

**Stability and Aggregation of Microplastics Suspended in Aqueous
Media**

By

Raziye Asoodeh

A thesis submitted

to the School of Graduate Studies in partial fulfillment of the
requirements for the degree of

Master of Science

Department of Earth Sciences

Memorial University of Newfoundland

August 2024

St. John's, Newfoundland and Labrador

Abstract

The accumulation of microplastics (MPs) has become a significant problem due to their non-biodegradable nature and ingestion by marine life. This study focused on three types of microplastics of approximate size 1 μm : polystyrene microplastics (PSMPs), carboxylate-modified polystyrene (PS-COOH), and amine-modified polystyrene (PS-NH₂). Their behavior was investigated in aqueous media at pH 5 and 9, with the inclusion of humic acid, different ions (Mg²⁺ or Na⁺) with ionic strength (IS) range (3mM and 15mM), and kaolinite. Results showed that a divalent cation, Mg²⁺, promoted aggregation by causing compression of the electric double layer. In lower IS scenarios, repulsion forces generated by electrical charges led to the stability of the PSMPs, inhibiting aggregation. Also, generally, suspensions were more unstable at higher pH values as the surface charge on microplastics may reverse, leading to reduced electrostatic repulsion. Humic acid improved the stability of suspensions through electrostatic or steric repulsion forces. Conversely, kaolinite reduced electrostatic repulsion, making suspensions less stable. Moreover, PS-NH₂ suspensions generally exhibited stability with high energy barriers, affected by kaolinite and IS. PS-COOH suspensions remained stable in higher IS NaCl, suggesting that the carboxylic acid groups contributed to their stability. These findings contribute to developing strategies to mitigate the environmental impact of microplastics.

Keywords: Microplastics, Stability, Aggregation, Polystyrene, Functional groups, Ionic strength, Humic acid, Clay,

General Summary

The accumulation of microplastics (MPs) has become a significant problem due to their non-biodegradable nature and ingestion by marine life. This study focused on three types of microplastics of approximate size 1 μm : polystyrene microplastics (PSMPs), carboxylate-modified polystyrene (PS-COOH), and amine-modified polystyrene (PS-NH₂). Experiments were conducted in water at pH levels of 5 and 9, with added humic acid (HA), ions (Mg²⁺ and Na⁺), and kaolinite. Results revealed that Divalent cations (Mg²⁺) caused the MPs to aggregate by compressing their electric layers. At lower ionic strength (IS), the MPs remained stable due to electric repulsion. Higher pH levels made the suspensions less stable, while HA improved stability through repulsion forces. Conversely, kaolinite reduced stability in most cases. PS-NH₂ MPs were generally stable, while PS-COOH MPs remained stable in higher IS conditions. These findings help develop ways to reduce the environmental impact of MPs.

Acknowledgments

I would like to express my sincere gratitude to the following individuals and organizations for their invaluable support and contributions during my research: I would like to express my sincere gratitude to my supervisors, Drs Tao Cheng and Alison Leitch, for all their support and guidance throughout my studies.

Furthermore, I would like to thank the previous and current faculty members at the Memorial University of Newfoundland for their invaluable contributions to my education. My gratitude to Memorial University of Newfoundland for providing financial support through the School of Graduate Studies Fellowship. Finally, I would like to thank my family and friends for their unwavering love, support, and encouragement. Their care and love will be forever appreciated.

Table of Contents

1	Introduction.....	1
1.1	Plastic production and breakdown.....	1
1.2	Functional groups	9
1.3	Research objectives	12
1.4	Thesis organization and layout.....	13
2	Literature review	15
2.1	Overview of relevant concepts	15
2.1.1	Colloids	15
2.1.2	Colloid stability and DLVO theory.....	15
2.1.3	Divalent cation bridging theory.....	19
2.1.4	Van-der-Waals attraction	20
2.1.5	Electric double layer and Zeta Potential	20
2.1.6	Debye length	22
2.1.7	Charge screening.....	24
2.1.8	Steric repulsion.....	24
2.1.9	Hydrodynamic diameter (HDD).....	25
2.1.10	Stokes' settling and Brownian motion	26
2.1.11	Point of zero charge (pH_{PZC}).....	28
2.2	Review of previous Studies	28

2.2.1	Stability or aggregation of MPs	28
2.2.2	Ionic strength and valence.....	30
2.2.3	Natural organic matter.....	32
2.2.4	pH.....	33
2.2.5	Clay	35
2.2.6	Functional groups: Effect of cation valence, humic acid, and clay colloids.....	37
3	Materials and methods	39
3.1	Dynamic light scattering (DLS)	39
3.2	Preparation of materials.....	41
3.2.1	Preparation of humic acid (HA).....	44
3.2.2	Preparation of kaolinite clay particle suspension.....	45
3.2.3	Preparation of suspensions	46
3.2.4	Preparation of colloidal suspension for batch experiments.....	49
3.3	DLVO calculation.....	51
4	Results and discussion	55
4.1	Measuring light absorbance of the microplastic suspensions: wavelength selection.....	55
4.2	Particle size analysis.....	56
4.3	Concentration of particles.....	57
4.4	Stability of plain polystyrene microplastic suspensions.....	58
4.4.1	Effect of ionic strength and salt types	59

4.4.2	Effect of kaolinite.....	62
4.4.3	Effect of humic acid	64
4.4.1	Effect of humic acid and kaolinite	65
4.5	Amine-modified polystyrene stability	72
4.6	Carboxylate-modified polystyrene stability	82
4.7	Comparative analysis of microplastic behavior: insights from three types of MPs	90
5	Conclusions and Recommendations	93
5.1	Conclusions	93
5.2	Recommendations for the future studies	95
6	References:.....	97
7	Appendix.....	110
7.1	Product specification of polystyrene	110
7.2	Product specification of amine-modified polystyrene.....	111
7.3	Product specification of carboxylate-modified polystyrene.....	112
7.4	Specification of humic acid	113
7.5	Specification of kaolinite.....	115

List of Tables

Table 1. Classification of plastic debris in the environment (Andrady, 2017).	3
Table 2. Common consumer plastics and applications (Brandon, 2017).....	5
Table 3. Polystyrene (PS), kaolinite, and humic acid (HA) concentrations in the suspensions for the stability tests	42
Table 4. Kaolinite concentration of the stock suspension.....	46
Table 5. Key parameters used in DLVO calculations (Xinjie Wang et al., 2020).....	53
Table 6. Hamaker constants	54
Table 7. The Hamaker constant (A) for the interaction between particles 1, which represents polystyrene (PS), and 2, which represents kaolinite or PS, across the medium 3, which is water.	54
Table 8. Energy Barrier (ϕ_{max}), Secondary Minimum (ϕ_{2min}) in NaCl solutions calculated for polystyrene microplastics based on DLVO theory.	70
Table 9. Energy Barrier (ϕ_{max}), Secondary Minimum (ϕ_{2min}) in MgCl ₂ solutions calculated for polystyrene microplastics based on DLVO theory.	71
Table 10. Energy Barrier (ϕ_{max}), Secondary Minimum (ϕ_{2min}) in NaCl solutions calculated for amine-modified polystyrene based on DLVO theory.	80
Table 11. Energy Barrier (ϕ_{max}), Secondary Minimum (ϕ_{2min}) in MgCl ₂ solutions calculated for amine-modified polystyrene based on DLVO theory.	81
Table 12. Energy Barrier (ϕ_{max}), Secondary Minimum (ϕ_{2min}) in NaCl solutions calculated for carboxylate-modified polystyrene suspensions based on DLVO theory.	88
Table 13. Energy Barrier (ϕ_{max}), Secondary Minimum (ϕ_{2min}) in MgCl ₂ solutions calculated for carboxylate-modified polystyrene suspensions based on DLVO theory.	89

List of Figures

Figure 1. Global plastic volume in different areas - modified from (Rosenboom et al., 2022).....	2
Figure 2. Average global plastic production in 2016 – modified from (Danso et al., 2019)	4
Figure 3. Primary and secondary sources of microplastics and their effect on human health- modified from (Debroy et al., 2022).	7
Figure 4. Schematic of carboxyl-modified polystyrene (COOH) and amine-modified polystyrene (NH ₂) - modified from (Anguissola et al., 2014)	10
Figure 5. Illustration of various particle interactions in a suspension – modified from (Sharma et al., 2021).....	16
Figure 6. Interaction potentials as a function of interparticle distance with interparticle distance (a) example calculation from an experiment in the current research; (b) illustration of electrostatic repulsion; (c) illustration of van der Waals interactions- modified from (Matter et al., 2020).....	18
Figure 7 . Divalent cation bridging theory- modified from (Ibrahim et al., 2018)	19
Figure 8. Cartoon showing the EDL on a negatively charged particle- modified from (Park et al., 2011).....	21
Figure 9. Debye length as a function of salt types according to the valency of the constituent ions, e.g. NaCl is type 1:1, MgCl ₂ is type 2:1- modified from (Kontogeorgis et al., 2016).....	23
Figure 10. Schematic representation of steric stabilization- modified from (Selvamani, 2019). ..	25
Figure 11. Hydrodynamic diameter measured with dynamic light scattering (DLS), compared with particle diameter measured with transmission electron microscopy (TEM). Modified from (Lafi, 2020).....	26
Figure 12. Effect of water chemistry and other suspended materials in natural habitats on MP behavior- modified from (Dong et al., 2022)	30

Figure 13. Zeta potential and z-average HDD variation of amidine PS nanoplastic particles (10 mg/L) as a function of pH in ultrapure water- modified from (Ramirez et al., 2019).35

Figure 14. Anisotropic surface charge of clay colloids (Montmorillonite)- modified from (Zhou et al., 2012).37

Figure 15. Zeta sizer, a device for analyzing particle suspensions by measuring light scattering, particle size, and zeta potential (ZP).40

Figure 16. Folded capillary cell used in the zeta sizer for measuring zeta potential (ZP).40

Figure 17. Experimental conditions for 96 different types of suspensions of polystyrene microplastics (PSMPs) studied in this research.43

Figure 18. Humic acid stock suspension on magnetic stirrer.....44

Figure 19. Suspensions are sonicated by using an ultrasonic cleaner.47

Figure 20. Vortex mixer: a laboratory instrument used to mix liquid samples through rapid rotational movement.....48

Figure 21. UV-Vis spectrophotometer48

Figure 22. UV-Vis spectra of microplastics (MPs) (50 mg/L), kaolinite (10 mg/L), and humic acid (HA) (3 mg/L) in deionized water.....56

Figure 23. Size distributions of microplastic particles polystyrene in pH 5 in deionized water....57

Figure 24. Polystyrene concentration vs absorbance a) polystyrene (50 mg/L) b) mixture of polystyrene (50 mg/L), kaolinite (10 mg/L), and HA (3 mg/L) at wavelength 600 nm.58

Figure 25. Stability of the polystyrene suspensions at pH 5 (blue) and 9 (red) in 3 mM NaCl, 15 mM NaCl, 1 mM MgCl₂, and 5 mM MgCl₂ solutions. Data are expressed as mean ± standard deviation of duplicate experiment.66

Figure 26. Zeta potential (ZP) of the polystyrene suspensions at pH 5 (blue) and 9 (red) in 3 mM NaCl, 15 mM NaCl, 1 mM MgCl₂, and 5 mM MgCl₂ solutions. Data are expressed as mean ± standard deviation of triplicate measurements.67

Figure 27. Hydrodynamic diameter (HDD) of the polystyrene suspensions at pH 5 (blue) and 9 (red) in 3 mM NaCl, 15 mM NaCl, 1 mM MgCl₂, and 5 mM MgCl₂ solutions. Data are expressed as mean ± standard deviation of triplicate measurements.68

Figure 28. DLVO interaction plots for polystyrene microplastics according to DLVO theory, van der Waals and EDL forces. Different colors symbolize different pH, and dashed lines lower IS for NaCl and MgCl₂. a) polystyrene b) polystyrene+ kaolinite c) polystyrene+ humic acid (HA) d) polystyrene+ HA+ kaolinite69

Figure 29. Stability of the amine-modified polystyrene suspensions at pH 5 (blue) and 9 (red) in 3 mM NaCl, 15 mM NaCl, 1 mM MgCl₂, and 5 mM MgCl₂ solutions. Data are expressed as mean ± standard deviation of duplicate experiments.76

Figure 30. Zeta potential (ZP) of the amine-modified polystyrene suspensions at pH 5 (blue) and 9 (red) in 3 mM NaCl, 15 mM NaCl, 1 mM MgCl₂, and 5 mM MgCl₂ solutions. Data are expressed as mean ± standard deviation of triplicate measurements.77

Figure 31. The hydrodynamic diameter (HDD) of the amine-modified polystyrene suspensions at pH 5 (blue) and 9 (red) in 3 mM NaCl, 15 mM NaCl, 1 mM MgCl₂, and 5 mM MgCl₂ solutions. Data are expressed as mean ± standard deviation of triplicate measurements.78

Figure 32. DLVO interaction plots for amine-modified polystyrene (PS-NH₂) according to DLVO theory, van der Waals, and EDL forces. Different colors symbolize different pH, and dashed lines lower IS for NaCl and MgCl₂. a) PS-NH₂ b) PS-NH₂ + kaolinite c) PS-NH₂ + HA d) PS-NH₂ + HA+ kaolinite79

Figure 33. Stability of the carboxylate-modified polystyrene suspensions at pH 5 (blue) and 9 (red) in 3 mM NaCl, 15 mM NaCl, 1 mM MgCl₂, and 5 mM MgCl₂ solutions. Data are expressed as mean ± standard deviation of duplicate experiments.84

Figure 34. Zeta potential (ZP) of the carboxylate-modified polystyrene suspensions at pH 5 (blue) and 9 (red) in 3 mM NaCl, 15 mM NaCl, 1 mM MgCl₂, and 5 mM MgCl₂ solutions. Data are expressed as mean ± standard deviation of triplicate measurements.85

Figure 35. Hydrodynamic diameter (HDD) of the carboxylate-modified polystyrene suspensions at pH 5 (blue) and 9 (red) in 3 mM NaCl, 15 mM NaCl, 1 mM MgCl₂, and 5 mM MgCl₂ solutions. Data are expressed as mean ± standard deviation of triplicate measurements.....86

Figure 36. DLVO interaction plots for carboxylate-modified polystyrene suspensions (PS-COOH) according to DLVO theory, van der Waals, and EDL forces. Different colors symbolize different pH, and dashed lines lower IS for NaCl and MgCl₂. a) PS-COOH b) PS-COOH + kaolinite c) PS-COOH + HA d) PS-COOH + kaolinite+ HA87

Figure 37. Zeta potential (ZP) of the amine-modified polystyrene suspensions at pH 5 (blue) and 9 (red) in 3 mM NaCl, 15 mM NaCl, 1 mM MgCl₂, and 5 mM MgCl₂ solutions. Data are expressed as mean ± standard deviation of triplicate measurements.91

Figure 38. (a). Stability of the polystyrene+ kaolinite suspensions at pH 5 (blue) and 9 (red) in 15 mM NaCl, (b). Hydrodynamic diameter (HDD) of the polystyrene suspensions at pH 5 (blue) and 9 (red) in 3 mM NaCl and 15 mM NaCl solutions.....92

List of abbreviations and symbols

°C – Degree Celsius

cm – centimeter

DOM – dissolved organic matter

EDL– electrical double layer

EDX– energy dispersive

g – gram

HA – humic acid

h⁻¹ – per hour

IS – ionic strength

J – joule

K - Kelvin

k_B – Boltzmann constant 1.38×10^{-23} J/K

k_BT– energy unit equals 4.11×10^{-21} J (for T = 24.5 °C)

kg – kilogram

L – liter

mL/min – milliliter per minute

M – moles/L

mM – millimoles/L

mg – milligram

ml – milliliter

mg/kg – milligrams per kilogram

mg/L –milligrams per liter

mm – millimeter

MP – microplastic

mV – millivolts

nm – nanometer

NOM – natural organic matter

NP – nanoparticles

NPs – nanoplastics

pH – power of hydrogen; a measure of hydrogen ion activity

PS – polystyrene

PS-NH₂ amine- modified polystyrene

PS-COOH carboxylate- modified polystyrene

PZC – point of zero charge

SEM – scanning electron microscope

μg – microgram

μg/L – micrograms per liter

μm – micrometer

VDW – van der Waals

XRD – X-ray diffraction

ZP – zeta potential

DLVO- Derjaguin–Landau–Verwey–Overbeek

1 Introduction

1.1 Plastic production and breakdown

Synthetic polymers were developed with the aim of creating materials that possess the ability to be easily shaped and retain their form ([Andrady et al., 2009](#); [Smith, 1935](#)). The inception of the first synthetic polymer dates back to 1907, and since then, there have been significant advancements in the realm of plastics ([Andrady et al., 2009](#); [Smith, 1935](#)). Plastics offer a multitude of advantages, including cost-effectiveness, lightweight nature, strength, durability, and the ability to be molded into various shapes and forms. Consequently, plastics have replaced conventional materials in diverse industries, such as packaging (comprising 35.9% or 146 million metric tonnes), construction (16.0% or 65 million metric tonnes), textiles (14.5% or 59 million metric tonnes), and others (3.6%) on an annual basis as of 2015 ([Rosenboom et al., 2022](#)) (Figure 1). The growing utilization of plastics and the subsequent global demand have raised concerns regarding the escalating issue of plastic waste in the foreseeable future ([Hahladakis et al., 2018](#); [Mcnutt, 2017](#); [Wessel et al., 2016](#)).

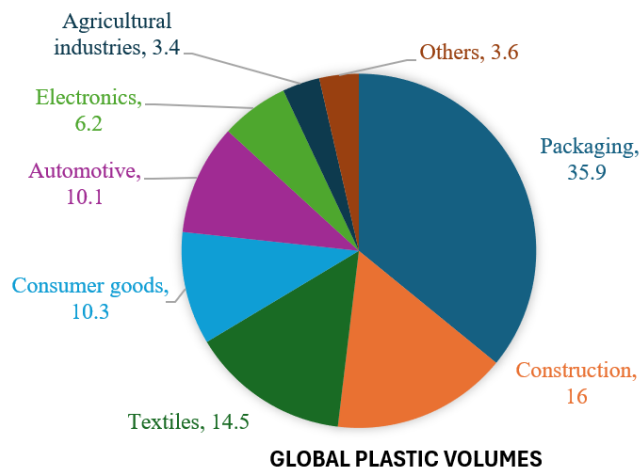


Figure 1. Global plastic volume in different areas - modified from ([Rosenboom et al., 2022](#))

Currently, global plastic production and its use are increasing in many areas of people’s lives, including domestic, industry, education, etc. ([Adyel, 2020](#); [Rochman et al., 2020](#)). The annual global production of plastic materials was more than 335 million tonnes in 2017, and it is predicted that this number will double in the next 20 years ([Garvey et al., 2020](#); [Sharma et al., 2021](#); [Wright et al., 2017](#)). China, North America, and Europe have been identified as prominent regions that have contributed significantly to the overall global production of plastic materials, producing 29%, 18%, and 18%, respectively ([Lv et al., 2019](#)).

As illustrated in Table 1, plastic fragments can be categorized into different groups based on their size, namely macroplastics, mesoplastics, microplastics (MPs), and nanoplastics. Macroplastics represent larger plastic fragments exceeding 2.5 cm, including items like small water bottles and cups. Mesoplastics encompass plastic particles ranging from 0.5 to 2.5 cm, such as small plastic toys and boxes. MPs are plastic particles smaller than 5 mm, commonly originating from sources like microbeads in personal care products and tire leachate. Lastly, nanoplastics (NPs) are MPs with sizes below 1 µm, typically formed unintentionally during manufacturing processes

or through the breakdown of larger plastic objects. These distinct categories aid in the identification and characterization of plastic fragments found in the environment ([Bhargava et al., 2018](#); [Debroy et al., 2022](#); [He et al., 2018](#); [Liu et al., 2018](#)) (Table 1).

There are two main ways that MPs can be produced; primary and secondary. Primary MPs are produced directly and can be found in some cosmetic and personal care products like toothpaste. In comparison, secondary MPs are made of larger plastics that break into smaller sizes due to factors like photooxidation, wind and water ([Sun et al., 2019](#)).

Plastics can undergo physical degradation through various mechanisms. Wind or wave-driven currents can result in collisions with rocks, cliffs, or the mixing of pieces of plastic with sand and sediments, causing their fragmentation into smaller particles. Additionally, photodegradation occurs as the polymer chains of plastics absorb UV light, leading to the formation of unstable bonds and subsequent breakdown. Biological degradation occurs when plastics interact with organisms, particularly aquatic species, which can ingest and break down the particles into smaller sizes. The combination of these various degradation processes leads to the formation of MPs.

Table 1. Classification of plastic debris in the environment ([Andrady, 2017](#)).

Class	Size ranges (MSFD GES)*	example
Macroplastics	> 2.5 cm	Water bottles and cups
Mesoplastics	0.5 cm–2.5 cm	Small plastic toys and boxes
Microplastics	0.5 cm (5000 µm) to 1 µm	Microbeads in personal care products and tire leachate
Nanoplastics	< 1 µm	Drug Delivery Systems

* MSFD GES Technical Subgroup on Marine Litter (2013) Monitoring Guidance for Marine Litter in European Seas.

MPs can be found in different sizes, compositions, types, and shapes. Based on the Table 2, the density of plastic determines its fate in the environment, as it influences whether the plastic will float on the surface or sink. Additionally, the structure is important to understand, particularly in terms of whether the material is hydrophobic or hydrophilic. The strong C-C bonds and the extremely hydrophobic surface of certain plastics play a crucial role in their environmental persistence and behavior. The most common MPs in the environment are polystyrene (PS), polyvinyl chloride (PVC), polyethylene (PE), polypropylene (PP), and polyethylene terephthalate (PET) ([Ahmed et al., 2022](#)). As illustrated in Figure 2, from an economic perspective, PE constituted the largest share of global plastic production in 2016, accounting for 38.2% of the total. Following PE, PP represented 22.4% of production, while PVC comprised 12.5%. PET contributed 10.9% to the overall production, while polyurethane (PUR) accounted for 8.9%. PS made up 4.6% of the production, and polyamide (PA) represented 2.6%. These percentages indicate the proportional distribution of these plastic types within the global plastics manufacturing industry ([Danso et al., 2019](#); [Hahladakis et al., 2018](#); [Mattsson et al., 2018](#)) (Table 2).

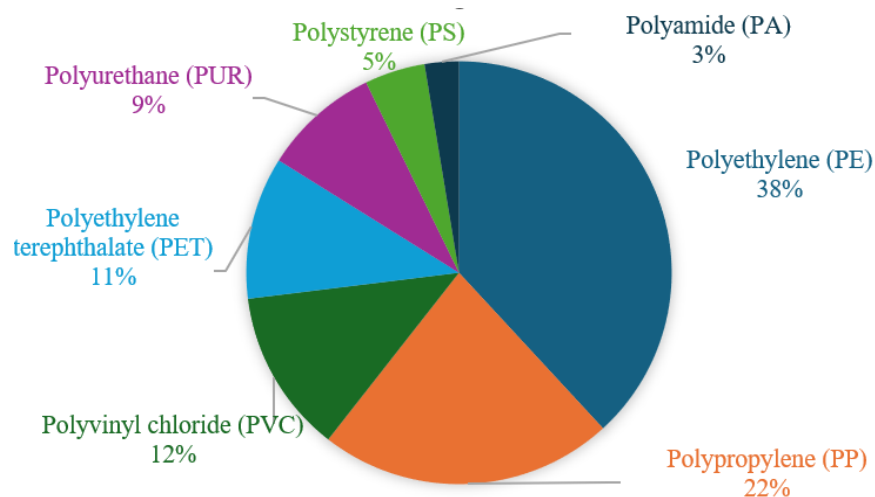


Figure 2. Average global plastic production in 2016 – modified from ([Danso et al., 2019](#))

Table 2. Common consumer plastics and applications ([Brandon, 2017](#))

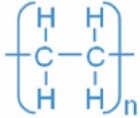
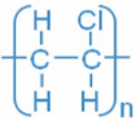

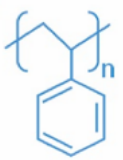
Plastic Type	Density (g/cm ³)	Common Applications	Structure
Polyethylene Terephthalate (PET)	1.35	Disposable clear plastic drink bottles, food jars	 <p>Polyethylene</p>
Polyvinyl Chloride (PVC)	1.35	Pipes and fittings, vinyl siding, synthetic-leather products, shampoo bottles	 <p>Polyvinyl chloride</p>
Polypropylene (PP)	0.89-0.91	Flexible containers, bottle caps, drink cups	 <p>Polypropylene</p>
Polystyrene (PS)	1.0-1.1	Disposable cutlery, packing peanuts, CDs	 <p>Polystyrene</p>

Figure 3 depicts that MPs can enter aquatic ecosystems via direct and indirect routes ([Auta et al., 2017](#)). The direct pathways encompass the introduction of plastic items into water bodies, including lakes, rivers, and oceans, either as litter or due to improper handling ([Sun et al., 2019](#)). In contrast, the indirect pathways involve the transfer of MPs from the soil or atmosphere. This transfer can occur through activities such as illegal dumping or inadequate management of landfills ([Cole et al., 2011](#)). Moreover, MPs can be transported from the soil into water bodies through

processes such as runoff, erosion, and wind dispersion ([Rezaei et al., 2019](#)). Under stormy conditions, the concentrations of MPs on land can intensify, thereby facilitating their entry into water systems ([Eerkes-Medrano et al., 2015](#)).

The stability of suspensions of MPs influences the distribution, mobility, and fate of MPs and their possible effects on ecosystem health and human health ([Xinjie Wang, 2021](#)). MPs pose a threat to marine organisms as MPs provide a surface for bacteria and biofilms to accumulate. These bacteria consume dissolved oxygen in the water and contribute to deoxygenation, leading to reduced oxygen levels in the water. This lack of oxygen adversely affects fish and other oxygen-dependent animals, jeopardizing their survival (Figure 3). Regrettably, the process of recovering from microplastic-induced marine deoxygenation is anticipated to take centuries. The persistent nature of MPs and their challenging removal from the ocean exacerbate the issue. As these particles degrade into smaller fragments, they are prone to ingestion by marine organisms, thus entering the food chain and intensifying the problem. Moreover, the detrimental effects caused by MPs persist for an extended period. Even if plastic usage were to cease immediately, the ocean would require a significant amount of time to recover from the existing damage inflicted by MPs ([Kvale et al., 2023](#)).

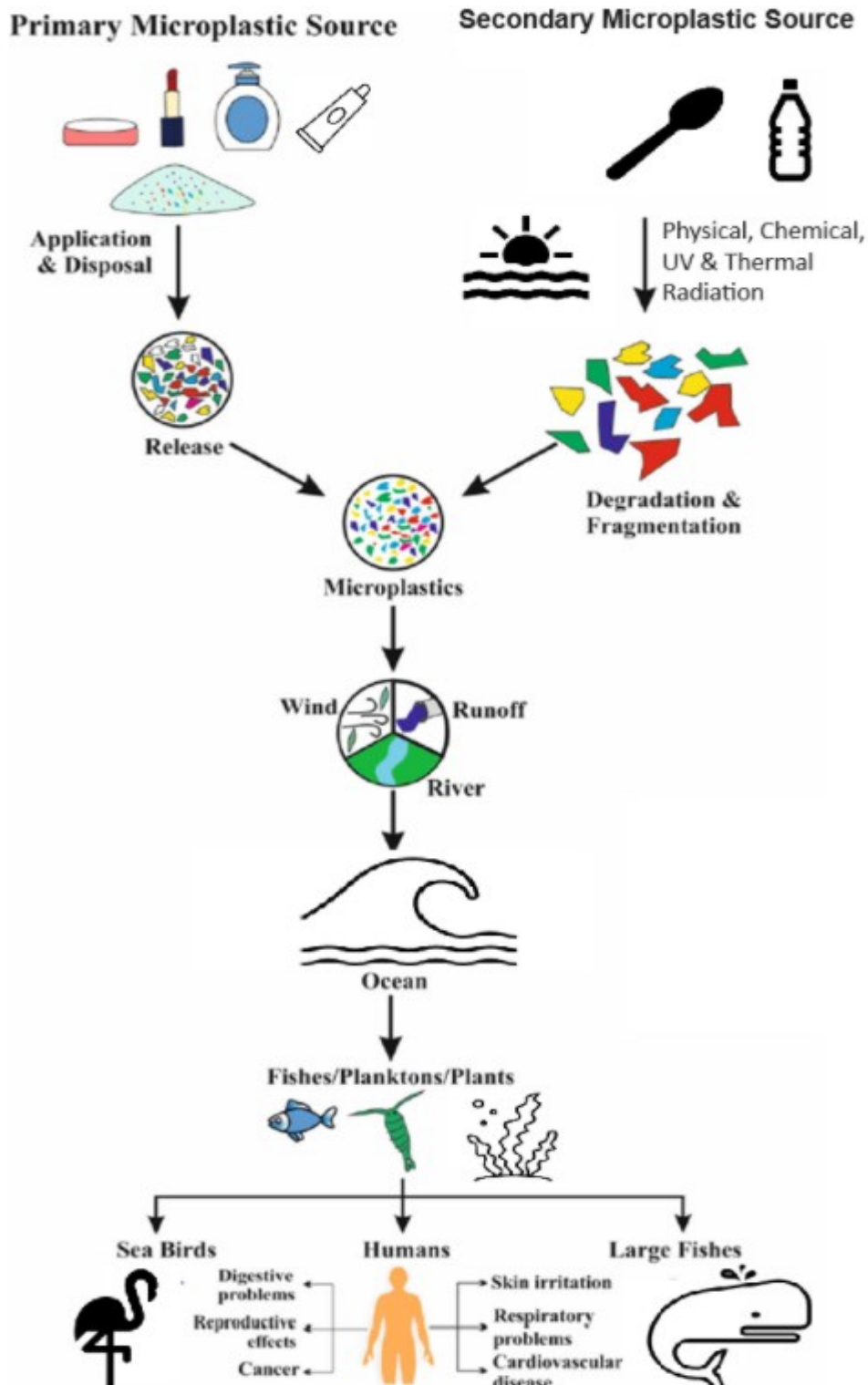


Figure 3. Primary and secondary sources of microplastics and their effect on human health-modified from (Debroy et al., 2022).

MPs and NPs have the ability to be consumed by various marine organisms, entering the food chain and posing a risk to human health. These small plastic particles, when present in water, can be ingested by phytoplankton and zooplankton, acting as a pathway for their entry into the human diet. The presence of plastics in marine ecosystems can also impact the population dynamics of marine organisms, like zooplankton, which are an essential source of energy in the aquatic environment. Ingestion of MPs has been linked to inflammation and cellular harm. One significant concern is their capacity to absorb toxic or harmful chemicals, including pesticides, onto their surfaces. The large surface area of MPs and NPs enhances their ability to absorb such chemicals. These problems are exacerbated by the prolonged degradation time of plastics, which amplifies the risks to both the environment and human well-being ([Wu et al., 2017](#)) (Figure 3).

The aggregation of MPs in aquatic environments is an important factor that profoundly impacts the fate of these particles and the ecological hazards they pose. This phenomenon entails the tendency of MPs to aggregate and form larger particles, thereby affecting their movement, dispersion, and potential interactions with organisms and ecosystems. Consequently, it contributes to the overall ecological risks associated with the contamination of aquatic systems by microplastics ([Alimi et al., 2018](#); [Besseling et al., 2017](#); [Carr et al., 2016](#)).

Aggregation is the mechanism through which two particles approach each other, ultimately to collide and attach. In the case where both particles involved in aggregation are MPs of the same nature, it is denoted as homoaggregation. Conversely, when the two MP particles differ in type, it is termed heteroaggregation ([Alimi et al., 2018](#)). Within natural aqueous settings, the occurrence of heteroaggregation between MPs and diverse particles, such as natural minerals, is more prevalent owing to the overwhelmingly greater number of natural colloids. This then leads to

phenomena like sedimentation and floating ([Long et al., 2017](#); [Oriekhova et al., 2018](#); [Singh et al., 2019](#)).

The surfaces of MPs commonly exhibit hydrophobic functional groups, which facilitate the attraction of dissolved organic matter (DOM) and organisms, especially algae and bacteria ([Zhang et al., 2020](#)). The formation of biofilms arises as a consequence of the adsorption processes occurring on the surface of MPs in the presence of natural water ([Harrison et al., 2018](#)).

1.2 Functional groups

By definition, functional groups denote distinct configurations of atoms found within molecules, exerting significant influence over the physiochemical characteristics of substances and their interactions with diverse compounds ([Bader et al., 1994](#)). The behavior and potential uses of MPs are determined by the characteristics of their outer surface, which might include attached functional groups. Functional groups are essential in determining the surface charge of MPs, thereby influencing their behavior and movement in different environments.

As illustrated in Figure 4, MPs can possess different functional groups on their surfaces, including carboxyl (-COOH) and amino (-NH₂) groups, which are introduced through processes like photodegradation and biodegradation ([Andrady, 2011](#)) (Figure 4). The aging of plastic materials in the environment, influenced by factors including photodegradation (caused by the action of light, often sunlight during outdoor exposure) and biodegradation (caused by the action of living organisms, typically microbes), can result in the formation of NPs or MPs with diverse functional groups. For instance, surface oxidation during weathering processes can lead to the presence of carboxyl groups on nanoparticles (NP) surfaces ([Luan et al., 2019](#)), while hydrolysis of polyamides can generate amine-modified NPs with positive charges ([Xiao Wang et al., 2020](#)).

These functional groups on the surfaces of MPs and NPs impact their properties and behavior, including interactions with other substances or organisms in aquatic environments. For example, the overabundance of PS-NH₂, a variant of polystyrene with amino groups, in the digestive systems of the larvae of *Paracentrotus lividus* (a type of sea urchin) adversely affected their initial growth stages. In contrast, PS-COOH, a different form of polystyrene with carboxyl groups, did not exhibit significant detrimental effects on the larvae ([Della Torre et al., 2014](#)).

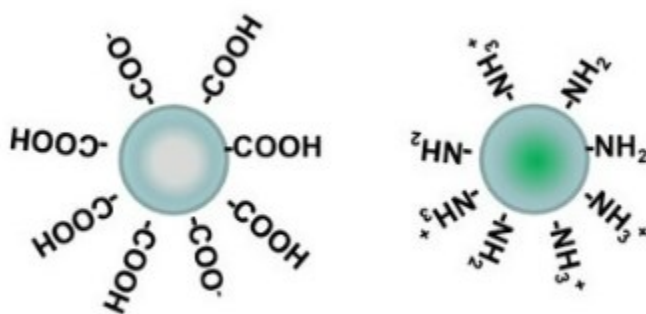


Figure 4. Schematic of carboxyl-modified polystyrene (COOH) and amine-modified polystyrene (NH₂) - modified from ([Anguissola et al., 2014](#))

To investigate the stability and migration characteristics of MPs, researchers often utilize polystyrene nanospheres (PSNPs) that have been modified with various functional groups. These modified PSNPs determine how different surface properties impact the behavior and interactions of MPs ([Wu et al., 2019](#)). The strategic design and incorporation of specific functional groups in nanoparticles have great importance and potential in various medical applications. For instance, previous research has demonstrated the effectiveness of PSNPs that have been modified with amino functional groups in treating prostate cancer cells. This modification enables the nanoparticles to interact specifically with the cancer cells, increasing the likelihood of successful treatment results

([Lunov et al., 2011](#)). When nanoparticles are suspended in biological fluids, they adsorb proteins and other biomolecules from the surrounding environment, forming a layer called the "corona". This layer defines the biological identity of the NPs and affects nanoparticle-cell interactions. Nanomaterials are taken up by cells through active, energy-dependent endocytic pathways and in many cases, they are transported to the lysosomes.

Commercial polystyrene nanospheres have widespread use as carriers in medicine for targeted drug delivery and controlled drug release. Nanoparticles possess the ability to infiltrate the human body via ingestion and inhalation, thereby potentially gaining entry into the bloodstream and becoming systemic. Preferential accumulation within vital organs, notably the liver and kidneys, is observed. These distinctive attributes render nanomaterials promising for biomedical drug delivery purposes. Additionally, they are commonly employed as model materials to study the fate and transport of MPs and NPs in the environment ([Dong et al., 2019](#)). To enhance the bioavailability of drugs, it is necessary to modify the surfaces of NPs with reactive functional groups. This surface modification allows for improved interactions with drugs, leading to enhanced drug delivery and therapeutic efficacy. PS-COOH finds wide application in the medical field, specifically for purposes such as cell imaging and drug delivery. The utilization of PS-COOH stems from its advantageous properties, which include favorable biocompatibility, straightforward synthesis, and remarkable durability. The presence of carboxyl functional groups on the PS surface allows for convenient coupling with targeting molecules or therapeutic agents, thereby enabling precise delivery and imaging of cells. Moreover, the inherent stability of PS-COOH ensures the sustained integrity and efficacy of drug delivery systems over extended periods ([Wang et al., 2017](#)).

1.3 Research objectives

MPs, especially polystyrene types, pervade our ecosystem, and their mobility and stability bear significant environmental consequences. PS is widely used in plastic products and has been identified as one of the most common types of MPs found in the environment ([Lei et al., 2018](#)). Polystyrene is the subject of interest in this investigation. Specifically, this study evaluates three variations of PSMPs, PS-Plain (unmodified), PS-COOH, and PS-NH₂, each approximately 1 μm in size. Their diverse surface charges can substantially influence their aggregation and stability in the environment ([Wu et al., 2019](#)).

Existing research underscores that factors like pH, ionic strength (IS) and type, particle size, surface functional groups, and natural organic matter influence the stability and mobility of MPs. Recent studies have concentrated on the aggregation and deposition of MPs and NPs - specifically spherical PS particles – that have been altered with sulfate, amine, or carboxyl groups ([Alimi et al., 2018](#)). However, most of these studies explored these factors individually, creating a gap in understanding their combined effects on MPs. This research sought to fill this gap.

One of the objectives of this research was to unravel the primary forces and mechanisms driving the mobility of MPs. This included an examination the competing influence of van der Waals attraction and electrical double layer repulsion as outlined in the Derjaguin–Landau–Verwey– Overbeek (DLVO) theory, which will be discussed in section 2.1.2 ([Ling et al., 2022](#)). The insights gained from this study will shed light on the environmental behavior of MPs and aid in devising effective strategies to mitigate their adverse effects on environmental and human health. The rationale behind selecting specific IS and pH values was to replicate the salinity conditions

found in soil, water and fresh groundwater. In this study, the chosen IS range (3 mM and 15 mM) and pH between 5 and 9 aim to closely resemble the natural characteristics of these environments.

1.4 Thesis organization and layout

The thesis is structured into five chapters. The organization and layout of the thesis are as follows:

Chapter 1: Introduction

The first chapter of the thesis outlines the research topic, its importance, and the study's specific goals. It defines the research questions and sets the context for investigating how microplastics behave in the environment. This chapter provides the foundation for later chapters by introducing key ideas and the motivations behind the research.

Chapter 2: Literature Review

In this chapter, an in-depth exploration of existing literature on microplastics in water is presented. Current knowledge is highlighted, important theories and models are discussed, and gaps in understanding microplastic behavior under different conditions are identified. The literature review provides the theoretical framework for the research, giving context for the empirical investigation.

Chapter 3: Materials and Methods

Chapter 3 explains the experimental setup and methods used to study microplastic behavior under various conditions, including different concentrations of the salts NaCl and MgCl₂. It describes the types of microplastics used, how samples were collected, the measurement techniques

employed, and how the data were analyzed. This chapter provides a thorough understanding of the experimental procedures, ensuring transparency and reproducibility.

Chapter 4: Results and Discussion

Chapter 4 presents the research findings. It details the results of the conducted experiments. The chapter covers results related to microplastic stability, aggregation tendencies, sizes, charges, and energy barriers. Each observation is explained within the context of research questions and existing theories. The results are discussed in relation to different microplastic types and the effects of different conditions, such as varying salt concentrations and $MgCl_2$ presence, HA, and kaolinite.

Chapter 5: Conclusions and Recommendations

The final chapter synthesizes the findings. It emphasizes important observations, patterns, and insights from the research. This chapter revisits research questions and objectives based on the results. Conclusions drawn are connected to the broader context of microplastic behavior in water. Additionally, the chapter summarizes the study and its findings with recommendations for future research.

2 Literature review

2.1 Overview of relevant concepts

2.1.1 Colloids

A colloidal system is typically composed of two main components: colloidal dispersions and a surrounding medium, which can exist in the forms of gas, liquid, or solid. Colloidal dispersions typically consist of particles ranging in size from 1 nanometer to 1 micrometer, although occasionally larger particles up to 10 or 50 micrometers may also be classified as colloids due to their small dimensions and large surface area. The unique properties exhibited by colloidal particles highlight the importance of studying and comprehending colloids and their stability ([Kontogeorgis et al., 2016](#)).

2.1.2 Colloid stability and DLVO theory

Of all the characteristics associated with colloids, stability is arguably the most crucial aspect deserving thorough investigation and comprehension. Colloidal dispersions exhibit a high surface area (sometimes higher than $100 \text{ m}^2/\text{g}$), which makes them susceptible to reacting with other suspended materials and potentially becoming unstable. The stability of colloidal systems is related to a balance between attractive and repulsive forces. Notably, the attractive forces found in colloidal systems, such as van der Waals interactions, tend to be significantly stronger than those encountered between individual molecules in a non-colloidal aqueous liquid.

Consequently, an abundance of attractive forces can lead to the aggregation of suspended particles and hence to instability of the suspension. However, repulsive forces, including electrical forces originating from charged particles, work in opposition to the attractive forces, thereby

contributing to the suspension's stability. Steric forces, which involve the physical hindrance of particles (e.g., from overlapping electron clouds), also play a role in repulsion, and contribute to the overall stability of colloids. As illustrated in Figure 5, the stability of colloidal systems is influenced by the interplay between attractive van der Waals forces, which can lead to aggregation (instability in suspension), and repulsive forces arising from the electrical charges present on the particles (stability in suspension). Interactions between colloidal particles are primarily determined by the van der Waals attraction and electrical double layer repulsion, as described by the Derjaguin–Landau–Verwey–Overbeek (DLVO) theory ([Kontogeorgis et al., 2016](#)).

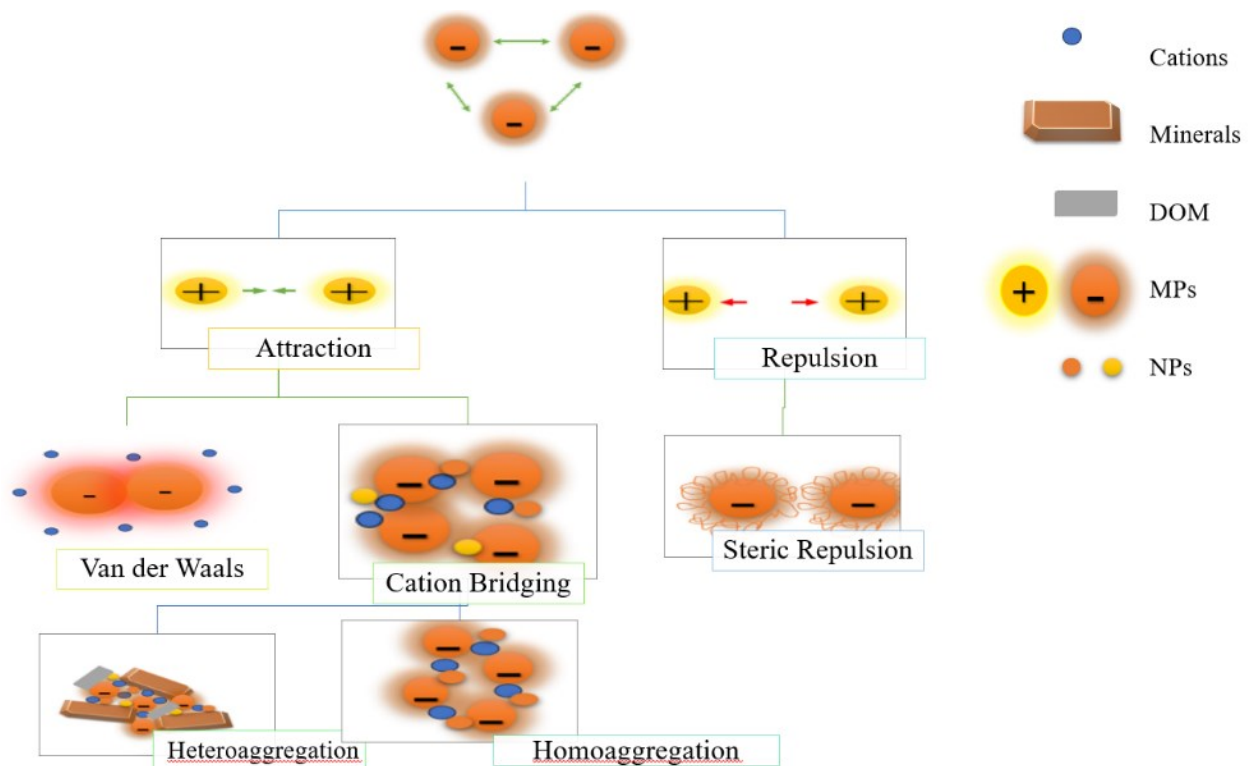


Figure 5. Illustration of various particle interactions in a suspension – modified from ([Sharma et al., 2021](#))

The DLVO theory takes into account the concurrent influence of attractive van der Waals forces (V_A) and repulsive forces arising from the double layer (V_R). The total potential energy (V) is the result of the combined effect of these forces, expressed as equation 1 is:

$$V = V_R + V_A. \tag{1}$$

As illustrated in Figure 6, to gain insight into the behavior of a colloidal system, potential energy-distance plots are frequently employed. These graphical representations (e.g., Figure 6) provide a visual depiction of the relationship between potential energy and distance. Negative potential energy due to van der Waals forces signifies attraction and instability of the suspension, while positive potential energy related to electrostatic repulsion denotes stability and repulsion. The combination of the two is depicted by the blue curve. The presence of a secondary minimum indicates a weak attractive force between two particles. The positive peak observed in the diagram corresponds to the energy barrier that particles must overcome to come into contact. It arises from electrostatic forces. Conversely, the primary minimum represents a strong attractive force between particles at very short distances, promoting their aggregation.

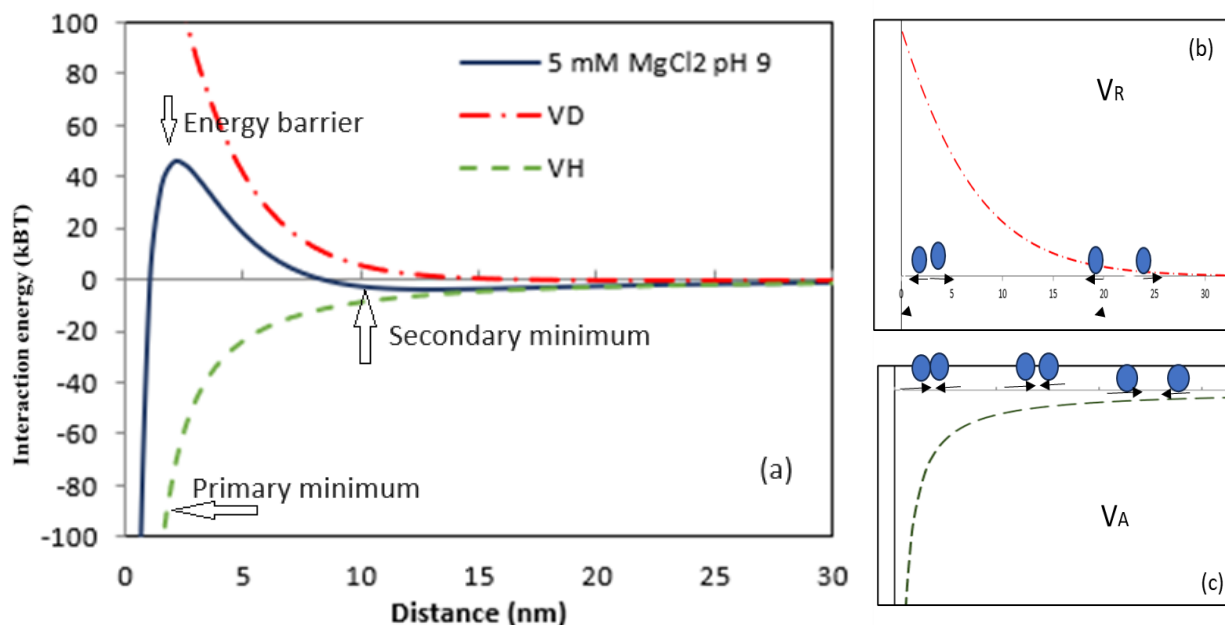


Figure 6. Interaction potentials as a function of interparticle distance with interparticle distance (a) example calculation from an experiment in the current research; (b) illustration of electrostatic repulsion; (c) illustration of van der Waals interactions- modified from ([Matter et al., 2020](#)).

When repulsive forces dominate, the system is stable. On the other hand, where attractive van der Waals forces prevail at all distances, aggregation takes place, resulting in an unstable dispersion.

As the majority of particles in a suspension possess an electric charge, electrostatic forces exist in the surrounding medium, particularly in polar solvents like water. Water's high relative permittivity strengthens the interactions among charged particles. The surface charge of particles may originate from the adsorption of ions present in the solution or the dissociation of surface groups. The strength of repulsion is significantly influenced by the physiochemical properties of the medium. Therefore the parameters of salinity, pH, IS, ion types (monovalent, divalent), natural

organic matter (NOM) and other factors of the aquatic environment strongly affect the stability of colloids ([Kalliola et al., 2016](#); [Pradel et al., 2021](#)).

2.1.3 Divalent cation bridging theory

Divalent cations, including Ca^{2+} and Mg^{2+} , have been found to promote particle aggregation when introduced into a suspension. The divalent cation bridging theory explains this observation by proposing that divalent cations serve as bridges between negatively charged particles, facilitating their aggregation. As depicted in Figure 7, in colloidal systems, where particles commonly bear negative charges, divalent cations act as bridges. This bridging effect is more pronounced compared to monovalent cations like Na^+ , as divalent cations possess two positive charges ([Sobeck et al., 2002](#)).

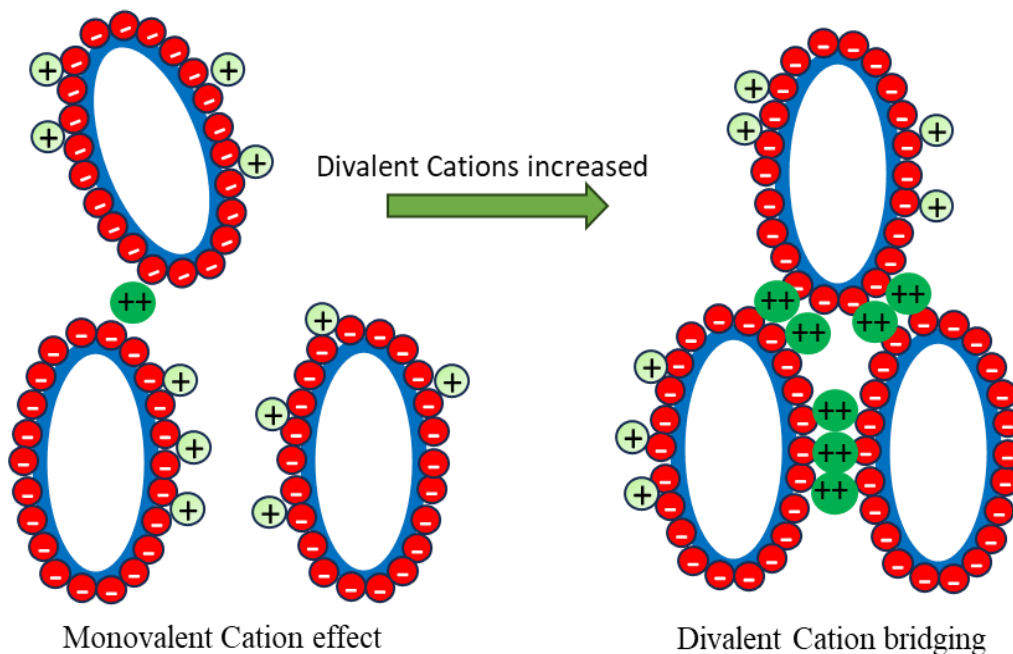


Figure 7 . Divalent cation bridging theory- modified from ([Ibrahim et al., 2018](#))

2.1.4 Van-der-Waals attraction

Van der Waals forces result from interactions between dipoles, which can be permanent in polar molecules or temporary due to changes in electron density. These forces, also referred to as London dispersion forces, occur between all atoms and molecules and are caused by temporary imbalances in electron distribution within the particles. Permanent dipoles arise from the uneven distribution of electrons in polar molecules, leading to attractive forces between positively and negatively charged regions of adjacent molecules. On the other hand, temporary dipoles occur when there is a momentary shift in electron density, resulting in attractive interactions. Van der Waals forces play a crucial role in the stability and interactions between particles ([Matter et al., 2020](#)).

2.1.5 Electric double layer and Zeta Potential

An electric double layer (EDL) is an essential factor in the electrostatic stabilization of colloids, as it involves the adsorption of negatively charged ions from the dispersion medium onto colloidal particles, resulting in their negative electric charge. The negatively charged particles adsorb the positively charged ions present in their surroundings. As depicted in Figure 8, the EDL encompasses the adsorbed ions on its surface and a layer of the oppositely charged ions within the dispersion medium. Notably, the EDL maintains electrical neutrality.

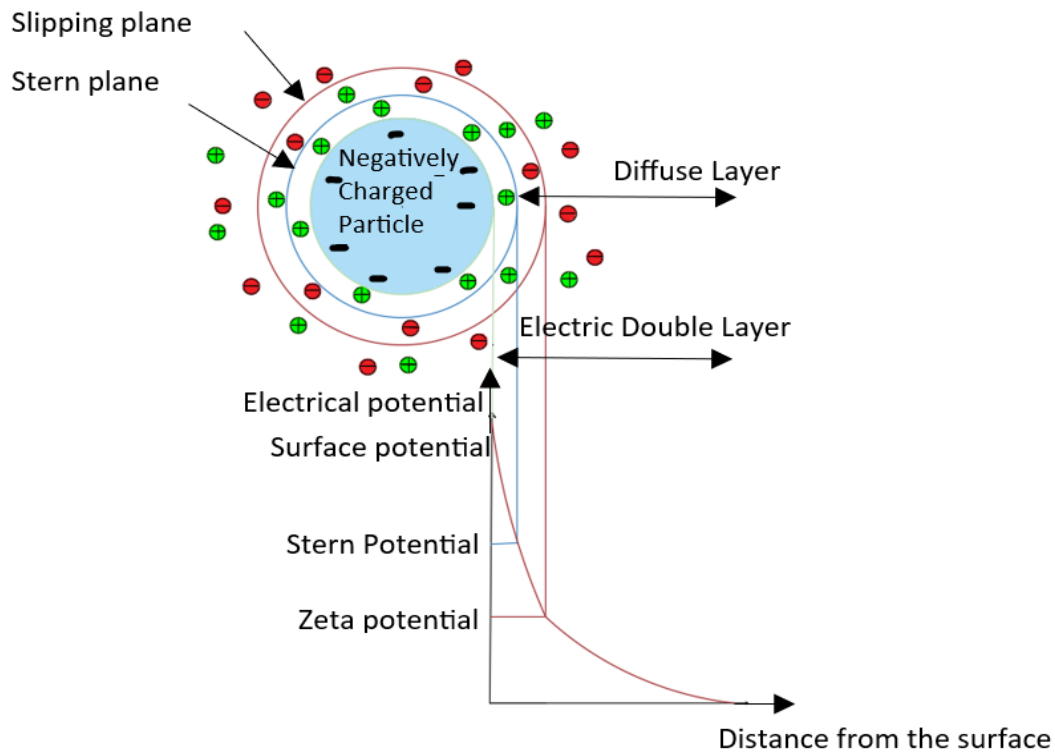


Figure 8. Cartoon showing the EDL on a negatively charged particle- modified from ([Park et al., 2011](#)).

An EDL is composed of three components:

- **Surface charge:** ions with a specific charge (typically negative) that adhere to the surface of the particle.
- **Stern layer:** counterions (oppositely charged to the surface charge) that are drawn to the particle surface and firmly attached to it due to electrostatic forces.
- **Diffuse layer:** a layer of the surrounding dispersion medium (solvent) located near the particle. The diffuse layer contains freely moving ions, particularly an increased concentration of oppositely charged ions. The ions within the diffuse layer experience the electrostatic force exerted by the charged particle.

The EDL exhibits its highest electrical potential (in absolute magnitude) at the particle surface (surface potential). The Stern potential applies at the outside edge of the Stern layer of oppositely charged adsorbed ions. Moving beyond the Stern layer, the electrostatic effects resulting from the particle's surface charge gradually diminish according to Debye's law. This law states that for each Debye length, the electric field strength reduces by a factor of $1/e$ ([Chen et al., 2013](#)). As the distance from the surface increases, the potential gradually decreases until it reaches (close enough to) zero at the boundary of the EDL.

During the movement of a colloidal particle in the dispersion medium, a layer of the surrounding liquid adheres to the particle, and the boundary of this layer is referred to as the slipping plane (shear plane). The electric potential value at the shear plane is known as the zeta potential (ZP) or electrokinetic potential, which holds significant importance in the theory of colloidal particle interaction ([Park et al., 2011](#)).

In other words, the ZP indicates the electric potential at a particular location where a colloid particle undergoes movement or sliding. This location serves as a dividing line separating the particle from the nearby fluid. Measuring the ZP means finding out the disparity in electric potential between this boundary and the EDL surrounding the particle. ZP serves as an indirect measurement of the stability of colloidal suspension ([Al Harraq et al., 2021](#)).

2.1.6 Debye length

The Debye length, symbolized as κ^{-1} , serves as a metric for quantifying the thickness of the electrical double layer within a colloidal configuration. It indicates the range within which the electrostatic interactions between charged particles propagate. A larger Debye length corresponds to an expanded ion cloud, thereby fostering the stability of colloidal entities. This expansion

effectively impedes particles from closely approaching each other at short distances, where the predominance of the highly attractive van der Waals forces emerges. The magnitude of the Debye length is contingent upon a multitude of factors including the thermal motion of ions, characteristics of the solvent, the IS of the solution, and the dielectric properties of the surrounding medium. Notably, the presence of salt in the solution, particularly monovalent ions, promotes a reduction in the Debye length ([Kontogeorgis et al., 2016](#); [Matter et al., 2020](#)). Figure 9 depicts the correlation between salt concentration in an aqueous solution and the Debye length, indicating that as the IS increases, reflecting an elevated ion concentration, the Debye length is reduced ([Kontogeorgis et al., 2016](#)).

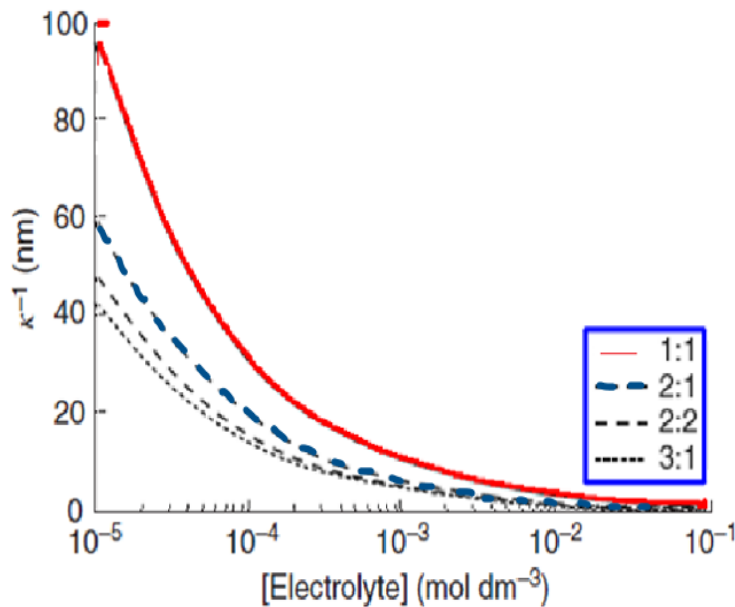


Figure 9. Debye length as a function of salt types according to the valency of the constituent ions, e.g. NaCl is type 1:1, MgCl₂ is type 2:1- modified from ([Kontogeorgis et al., 2016](#))

2.1.7 Charge screening

In the context of a solution containing charged particles and ions, the phenomenon of charge screening arises. When charged particles are in proximity within a suspension, particles with the same charge repel each other, while those with opposite charges attract. However, the presence of additional ions in the suspension solution can disrupt these forces and impact the behavior of the charged particles. “Charge screening” occurs when ions carrying opposite electric charges to the surface charge of the particles are introduced into the solution, subsequently diminishing the electrostatic repulsion between the particles. Consequently, charge screening promotes particle aggregation ([Israelachvili, 2011a](#)).

2.1.8 Steric repulsion

Steric repulsion is the consequence of large molecules attaching to micro or nanoparticles, producing a ‘hairy’ surface (Figure 10). The hairy surface of particles acts as a protective barrier. The repulsive force associated with overlapping electron clouds acts as a physical obstruction, preventing particles from approaching each other closely and forming aggregates. Steric repulsion is a vital factor in improving the stability of colloidal systems, as it helps to maintain the dispersion of particles. It is worth noting that steric repulsion operates over short distances – determined by the length of the attached molecules - and is influenced by the sizes of the particles involved ([Selvamani, 2019](#)).

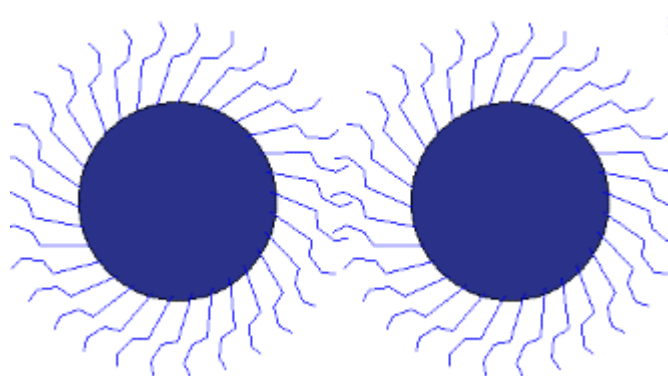


Figure 10. Schematic representation of steric stabilization- modified from ([Selvamani, 2019](#)).

2.1.9 Hydrodynamic diameter (HDD)

The HDD is a crucial parameter utilized to quantitatively define the effective size of particles present in a fluid medium. Experimental methods such as dynamic light scattering (DLS) are often employed to measure the HDD of suspended particles. As depicted in Figure 11, It is worth noting that the HDD generally exceeds the actual diameter obtained through transmission electron microscopy (TEM) due to several factors, including the electrical conductivity characteristics of the suspension. The disparity observed between these two size measurements is influenced by a multitude of factors, which collectively capture the intricate interplay between particles and their surrounding fluid environment ([Lafi, 2020](#)). HDD has emerged as a valuable parameter for assessing the inclination of MPs toward aggregation. The magnitude of HDD values serve as an indicator, reflecting the potential for particle aggregation and the formation of larger particle clusters. This physical characteristic offered valuable insights into the behavior of MPs across different experimental contexts, shedding light on their interactions and tendencies to either aggregate or maintain dispersion. When particles aggregate, their collective size expands, leading to an increase in the HDD of colloidal particles. Attached molecules can also increase

hydrodynamic diameter: for example, in a study after the protein A was attached to the gold nanoparticles, the HDD of the particles experienced an increase ([Jans et al., 2009](#)).

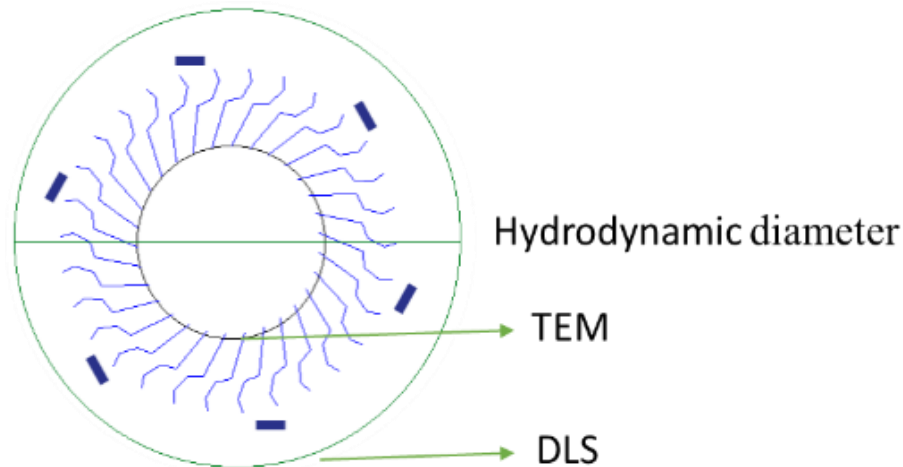


Figure 11. Hydrodynamic diameter measured with dynamic light scattering (DLS), compared with particle diameter measured with transmission electron microscopy (TEM). Modified from ([Lafi, 2020](#)).

2.1.10 Stokes' settling and Brownian motion

Stokes' equation is an equation used to calculate the rate of sinking or rising of spherical particles in a viscous liquid medium due to gravity. It considers the influences of gravity, buoyancy, and drag forces in laminar flow. Gravity causes negatively buoyant (relatively heavy) particles to move downward, while positive buoyancy acts in the opposite direction, pushing particles upward within the liquid. The drag force opposes the motion of particles and depends on their size and velocity. By considering these factors, Stokes' equation provides a method for estimating the maximum speed at which suspended particles settle in a dispersion medium.

The following equation is utilized to calculate the sedimentation velocities of idealized kaolinite particles and polystyrene spheres descending through water:

$$u = \frac{2R^2 g(\rho_{particle} - \rho_{water})}{9\eta_{water}} \quad (2)$$

In this equation, u represents the terminal velocity, R signifies the radius of the particles (0.05 micrometers for clay and 0.5 μm for polystyrene), ρ_{clay} is 2650 kg/m^3 , $\rho_{\text{polystyrene}}$ is 1050 kg/m^3 and ρ_{water} at 25 $^{\circ}\text{C}$ is 997 kg/m^3 . The dynamic viscosity of water at 25 $^{\circ}\text{C}$, η_{water} is $9 \times 10^{-4} \text{ kg m}^{-1} \text{ s}^{-1}$, and g represents the acceleration due to gravity ($9.81 \text{ m}/\text{s}^2$) ([Kontogeorgis et al., 2016](#)).

Solving this equation gives a terminal velocity of clay particles of $10^{-8} \text{ m}/\text{s}$, which corresponds to 0.9 mm/day . For 1-micron polystyrene spheres the settling velocity is $3.2 \times 10^{-8} \text{ m}/\text{s}$ or 2.8 mm/day . Therefore, over a 6-hour duration experiment, such spheres would settle about 0.7 mm (700 microns).

Suspended particles are also affected by Brownian motion. The square root of the mean squared displacement of a particle in a 3-dimensional space, \bar{x} , is often used to characterize how far a particle has moved in time t :

$$\bar{x} = \sqrt{6Dt} \quad (\text{Kontogeorgis et al., 2016}) \quad (3)$$

where the diffusion coefficient D is given by

$$D = \frac{k_B T}{6\pi\eta R} \quad (\text{Kontogeorgis et al., 2016}) \quad (4)$$

For 1 micron diameter polystyrene spheres in water at 25 $^{\circ}\text{C}$, $D \approx 2.45 \times 10^{-13} \text{ m}^2/\text{s}$. After 30 min, $\bar{x} = 51$ microns and after 6 h, $\bar{x} = 178$ microns. For the suspensions used in this study, at a concentration of 50 mg/L , if evenly distributed the suspended particles are about 22 microns apart, so over the course of the experiments they have time for close encounters.

This does not take into account the electric charge effects mentioned above. Surface effects which increase the hydraulic radius would slow settling by reducing the effective density difference, whereas aggregation of particles would increase the calculated settling velocity by increasing the diameter of the settling entities.

2.1.11 Point of zero charge (pH_{PZC})

The term "point of zero charge" (pH_{PZC}) pertains to the pH value at which a solid surface or particle exhibits no net electrical charge. At this specific pH, there exists neither attractive nor repulsive forces between the surface or particle and the surrounding solution, resulting in a condition of electrical neutrality. The determination of pH_{PZC} depends on the balance between the concentrations of hydrogen ions (H^+) and hydroxide ions (OH^-) on the surface. In suspensions where the pH of the suspension is lower than the pH_{PZC} , the surface charge becomes positive due to an excess of H^+ ions. Conversely, when the pH exceeds the pH_{PZC} , the surface charge of the particle becomes negative due to an excess of OH^- ions ([Chorover, 2023](#)).

2.2 Review of previous Studies

2.2.1 Stability or aggregation of MPs

MPs can accumulate in sediments or other environmental matrices, which may adversely affect the environment as aquatic organisms ingest MPs ([Darabi et al., 2021](#)). As depicted in Figure 12, various factors such as IS, NOM, and other materials can affect MPs. Investigating the affect of water chemistry and other suspended materials in natural habitats on MP behavior is important since the stability of suspensions affects these contaminants' bioavailability, toxicity, and transport

([Alimi et al., 2018](#)). Significant factors include pH ([Li et al., 2016](#); [Lin et al., 2017](#)), IS, and ion type (monovalent, divalent, and trivalent) ([Akaighe et al., 2012](#); [Shen et al., 2015](#)) of the medium, and the presence of natural organic matter (NOM) ([Cai et al., 2018](#); [Chekli et al., 2015](#)) (Figure 12). Understanding the stability or aggregation of suspended MPs in various environments is crucial for creating effective mitigation methods for their adverse consequences. The electrostatic interaction between MPs particles at various pH and IS dominates the stability of suspensions. Moreover, NOM and clay particles such as kaolinite, montmorillonite, and illite, which are abundant in the environment, also have influence on MPs mobility. Montmorillonite had the most significant impact on promoting aggregation of MPs. This is because montmorillonite has a larger surface area, which resulted in particle aggregation, as the surface charge was neutralized. ([C. Wang et al., 2020](#)). According to a study by ([Dong et al., 2019](#)), humic acid can improve the stability of MPs through electrostatic or steric repulsion forces. By adsorbing onto MPs surfaces, kaolinite particles can influence plastic stability behaviors as they have large surface area, high cation exchange capacity and surface charge heterogeneity ([Li et al., 2020](#)). In addition, a coating of surface-reactive functional groups on MP particles plays an important role in the stability of suspensions of MPs ([Dong et al., 2019](#)).

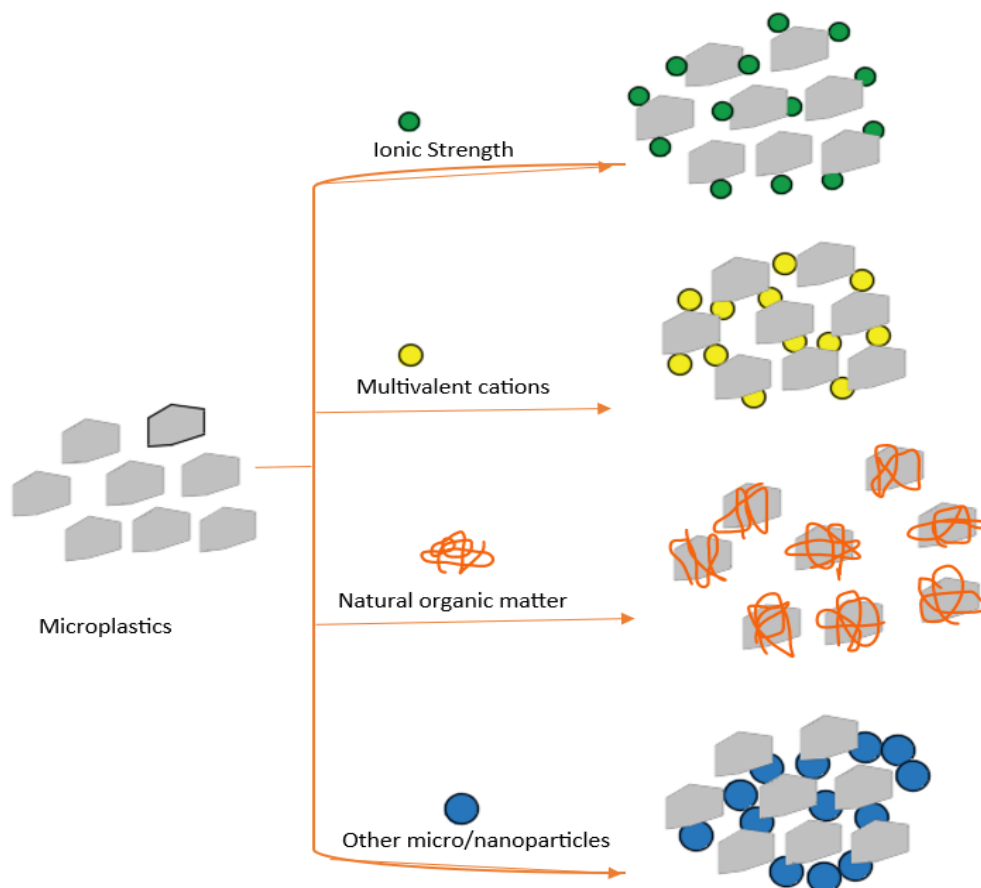


Figure 12. Effect of water chemistry and other suspended materials in natural habitats on MP behavior- modified from ([Dong et al., 2022](#))

2.2.2 Ionic strength and valence

Recent studies have advanced our understanding of how ions and IS affect the stability of MPs and NPs in aqueous solutions ([Singh et al., 2019](#); [Tallec et al., 2019](#)). The concentration and charge of ions in the background solution (or IS) significantly influence the aggregation behavior of MPs in aquatic environments, as it directly impacts the surface charge of MPs ([Alimi et al., 2018](#)). Typically, when IS increases, it reduces the stability of the suspension. According to the

DLVO theory, an increase in IS leads to the compression of the double layer and reduces repulsive forces between the particles, which in turn promotes the aggregation of MPs ([Sharma et al., 2021](#)) ([Li et al., 2021](#)).

For instance, in a study conducted by Wegner et al. (2012), the aggregation behavior of carboxylate-modified polystyrene (PS) particles measuring 30 nm was examined. The results revealed that these particles exhibited rapid aggregation in seawater, with the aggregated particle size increasing to 1000 nm in less than 30 min ([Wegner et al., 2012](#)).

Similarly, in another study investigating 100 nm-sized polystyrene nanoparticles (PSNP) in 0.01 mM FeCl₃ solution, the suspension exhibited stability. However, as the IS was increased from 0.01 mM to 1 mM, the particle size significantly increased from 100 nm to 350 nm in 10 min ([Cai et al., 2018](#)). In a related study conducted on nanoparticles (NP), it was observed that as the IS increased, the ZP values became less negative. Specifically, the ZP values decreased when the IS was increased in a background solution of NaCl. This reduction in ZP can be attributed to the compression of the EDL, resulting in a decrease in the repulsive forces between particles. Consequently, aggregation occurs due to the influence of van der Waals forces, as explained by the DLVO theory ([Birdi, 2016](#)).

The ionic valence of ions plays a pivotal role in shaping the behavior of MPs within aquatic ecosystems ([Wang et al., 2021](#)). Another study highlighted the unique characteristics exhibited by nanoscale plastic particles when exposed to varying salt solutions, encompassing both monovalent NaCl and divalent cations. The impact of divalent cations, specifically Ca²⁺ and Mg²⁺, exerted a more pronounced effect, inducing notable compression of the electrical double layer and fostering aggregation ([Shams et al., 2020](#)). Similarly, it has been observed that polyethylene nanoscale plastics exhibit a higher sensitivity to divalent cations, particularly Ca²⁺ ions, in contrast to

monovalent ([Wu et al., 2019](#)). It is evident that the aggregation of MPs is predominantly influenced by the ionic valency of ions with charges opposing those of the colloids. Furthermore, studies have demonstrated that trivalent cations have a more significant impact on the aggregation and stability of nanoscale plastics within aquatic environments when compared to monovalent and divalent cations ([Wu et al., 2019](#); [Xiao et al., 2018](#)).

Because of their higher charge screening, the divalent electrolytes, such as CaCl_2 and BaCl_2 , have a more pronounced effect on the hydrodynamic diameters of MPs compared to the monovalent electrolytes like NaCl , NaNO_3 ([Li et al., 2018](#)). Divalent cations (Ca^{2+}) aid in the formation of bridges between HA and NPs (see section 2.1.8), thereby reducing stability in the aquatic environment ([Singh et al., 2019](#)).

2.2.3 Natural organic matter

Natural organic matter (NOM) comprises polysaccharides, humic substances (HSs), and proteins and is found in various environmental settings, including soil, groundwater, sediments, surface water, and rivers. HSs are commonly categorized as fulvic acid, humic acid, and humin. Dissolved organic matter (DOM) specifically refers to the portion of organic matter that is dissolved in water. Recent research has revealed a range of effects associated with DOM on the stability and aggregation of MPs and NPs in water environments. However, there is still a need for a comprehensive understanding of the influence of DOM on MPs and NPs ([Sharma et al., 2021](#)). DOM possesses the capacity to attract and adhere to the surfaces of particles, such as MPs, through intricate interactions like hydrophobic and electrostatic forces ([Tallec et al., 2019](#)). The impact of DOM on the aggregation or dispersion of MPs in natural water is influenced by factors such as the valence of ions and the presence of diverse functional groups or charges on the particle surfaces ([Cai et al., 2018](#)). When DOM and MPs or NPs possess opposite net charges on their surfaces, an

increase in DOM concentration can lead to a reduction in the ZP of MPs or NPs, resulting in their heteroaggregation ([Sharma et al., 2021](#)).

HA, which is a component of NOM, demonstrates a negative charge within the pH range of 4.0 to 8.0 ([Zhu et al., 2014](#)). Studies have also shown that HA can alter the aggregation of colloids by stabilizing or dispersing particles through interaction with colloids ([Li et al., 2021](#)). It has been observed that when NOM is present, it can stabilize suspensions of micro and nano plastics ([Shams et al., 2021](#)). This stabilization is primarily due to the NOM's ability to provide steric repulsion. As a result, this leads to a decrease in aggregation, less settling, and increased movement of NPs ([Alimi et al., 2018](#)). Additionally, HA may affect the heteroaggregation of MPs-bentonite by adsorbing onto bentonite, MPs, or MPs-bentonite ([Li et al., 2021](#)).

Another study found that NOM affects the stability of negatively and positively charged nanoparticles through electrostatic attraction, by stabilizing suspensions of negatively charged particles (coated with carboxyl groups) and promoting the aggregation of positively charged particles (coated with amino groups) ([Wu et al., 2019](#)). Divalent cations like Ca^{2+} in the presence of NOM, such as humic acid, fulvic acid, and lysozyme, can lead to an increase in aggregation of pristine-PS-NPs, due to the cation's ability to neutralize surface charges and overcome the steric hindrance caused by NOM adsorption or particles ([Ali et al., 2022](#)).

2.2.4 pH

Numerous investigations have explored the impact of pH on the stability of nanoplastics (NPs) or microparticles (MPs) through the analysis of ZP, HDD, and surface charge ([Sharma et al., 2021](#)). The pH in aquatic environments typically fall within the range of 5 to 9 (often observed) ([Chowdhury et al., 2015](#); [Wang et al., 2016](#)). The surface charge of particles, including MPs, and

the ionization of surface functional groups, is influenced by pH. As a result, the strength of electrostatic repulsion between particles is affected. The aggregation behavior of particles is impacted by pH values both higher and lower than pH_{PZC} due to their effect on surface charge and electrostatic interactions ([Li et al., 2018](#)). In a study, ZP measurements were conducted on amine-modified polystyrene (PS) particles across different pH values. As illustrated in Figure 13, at pH below 7, the ZP was positive, peaking at approximately +50 mV. With increasing pH up to 11, the ZP progressively decreased. At around pH 9.5, the ZP shifted from positive to zero, indicating the occurrence of the point of zero charge (pH_{PZC}) ([Cross et al., 1999](#)): for the amine-modified PS particles, estimated to be approximately 9.9 ± 0.1 . Within the region of the pH_{PZC} , aggregation became evident, resulting in a maximum HDD value of 1260 ± 190 nm. Below pH 9, when the ZP was positive and the particles carried a positive charge on their surface, electrostatic repulsion hindered particle aggregation and NPs exhibit stability, maintaining a consistent HDD of 98 ± 2 nm ([Ramirez et al., 2019](#)).

Increasing the pH in a solution containing monovalent cation Na^+ was found to enhance the stability of suspensions of PSNPs (100 nm diameter) and PSNPs-COOH (303 nm diameter) in certain studies. This increase in stability is attributed to the presence of additional hydroxyl groups that are attracted to the particle surface, rendering particles more negatively charged. As a consequence, electrostatic repulsion is intensified, leading to enhanced stability of the suspension ([Romero-Cano et al., 2001](#)).

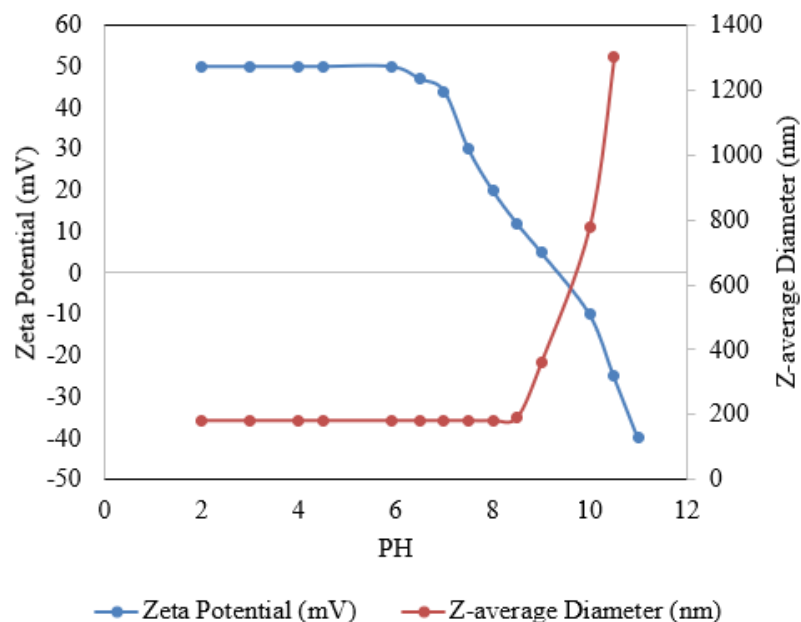


Figure 13. Zeta potential and z-average HDD variation of amidine PS nanoplastic particles (10 mg/L) as a function of pH in ultrapure water- modified from ([Ramirez et al., 2019](#)).

Similarly, variations in pH alter the overall charge distribution in the double layer, altering the ZP, which serves as an indirect measurement of the stability of colloidal suspensions ([Al Harraq et al., 2021](#)). According to a study by ([Li et al., 2019](#)), the range of point of zero charge (pH_{PZC}) for different types of MP, including polystyrene, polypropylene, polyethylene, polyamide, polyethylene, and polyvinylchloride MPs, is 5.59–5.85. The pH_{PZC} value for polystyrene is 5.85. When pH_{PZC} is lower than pH values, the net charge of the MP surface is negative, which provides favorable conditions for interaction with positively charged chemicals, such as certain proteins ([Li et al., 2019](#)). Electrostatic repulsion allows MPs and NPs to prevent aggregation over a broad range of pH ([Sharma et al., 2021](#)).

2.2.5 Clay

Minerals, such as clay minerals, can affect the stability of MP and NPs suspensions. The stability of suspensions is determined by the ZP between particles and clay. When particles have

the same charge, they repel each other due to electrostatic forces, which stabilizes the suspension. A study explored the stability of PSNPs in the presence of clay colloids, specifically bentonite. The study found that bentonite colloids contribute to heteroaggregation with NPs when salts are present. The anisotropic surface charge of clay colloids is responsible for this heteroaggregation mechanism. The faces of bentonite particles carry a negative charge, while the edges can have both negative and positive charges. At low IS, bentonite can stabilize NPs suspensions. However, as the IS increases, heteroaggregation between clay and NPs may occur due to a reduction in electrostatic forces between clay and PSNPs. The presence of monovalent cation Na^+ can also bridge between negatively charged particles and cause aggregation ([Singh et al., 2019](#)).

The charge on the edges of clay particles can change with varying pH and IS conditions. A study on citrate-functionalized Ag and TiO_2 nanoparticles observed increased aggregation in the presence of clay colloids like kaolin and montmorillonite clays (Figure 14) ([Wang et al., 2015](#); [Zhou et al., 2012](#)).

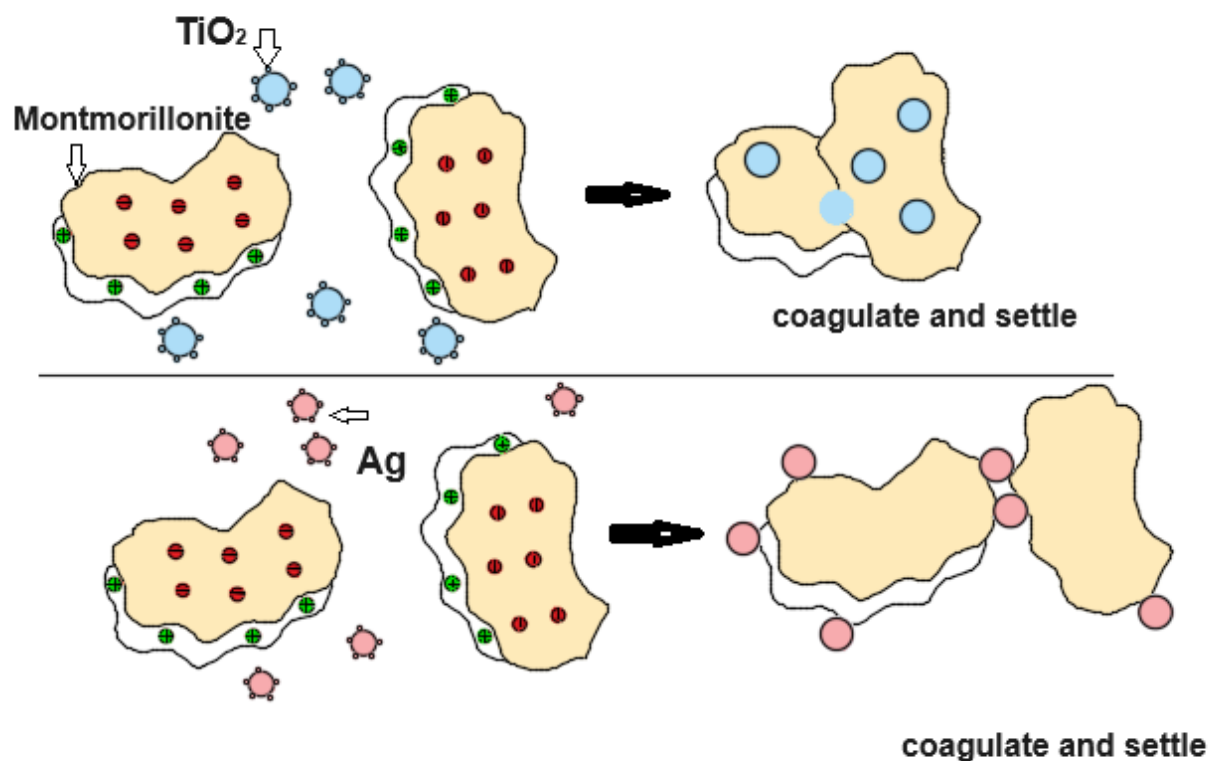


Figure 14. Anisotropic surface charge of clay colloids (Montmorillonite)- modified from ([Zhou et al., 2012](#)).

2.2.6 Functional groups: Effect of cation valence, humic acid, and clay colloids.

The hydrodynamic properties and stability of colloids are greatly impacted by the chemical properties of the surface of the suspended particles ([Dong et al., 2019](#)). For instance, ([Della Torre et al., 2014](#)) found that polystyrene nanoparticles in seawater with different surface charges exhibit different aggregation behaviors: they found that NPs modified with negatively charged carboxyl groups rapidly formed larger aggregates while positively charged particles remained in suspension with smaller aggregates. The overall conclusion is that the hydrochemical properties and surface chemical properties of colloids play a significant role in NPs aggregation. Another study by Tallec

et al. (2019) investigated the effect of the surface charge of NPs by measuring the HDD and ZP of the particles in different mediums such as ultrapure water (UW), artificial seawater (ASW) and filtered seawater (FSW). The result showed that the size of amines-PS (positively charged surfaces) remained stable in all of the media. This stability is believed to be due to a specific coating that leads to repulsion. However, negatively charged particles such as PS-COOH and plain PS aggregated in the sea water media ([Sharma et al., 2021](#)); ([Li et al., 2021](#)).

In summary, the literature review examines the stability and aggregation behavior of MPs and NPs in various environmental contexts, highlighting key factors like IS, NOM, pH, and clay minerals. Studies indicate that IS and ionic valence significantly influence MP aggregation, with divalent cations such as Ca^{2+} and Mg^{2+} promoting particle aggregation by compressing the electrical double layer, as the DLVO theory explains. NOM, particularly HA, stabilizes MPs through steric repulsion and electrostatic interactions, while variations in pH affect the surface charge and electrostatic repulsion of MPs, influencing their stability. Clay minerals, with their anisotropic surface charges, contribute to heteroaggregation, particularly in the presence of salts. Additionally, the chemical properties of MP surfaces, such as the presence of functional groups, play a crucial role in determining their behavior and aggregation in different media. This comprehensive review underscores the complexity of MP and NP interactions in aquatic environments and the need for further research to develop effective mitigation strategies for their environmental impact.

3 Materials and methods

This study investigates the stability and aggregation behavior of polystyrene microplastics (PSMPs) in different environmental conditions, with a focus on how different functional groups and environments influence these processes. By utilizing Dynamic Light Scattering (DLS) and Zeta Potential (ZP) measurements, the hydrodynamic diameter (HDD) and surface charge of the PSMPs are assessed under varying conditions, including the presence of monovalent and divalent cations, kaolinite, and humic acid (HA). The research involves preparing different suspension types, adjusting ionic strength (IS) and pH levels, and measuring the stability and interaction energies using the Derjaguin–Landau–Verwey– Overbeek (DLVO) theory. A detailed workflow and experimental methodology are provided to ensure reproducibility.

3.1 Dynamic light scattering (DLS)

Dynamic light scattering (DLS) (also referred to as photon correlation spectroscopy or quasi-elastic light scattering) and ZP are now commonly used techniques in industry to determine respectively the HDD and surface charge of nanoparticles. These techniques can be easily performed in a laboratory setting. Moreover, these techniques are non-intrusive and do not require extensive sample preparation or calibration before measurements ([Bhattacharjee, 2016](#)). In this study, the HDD values are presented as z-average (Z-avg). The Z-avg is used as a metric of the average size of particles in a given particle collection, established by analyzing the intensity of the light they disperse. This process encompasses fitting the correlation curve of the scattered light to a singular exponential function, presuming a Gaussian distribution of particle sizes. The Z-avg is also known by other terms such as the intensity-weighted mean hydrodynamic size or the cumulant mean. The HDD and ZP are measured with a Zetasizer (Figure 15Figure 16). A syringe was used

to inject the suspension into a Folded capillary cell (as shown in Figure 16) for measuring ZP, and a cuvette was used for measuring HDD.



Figure 15. Zeta sizer, a device for analyzing particle suspensions by measuring light scattering, particle size, and zeta potential (ZP).

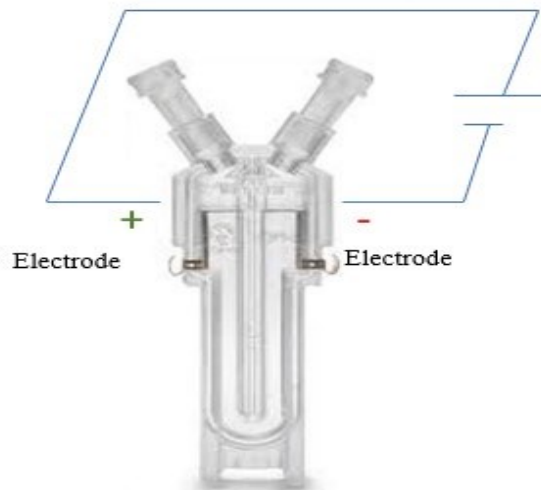


Figure 16. Folded capillary cell used in the zeta sizer for measuring zeta potential (ZP).

The polydispersity index (PDI) is a measure of the heterogeneity of a sample based on size. It describes the width or spread of particle sizes and may fluctuate between 0 and 1. If the PDI value falls below 0.1, it suggests that the particles are monodisperse, whereas values above 0.1 might indicate polydisperse particle size distributions. Polydispersity can arise from the diversity in size within a sample or from the clumping or clustering of the sample during separation or examination ([Raval et al., 2019](#)).

3.2 Preparation of materials

As illustrated in Figure 17, in the initial phase of this research, I experimentally studied how varying conditions such as the presence of monovalent and divalent cations (Na^+ and Mg^{2+}), kaolinite colloids, and humic acid, singly and in combination, affect the stability of PS-Plain suspensions. This investigation examined these suspensions under different background solutions and pH values and used ZP and HDD measurements to assess the stability and particle charges.

In the subsequent phase, the research expanded to study suspensions of PS with distinct functional groups - amine-modified and carboxylate-modified polystyrene. This analysis enhanced our understanding of the role of functional groups in the stability and aggregation of MPs in media with diverse water chemistry.

Four different types of suspensions (PSMPs, PSMPs + Kaolinite, PSMPs + Humic Acid (HA), and PSMPs +HA+ Kaolinite) were prepared. The stability of these suspensions was evaluated in four different background solutions (by concentration: 3 mM NaCl, 15 mM NaCl, 1 mM MgCl_2 , and 5 mM MgCl_2) at different pH values (5 and 9), as shown in Figure 17 and Table

3. Note that the ionic strength (IS) of 3 mM NaCl and 1 mM MgCl₂ is the same (3 mM), and the IS of 15 mM NaCl and 5 mM MgCl₂ is the same (15 mM).

Table 3. Polystyrene (PS), kaolinite, and humic acid (HA) concentrations in the suspensions for the stability tests

Suspension types	Components	PS concentration (mg/L)	kaolinite concentration (mg/L)	HA concentration (mg HA/L)
1	Polystyrene	50	–	–
2	Polystyrene +Kaolinite	50	10	–
3	Polystyrene +HA	50	–	3
4	Polystyrene +Kaolinite + HA	50	10	3
5	Carboxylate-modified polystyrene	50	–	–
6	Carboxylate-modified polystyrene +Kaolinite	50	10	–
7	Carboxylate-modified polystyrene +HA	50	–	3
8	Carboxylate-modified polystyrene +Kaolinite + HA	50	10	3
9	Amine-modified polystyrene	50	–	–
10	Amine-modified polystyrene +Kaolinite	50	10	–
11	Amine-modified polystyrene +HA	50	–	3
12	Amine-modified polystyrene +Kaolinite + HA	50	10	3

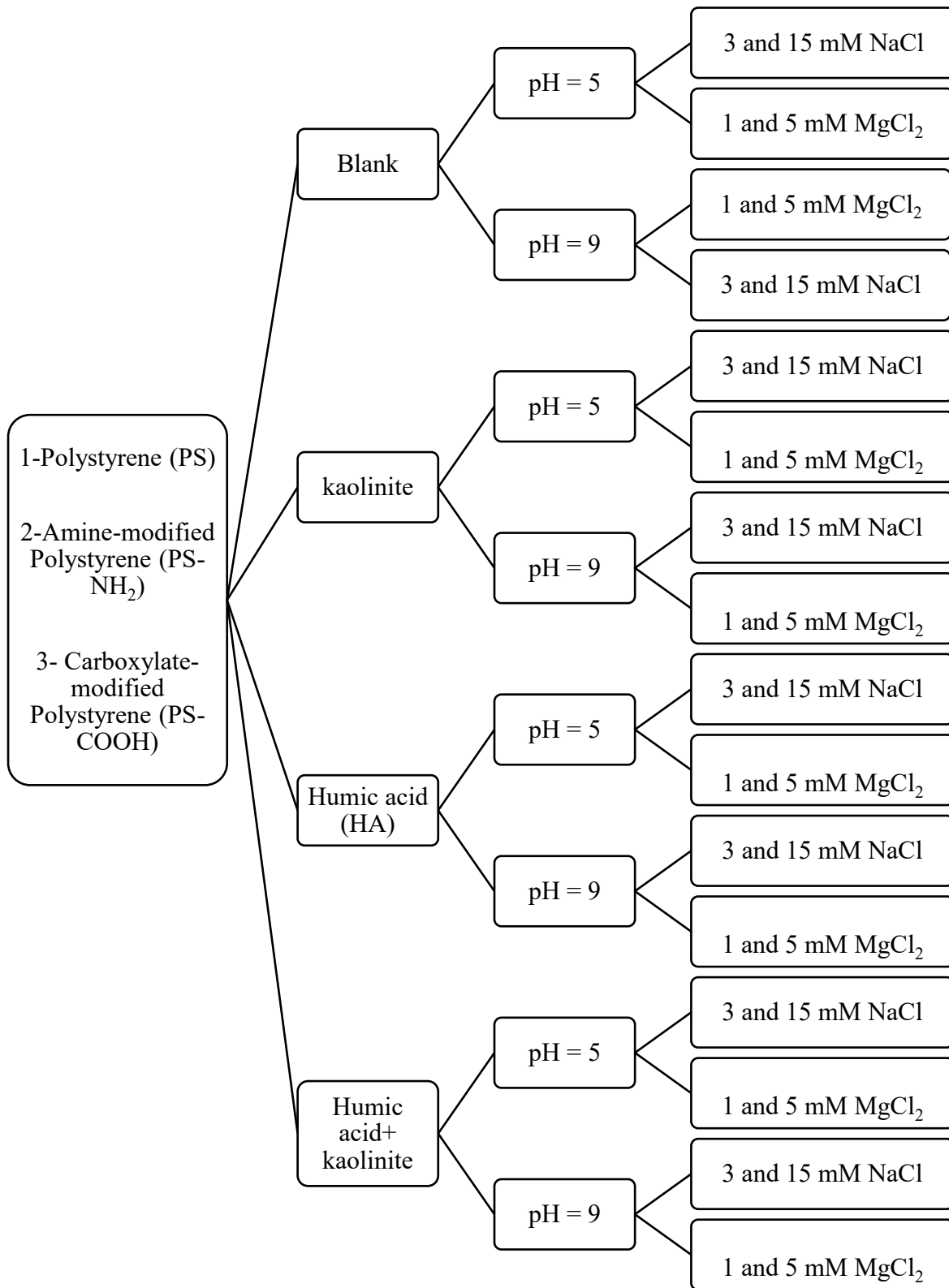


Figure 17. Experimental conditions for 96 different types of suspensions of polystyrene microplastics (PSMPs) studied in this research.

Three varieties of PSMPs (PS, PS-COOH, and PS-NH₂) were employed. The PS and PS-COOH suspensions, where the MPs possess negative charges, were procured from Sigma-Aldrich (Canada) at concentrations of 10% and 2.5% w/v, respectively. The suspension of positively charged particles PS-NH₂ (2.5% w/v) was also obtained from Sigma-Aldrich (Canada). The reported nominal size of PS in the vendor's documentation is 1 µm, determined by transmission electron microscopy (TEM). Similarly, the sizes of PS-COOH and PS-NH₂ were documented as 1 µm. Specifics are provided in the Appendix.

3.2.1 Preparation of humic acid (HA)

To represent dissolved organic matter (DOM), HA (with a fulvic acid content exceeding 90%) was acquired from VWR (Canada). The HA stock solution was prepared by dissolving 100 mg of HA powder (Alfa Aesar) in 100 mL of deionized water, resulting in a concentration of 1000 mg/L. The solution was thoroughly mixed and shaken, using a VWR shaker (Figure 18) and then stored in a dark refrigerator at a temperature of 4 °C until needed.



Figure 18. Humic acid stock suspension on magnetic stirrer.

3.2.2 Preparation of kaolinite clay particle suspension

For preparation of the kaolinite clay particle suspension, 4 g of kaolinite powder (obtained from The Clay Mineral Society ("https://www.clays.org/sourceclays_source_and_special/,")) were mixed with 1000 mL of deionized water. This was done to disperse the kaolinite particles in the water. The mixture of kaolinite powder and water was subjected to sonication using an ultrasonic Sonifier VWR for a duration of 60 min. Sonication helped in achieving proper dispersion of the kaolinite particles throughout the water, breaking up any agglomerations or clumps of particles. After sonication, the mixture was allowed to stand undisturbed for 24 h in a dark refrigerator at 4 °C ([Wu et al., 2019](#)). This standing time allowed larger kaolinite particles to settle down due to gravity, separating larger particles from the suspension.

Once the settling process was complete, the supernatant liquid (the homogeneous whitish liquid above the settled particles) was carefully transferred into a high-density polyethylene (HDPE) bottle for storage. The supernatant liquid contained the dispersed kaolinite particles, creating the kaolinite colloid stock solution. This kaolinite colloid stock solution was utilized in subsequent experiments for the preparation of particle suspensions.

To determine the concentration of kaolinite in the stock suspension, a 100 mL sample of the stock suspension was filtered through a 0.1 µm polyethersulfone membrane filter, which captured the kaolinite particles while allowing the liquid to pass through. The filter containing the captured kaolinite particles was then dried in an oven at 60 °C until all the liquid evaporated, leaving only the dry filter with the kaolinite particles. The weight difference between the dried filter and the initial filter (before filtration) was measured. The weight difference obtained was divided by the volume of the filtered sample (100 mL) to calculate the concentration of kaolinite

in the stock suspension. This process was repeated three times to obtain an average result. The mean value of the concentration obtained from the three measurements was considered as the kaolinite concentration of the stock suspension. The mean concentration value obtained from the data was 477 mg/L, with a corresponding standard deviation of 6 (Table 4).

Table 4. Kaolinite concentration of the stock suspension

Number	Weight difference between the dry filter and the initial filter (g)	Kaolinite concentration (mg/L)
1	0.048	480
2	0.048	480
3	0.047	470

3.2.3 Preparation of suspensions

To prepare these suspensions, the appropriate quantity of MPs was mixed with stock suspensions of HA and kaolinite. The term "stock suspensions" referred to pre-prepared suspensions of HA and kaolinite in a liquid medium (see above).

The different suspensions that were prepared are designated as follows:

- PSMPs: This referred to a suspension containing only MPs.
- PSMPs + Kaolinite: This suspension included MPs mixed with the kaolinite suspension.
- PSMPs + HA: This suspension consisted of MPs mixed with the HA suspension.
- PSMPs + HA + Kaolinite: This suspension was prepared by first thoroughly mixing the MPs and HA, and then adding the kaolinite suspension.

The order in which the components were mixed was kept consistent in the PSMPs + HA + kaolinite suspensions. First, the MPs and HA were mixed together, ensuring they were thoroughly combined. Afterward, the kaolinite suspension was added to this mixture.

The ionic strength (IS) of the solutions was adjusted by measuring and adding a specific amount of NaCl or MgCl₂ powder to the suspensions using an analytical balance. The suspensions were then sonicated by using an ultrasonic cleaner (Figure 19) for 30 min to mix and disperse the particles.



Figure 19. Suspensions are sonicated by using an ultrasonic cleaner.

The pH of the suspensions was then modified by adding small amounts of 0.1 M NaOH and/or HCl solutions. The 'small amounts' (approximately 0.005 mL) added were not enough to change the IS of the solutions. The salt solution was shaken by a Vortex Mixer (Figure 20). Suspensions were kept in 200 mL volumetric flask and sonicated with an ultrasonic cleaner (Figure 20).



Figure 20. Vortex mixer: a laboratory instrument used to mix liquid samples through rapid rotational movement.

A UV-Vis spectrophotometer (Genesys 10S UV-Vis, Thermo Scientific) was used to measure the absorbance of the suspensions (Figure 21). Also, ZP and size distribution of the MPs were measured with a zeta sizer (Malvern Instruments). These were done in triplicate at room temperature (25 °C).



Figure 21. UV-Vis spectrophotometer

3.2.4 Preparation of colloidal suspension for batch experiments

Stock suspensions were prepared in advance to facilitate the preparation of the experimental suspensions (as mentioned in section 3.2 Preparation of materials). The concentrations of the stock suspensions were as follows:

- Humic Acid (HA): 1000 mg/L
- Kaolinite: 477 mg/L
- Magnesium Chloride ($MgCl_2$): 1000 mg/L
- Sodium Chloride (NaCl): 1000 mg/L
- Polystyrene (PS): 100,000 mg/L

These concentrations served as the basis for creating specific suspension mixtures required for the batch experiments.

To prepare a specific suspension, the dilution principle $C_1V_1=C_2V_2$ was applied, where C_1 and C_2 represent the stock and final concentrations, respectively, while V_1 and V_2 correspond to the volumes of the stock solution and the final suspension. For instance, to achieve a final concentration of 50 mg/L of polystyrene in a 200 mL suspension, the following calculations were employed:

For polystyrene (PS):

$$50 \text{ mg/L} \times 200 \text{ mL} = 100,000 \text{ mg/L} \times V_1$$

$$V_1 = (50 \text{ mg/L} \times 200 \text{ mL}) / (100,000 \text{ mg/L}) = 0.1 \text{ mL}$$

Suspension Mixture Preparation

Following the calculated volumes for each component, the suspension was prepared by combining 0.1 mL of polystyrene stock and the necessary volume of NaCl or MgCl₂ stock solution, with the balance of the volume made up with deionized water to total 200 mL. Each component was added sequentially to the volumetric flask, with deionized water used to achieve the final volume, ensuring complete mixing and homogeneity of the suspension. After suspensions were carefully prepared in a 200 mL volumetric flask, the suspensions were then sonicated by using an ultrasonic cleaner for 30 min to mix and disperse the particles (Figure 17). The pH of the suspensions was adjusted to 5 or 9.

Stability Test

After pH adjustment, the suspension in the 200 mL volumetric flask was divided into 7 mL portions and each portion was transferred to a 15 mL centrifuge tube, with each tube intended for a single measurement point. The tubes were hand shaken and then let stand at room temperature. At time 0 (i.e., the time immediately after hand shaking) and after every 30 min, 3 mL suspension sample was extracted using a pipette from the middle depth of the water column in the tube, which was then transferred into a cuvette for measurement of light absorbance as shown in Figure 12. A stability test was completed after 360 min when the sample was taken. All stability tests were done in duplicate.

Zeta Potential and Hydrodynamic Diameter Measurements

For the assessment of ZP and HDD, initially, 10 mL tubes were utilized. At the end of 6-hour duration, the suspension samples were transported to the Zetasizer instrument stationed in the Core

Science building. The ZP was determined by injecting the suspension into a Folded capillary cell, as delineated in Figure 13. The HDD measurements were conducted using a standard cuvette.

3.3 DLVO calculation

The classical DLVO theory was utilized to assess the interaction energy and aggregation behavior of particles in various environments. The sum of van der Waals (Φ_{LW}) attraction and the electrical double layer (EDL) repulsion (Φ_{ED}) forces indicates, for two equal-sized spheres, whether the particle interaction is attractive or repulsive using equations (4) and (5). These formulae are based on the sphere-sphere geometry assumption ([Kontogeorgis et al., 2016](#)).

$$\Phi_{\text{total}} = \Phi_{LW} + \Phi_{ED} \quad (5)$$

$$\Phi_{LW} = -\frac{A_{132}R}{12D} \left[1 - \frac{5.32D}{\lambda} \ln \left(1 + \frac{\lambda}{5.32D} \right) \right] \quad (6)$$

$$\Phi_{ED} = -\frac{2\pi R n_{\infty} k_B T}{\kappa^2} \psi^2 \left[\ln \left(\frac{1+e^{-\kappa D}}{1-e^{-\kappa D}} \right) + \ln(1 - e^{-2\kappa D}) \right] \quad (7)$$

where A_{132} (J) is the Hamaker constant between two media, labeled as 1 and 2, across a third medium, which in this case is water.

$$A_{132} = \left(\sqrt{A_{11}} - \sqrt{A_{33}} \right) \left(\sqrt{A_{22}} - \sqrt{A_{33}} \right) \quad (8)$$

D (m) is the separation distance between the surface of two particles, R (m) is the MPs radius, n_{∞} is the number concentration of bulk ions, ψ is the reduced ZP, and κ (m^{-1}) is the inverse of the Debye length; ([Cai et al., 2018](#); [Dong et al., 2018](#)) (Table 5).

The reduced ZP is given by.

$$\psi = \frac{Z q_e ZP}{k_B T} \quad (9)$$

where Z is the valency of the ions in solution and q_e is the charge on an electron.

κ is the inverse Debye length (m^{-1}) and can be calculated as ([Tan et al., 2021](#)):

$$\kappa = \sqrt{\frac{2 \cdot 1000 \cdot N_A \cdot q_e^2 \cdot IS}{\epsilon_r \cdot \epsilon_0 \cdot k_B \cdot T}} \quad (10)$$

where ϵ_r is the relative permittivity of the water, and ϵ_0 is the permittivity of a vacuum.

$\kappa^{-1} = \frac{0.304}{\sqrt{C}}$ for monovalent cations like NaCl. $\kappa^{-1} = \frac{0.176}{\sqrt{C}}$ for divalent cations like $MgCl_2$

([Kontogeorgis et al., 2016](#)).

The ionic strength, IS (M) = $1/2 \sum_i C_i Z_i^2$ where C_i and Z_i are the molar concentration and valence of the ions.

The Hamaker constant for the interaction between particles 1, which represents polystyrene (PS), and 2, which represents kaolinite, across the medium 3, which is water, are given in Table 6 and Table 7.

Table 5. Key parameters used in DLVO calculations ([Xinjie Wang et al., 2020](#))

Parameter	Description
μ	Radius of polystyrene (m)
λ_c	Characteristic wavelength of interaction (nm) often assumed to be 100 nm.
A_{132}	Hamaker constant for interacting subject 1 and subject 2 in the medium 3
Ψ	Reduced ZP of PS under different conditions (mV) (equation (9))
D	Separation distance between interacting particles (nm)
κ	Inverse Debye length (m^{-1})
N_A	Avogadro's number ($6.02 \times 10^{23} \text{ mol}^{-1}$)
C_i	Molar concentration of ions ($\text{mol} \cdot \text{L}^{-1}$)
ϵ_0	Dielectric permittivity of vacuum ($8.854 \times 10^{-12} \text{ C} \cdot \text{V}^{-1} \cdot \text{m}^{-1}$)
ϵ_r	Relative permittivity of water (78.5 dimensionless)
Z_i	Valence of the i th ion
k_B	Boltzmann's constant ($(1.38 \times 10^{-23} \text{ J} \cdot \text{K}^{-1})$)
T	Absolute temperature (K)
z	Charge number for the electrolyte. For example, for NaCl, the charge number is 1

Table 6. Hamaker constants

Sample	Hamaker constant, (J)	References
PS	6.5×10^{-20}	(Bizmark et al., 2020)
PS-NH ₂	6.5×10^{-20}	(Bizmark et al., 2020)
PS-COOH	8.7×10^{-20}	(Filby, 2010)
Kaolinite-Kaolinite	1.5×10^{-19}	(Novich et al., 1984)
H ₂ O-H ₂ O	3.7×10^{-20}	(Israelachvili, 2011b)

Thus, the Hamaker constant (A) for PS-plain and PS-NH₂ are assumed to be the same, an approach similar to ([Bizmark et al., 2020](#)).

Table 7. The Hamaker constant (A) for the interaction between particles 1, which represents polystyrene (PS), and 2, which represents kaolinite or PS, across the medium 3, which is water.

Interacting media (1-3-2) 3 is the medium	A ($\times 10^{-20}$ J) particle 1	A ($\times 10^{-20}$ J) medium 3	A ($\times 10^{-20}$ J) particle 2	A ₁₂₃ ($\times 10^{-20}$ J)
PS–water–PS	6.5	3.7	6.5	0.4
PS–water– kaolinite	6.5	3.7	15	1.22
PS-NH ₂ - water- PS-NH ₂	6.5	3.7	6.5	0.4
PS-NH ₂ - water- kaolinite	6.5	3.7	15	1.22
PS-COOH - water- PS-COOH	8.7	3.7	8.7	1.05
PS-COOH - water- kaolinite	8.7	3.7	15	2

4 Results and discussion

4.1 Measuring light absorbance of the microplastic suspensions: wavelength selection

A UV-Vis spectrophotometer was employed to determine the suitable wavelength for measuring light absorption in suspensions containing microplastics (MPs). The provided Figure 22 displays the UV-Vis spectra of the MPs suspension (50 mg/L), kaolinite colloid suspension (10 mg/L), and 3 mg/L HA. Notably, the absorbance of the MPs suspension surpasses that of the kaolinite and humic acid (HA) within the wavelength range of 200 to 900 nm. Additionally, at longer wavelengths, the absorbance of kaolinite and HA diminishes significantly, approaching zero, whereas the absorbance of the MPs suspension remains considerable and can be detected using UV-Vis spectroscopy. Based on these observations, a wavelength of 600 nm was chosen to measure the absorbance (and hence the concentration) of the MPs suspensions, effectively minimizing the impact of kaolinite colloids and/or HA.

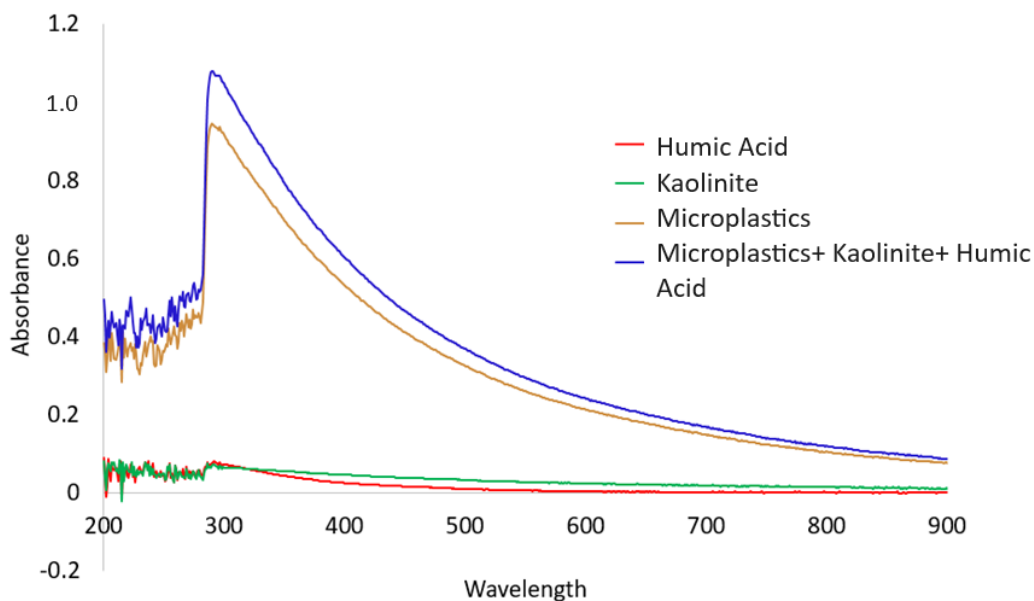


Figure 22. UV-Vis spectra of microplastics (MPs) (50 mg/L), kaolinite (10 mg/L), and humic acid (HA) (3 mg/L) in deionized water.

4.2 Particle size analysis

In order to measure the particle size, dynamic light scattering (DLS) was employed. The z-average (Z-avg) provided information on the cumulant size of the particles, while the polydispersity index (PDI) indicated the level of particle dispersion within the medium. A lower PDI value indicated a more uniform sample. In particular, a value less than 0.1 implies particles have a uniform size. Figure 23 presented the size distribution and intensity profiles of the particles.

	Size (d.nm):	% Intensity:	St Dev (d.nm):
Z-Average (d.nm): 1023	Peak 1: 1130	100.0	139.3
Pdl: 0.046	Peak 2: 0.000	0.0	0.000
Intercept: 0.923	Peak 3: 0.000	0.0	0.000

Result quality : Refer to quality report

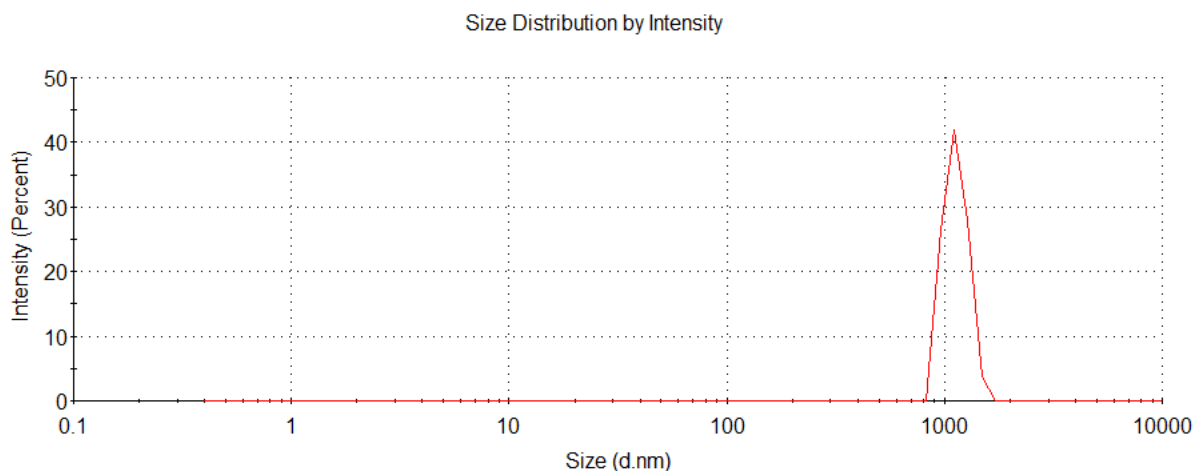


Figure 23. Size distributions of microplastic particles polystyrene in pH 5 in deionized water.

4.3 Concentration of particles

The wavelength of 600 nm was chosen as the measurement parameter for determining the concentrations of various plastic particles in the samples and establishing a relationship between their concentrations and absorbance values. Figure 24 demonstrates a linear correlation between concentration values, encompassing a range of 0 to 50 mg/L for MPs. A linear equation was employed, with respective R values of 0.9995 and 0.9999, to correlate the readings with the concentrations of polystyrene (50 mg/L) and the mixture of polystyrene (50 mg/L), kaolinite (10 mg/L), and HA (3 mg/L) in deionized water. It shows that the absorbance values for these substances fall within the range of 0 to 1, representing the optimal accuracy range of the measurement instrument.

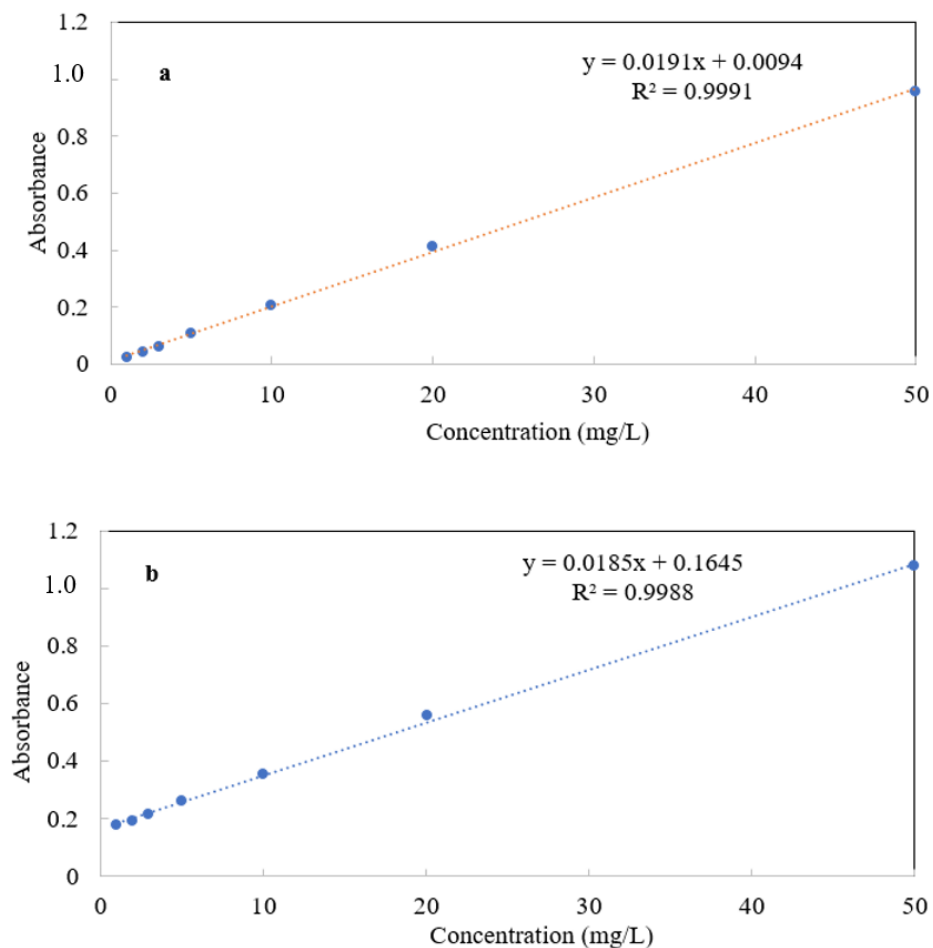


Figure 24. Polystyrene concentration vs absorbance a) polystyrene (50 mg/L) b) mixture of polystyrene (50 mg/L), kaolinite (10 mg/L), and HA (3 mg/L) at wavelength 600 nm.

4.4 Stability of plain polystyrene microplastic suspensions

This section is devoted to examining the stability of suspensions consisting of unmodified PSMPs, having a dimensional measure of 1.1 micrometers, in an aqueous environment. I elucidate my results through a series of experiments that examined the varying factors influencing stability. The focus lies on observing the changes in relative absorbance, hydrodynamic radius, ZP, and the

DLVO theoretical outputs, under differing experimental conditions. Findings are summarized in Tables 8 and 9 and in Figures 25 to 28, where the different panels refer to different experimental conditions: the two values of pH, 5 and 9, are indicated by blue and red symbols respectively.

Figure 25 shows the relative absorbance (A/A_0) of the PSMPs particle suspension as a function of time. A decreasing value with time indicates aggregation of the particles, i.e., instability of the suspension. Figure 26 shows the ZP of particles, measured at the end of each experiment (360 min). The PSMPs are negatively charged, so larger negative values suggest suspensions should be more stable. Figure 27 shows the HDD of particles, again measured at the end of each experiment. Values greater than 1000 nm (1 μm) indicate aggregation of particles. Figure 28, Tables 8 and 9 show the results of DLVO calculations. Here, higher positive values of the maximum interaction energy suggest greater stability. Ideally, these four indications of stability would agree with each other. However, practical experiments can result in variations and discrepancies among these indicators due to complex factors such as particle surface chemistry and additives.

4.4.1 Effect of ionic strength and salt types

The top row of Figure 25 – panels a to d – shows the relative absorbance (A/A_0) of the PSMPs particle suspension as a function of time for the two salts (NaCl and MgCl_2) at two different IS and for the two pH (5 and 9). According to these panels, all the suspensions exhibit instability at early time. At pH 5, there was a slow decrease in the A/A_0 ratio over 6 h. For pH 9, the A/A_0 ratio decreased sharply over the first 20 to 60 min and then was relatively flat with no consistent trend. The change was least for NaCl at low IS.

The ZP values, listed in Tables 8 and 9 and depicted in Figure 26 (a) and (e), add to these observations. The ZP values are negative at -10 to -20 mV, except those for the NaCl solutions at IS=3 mM, which were more negative (-26 to -34 mV). These higher negative values signify a larger electrostatic repulsion and increased stability, in general agreement with the A/A_0 results for pH 9. As pH increased, ZP became slightly more negative.

Hydrodynamic sizes, represented in Figure 27 (a) and (e), the assessment of PSMPs' aggregation behavior under varying ionic conditions revealed patterns consistent with those for ZP measurements. For NaCl solutions, at IS of 3 mM the HDD was close to 1000 nm (the actual size of the particles, according to the manufacturer's specifications is 1000nm. Appendix 1), indicating the suspension was stable. A moderate increase in HDD was observed as the IS increased, suggesting enhanced aggregation, consistent with the decrease in the negative ZP (Figure 26 (a)). For MgCl₂ solutions, the HDD was about one and a half to two times the particle size, indicating aggregation and consistent with the small negative ZP values. The slight decrease in HDD with pH increase was consistent with the slight decrease of ZP (i.e., more negative ZP) with increasing pH.

Figure 28 (top row) portrays the calculated energy barrier values from DLVO theory, providing insight into the barrier that PSMPs show against aggregation (see also Table 8 and 9). Higher energy barrier values indicate greater stability. For NaCl solutions, the energy barriers were significantly lower in solutions with higher IS, suggesting reduced resistance to aggregation. This is consistent with the observed increase in HDD and decrease in ZP values. The range of energy barrier values was observed to be lower for MgCl₂ (from 16 to 87 K_BT) in comparison to NaCl (up to 370 K_BT).

In low IS NaCl solutions (3 mM NaCl), PS suspensions were moderately stable. The HDD of the particles remained low. This can be attributed to their high ZP values, providing electrostatic forces that prevent aggregation ([Badawy et al., 2010](#); [Lin et al., 2010](#)). At higher IS (15 mM NaCl), the plain PSMPs suspensions became more unstable, with the (A/A_0) ratio decreasing from 1 to almost 0.8 over 6 h and a modest increase in the HDD. This is consistent with previous studies that have reported aggregation of plain PS in seawater under high IS conditions. The rise in salt concentrations led to a notable decrease in the ZP. ([Tallec et al., 2019](#)).

In the field of microplastic research, aggregation of MPs is a commonly observed behavior, typically attributed to the interaction between the negative surface charge of the MPs and cations present in the surrounding solution, such as Na^+ and Mg^{2+} . As a result of this interaction, the ZP values of PS become less negative with increasing IS of the solution. This decrease in ZP is consistent with the DLVO theory, which predicts a decrease in repulsive electrostatic interactions in the presence of salts ([Alimi et al., 2018](#)). This increase in electrolyte concentration results in the compression of the electric double layer (EDL), leading to a decrease in repulsive forces between particles and thus, an increased likelihood of aggregation and instability.

The addition of divalent cations, such as Mg^{2+} , to the solution resulted in increased instability of the PSMPs. At the lower IS (3 mM), after addition of Mg^{2+} , the ZP of PSMPs were found to be relatively less negative compared to the values obtained after addition of Na^+ , and the HDDs were larger, indicating the more efficient compression of EDL by divalent ions than monovalent ions ([Wu et al., 2019](#)). At the higher IS (15 mM), larger HDDs were observed for the Mg^{2+} solutions, although the ZPs were not reduced. This is because divalent cations can act as bridges between the negatively charged PSMPs particles, facilitating their aggregation and ultimately leading to their destabilization ([Wu et al., 2020](#)).

4.4.2 Effect of kaolinite

The way that the addition of kaolinite to PSMPs suspensions affects A/A_0 , is shown in Figure 25, panels e to h. In NaCl solutions (panels e and f), PSMPs' stability was notably affected by IS and pH. In low IS and pH 5, the A/A_0 ratio decreased over time, indicating instability. The effect was more pronounced in higher IS. At pH 9, the suspension was relatively stable at low IS, while A/A_0 decreased significantly over time at higher IS. These results underline the role of salt concentration in destabilization.

In $MgCl_2$ solutions (Figure 25, panels g and h) the suspensions with kaolinite appear slightly more unstable at lower pH, the opposite to the suspensions of plain polystyrene. Higher IS is associated with increased instability, as it is for NaCl solutions, though the effect is not as pronounced.

ZP measurements (Figure 26, second column) demonstrated scattered results that do not correspond well with the trends in A/A_0 (Figure 25, second row). Overall, however, the ZP values decreased compared with those for plain PS (Figure 26, first column), suggesting that introduction of kaolinite promotes instability due to the presence of surface chemical heterogeneity (Figure 26).

In Figure 27 (second column), HDD results revealed that for NaCl solutions (panel b), as IS increased, HDD values also increased significantly at both pH 5 and 9. The values are consistent with the patterns shown in A/A_0 (Figure 25, panels e and f), indicating that IS plays a significant role in promoting particle aggregation. Also consistent with the A/A_0 results, the effect of IS in $MgCl_2$ solutions was much less pronounced than it was for NaCl solutions, though increased IS also tended to slightly increase aggregation.

Lastly, regarding Figure 28, Table 8 and Table 9, the energy barrier data highlighted that the addition of kaolinite impacted the interaction energy between particles. The absence of energy barriers in 15 mM NaCl solutions suggests favorable conditions for particle aggregation. In MgCl₂ solutions, the energy barrier values were notably lower compared to NaCl, indicating differences in the stability mechanisms between NaCl and MgCl₂ solutions.

Energy barrier analysis displayed altered interaction energies due to kaolinite introduction. Notably, higher energy barriers were observed at pH 5 with kaolinite in NaCl solutions. However, the absence of energy barriers in 15 mM NaCl suggests favorable conditions for aggregation. Furthermore, the presence of kaolinite seemed to enhance these effects, resulting in the reduction or absence of energy barriers.

Kaolinite and PSMPs are both negatively charged. However, an increase in NaCl or MgCl₂ concentration (IS) resulted in reduced electrostatic repulsion between kaolinite colloid and PSMPs, leading to unstable or heteroaggregation. Moreover, Mg²⁺ ions may act as a bridge between two negatively charged particles (electrostatic attraction between the positively charged ion and the negatively charged surface of the particle) to facilitate aggregation ([Sharma et al., 2021](#)). The reduced repulsive forces between the particles due to the compression of the EDL and the presence of kaolinite colloids caused by the increase in electrolyte concentration could explain the higher instability and increased aggregation of the MPs. The less negative values of ZP of MPs with kaolinite in MgCl₂ solutions compared to NaCl solutions can be attributed to the higher adsorption and screening ability of Mg²⁺ ions as compared to Na⁺ ions ([Chowdhury et al., 2014](#)).

4.4.3 Effect of humic acid

In this section, the effect of adding HA on MP stability is examined within various suspensions. Based on the results, it is evident that the addition of HA promotes the stability of suspensions, as seen in Figure 25. A/A_0 in panels i to l all show increased stability compared with panels for plain polystyrene in panels a to d. The inclusion of HA induced a negative charge in PSMPs, leading to an increased negative value in their ZP (Figure 26, third column), except for $MgCl_2$ solutions at high IS (Figure 26 g vs. e). The ZP values of the MPs were most negative at low IS, becoming less negative (therefore less stabilizing) with increasing concentration in both NaCl and $MgCl_2$ solutions, particularly for $MgCl_2$ solutions. Unlike for the case of kaolinite addition, the values of ZP for solutions with HA are consistent with the behaviour of A/A_0 , as can be seen by comparing the third column in Figure 24 with the third row in Figure 23.

The HDD values (Figure 27, third column) of the MPs were mostly smaller when HA was introduced, compared with plain polystyrene, highlighting the role of HA in potentially stabilizing the particles. The only exception was for pH 9 $MgCl_2$ solutions at high IS, where the HDD was similar to that for plain polystyrene. The HDD values are consistent with the values of A/A_0 and ZP in Figure 25 and 26.

Regarding the energy barrier values (Figure 28, Table 8 and Table 9), the data suggested that the introduction of HA altered the interaction energies between the particles. The curves show that the presence of HA usually significantly increased the energy barriers, which plays a significant role in the stability of the suspensions. The exception again was for $MgCl_2$ solutions at high IS, where the energy barriers were similar for pH 5 and lower for pH 9. The energy barrier range in NaCl solutions is from 458 to 1148 $K_B T$, the highest observed in the study.

It is known that natural organic matter enhance steric surface repulsive forces and stabilizes nanoparticles, however, the presence of cations can lead to aggregation due to mechanisms such as bridging, reducing electrical repulsion, and compression ([Wang et al., 2021](#)). Interestingly, the suspensions were found to be most stable in 3 mM NaCl, and most unstable in 5 mM MgCl₂. This outcome is consistent with a previous study that reported HA caused a decline in aggregation of suspensions through steric repulsion in the presence of monovalent ions (Na⁺) and aggregation via cation bridging facilitated by NOM in the presence of divalent ions (Ca²⁺) ([Wang et al., 2021](#)).

4.4.1 Effect of humic acid and kaolinite

The combined presence of HA and kaolinite had a stabilizing effect on PSMPs at low IS at the two pH levels, very similar to the presence of HA alone. However, at higher IS, the ratio of absorbance (A/A_0) exhibited a consistent downward trend over 6 h, indicating reduced stability with higher concentrations (Figure 25, panels m to p). The ZP values were similar to those obtained for the addition of HA alone (Figure 26, third and fourth columns). They were consistently negative across conditions, with less variation for NaCl solutions than for MgCl₂ solutions (Figure 26, panels d vs h).

The addition of HA and kaolinite induced aggregation at higher IS. Under lower IS conditions at both pH 5 and 9, the HDD values remained small (Figure 27, fourth column), while the energy barrier was high (Figure 28, fourth row), indicating high repulsive forces and resulting in stable suspensions. As IS increased, HDD values increased (Figure 27). The largest change was for NaCl solutions at pH 9 and high IS, consistent with A/A_0 results. Higher MgCl₂ concentrations resulted in absence of energy barriers, underscoring the influence of MgCl₂ concentration on particle aggregation (Figure 26, Table 8 and Table 9).

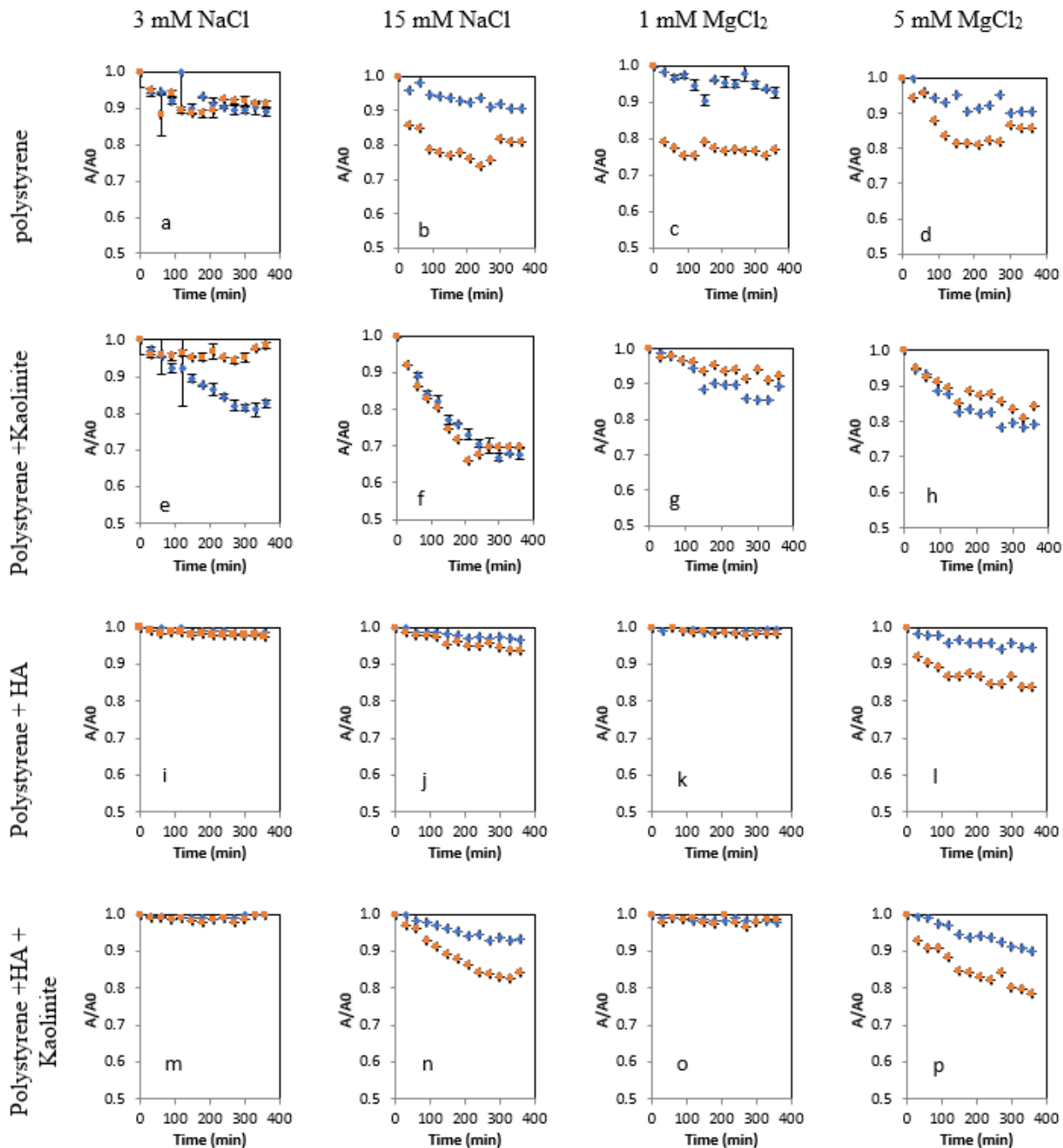


Figure 25. Stability of the polystyrene suspensions at pH 5 (blue) and 9 (red) in 3 mM NaCl, 15 mM NaCl, 1 mM MgCl₂, and 5 mM MgCl₂ solutions. Data are expressed as mean \pm standard deviation of duplicate experiment.

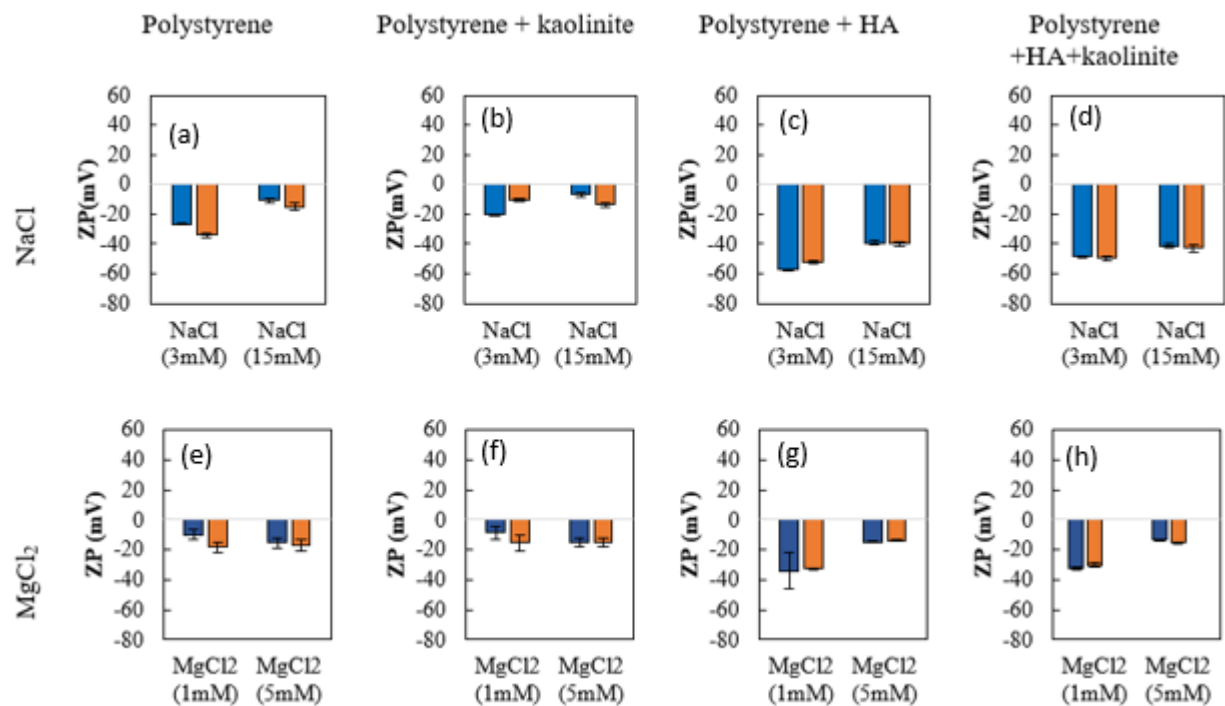


Figure 26. Zeta potential (ZP) of the polystyrene suspensions at pH 5 (blue) and 9 (red) in 3 mM NaCl, 15 mM NaCl, 1 mM MgCl₂, and 5 mM MgCl₂ solutions. Data are expressed as mean \pm standard deviation of triplicate measurements.

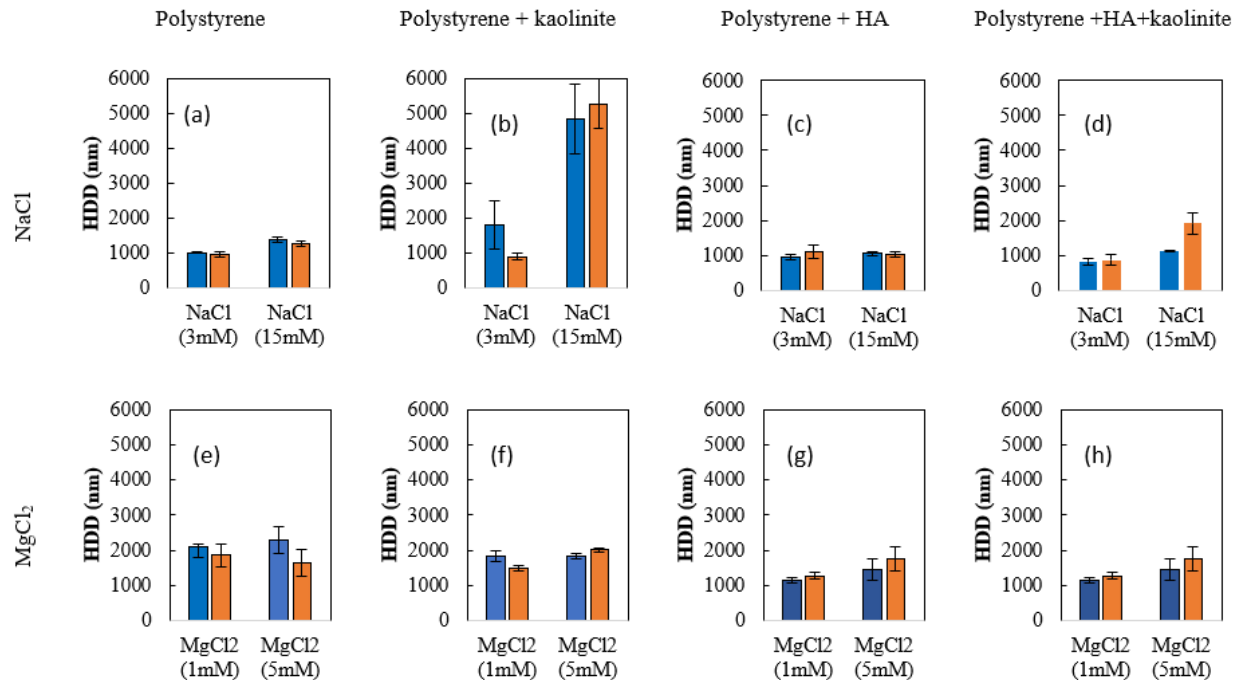


Figure 27. Hydrodynamic diameter (HDD) of the polystyrene suspensions at pH 5 (blue) and 9 (red) in 3 mM NaCl, 15 mM NaCl, 1 mM MgCl₂, and 5 mM MgCl₂ solutions. Data are expressed as mean \pm standard deviation of triplicate measurements.

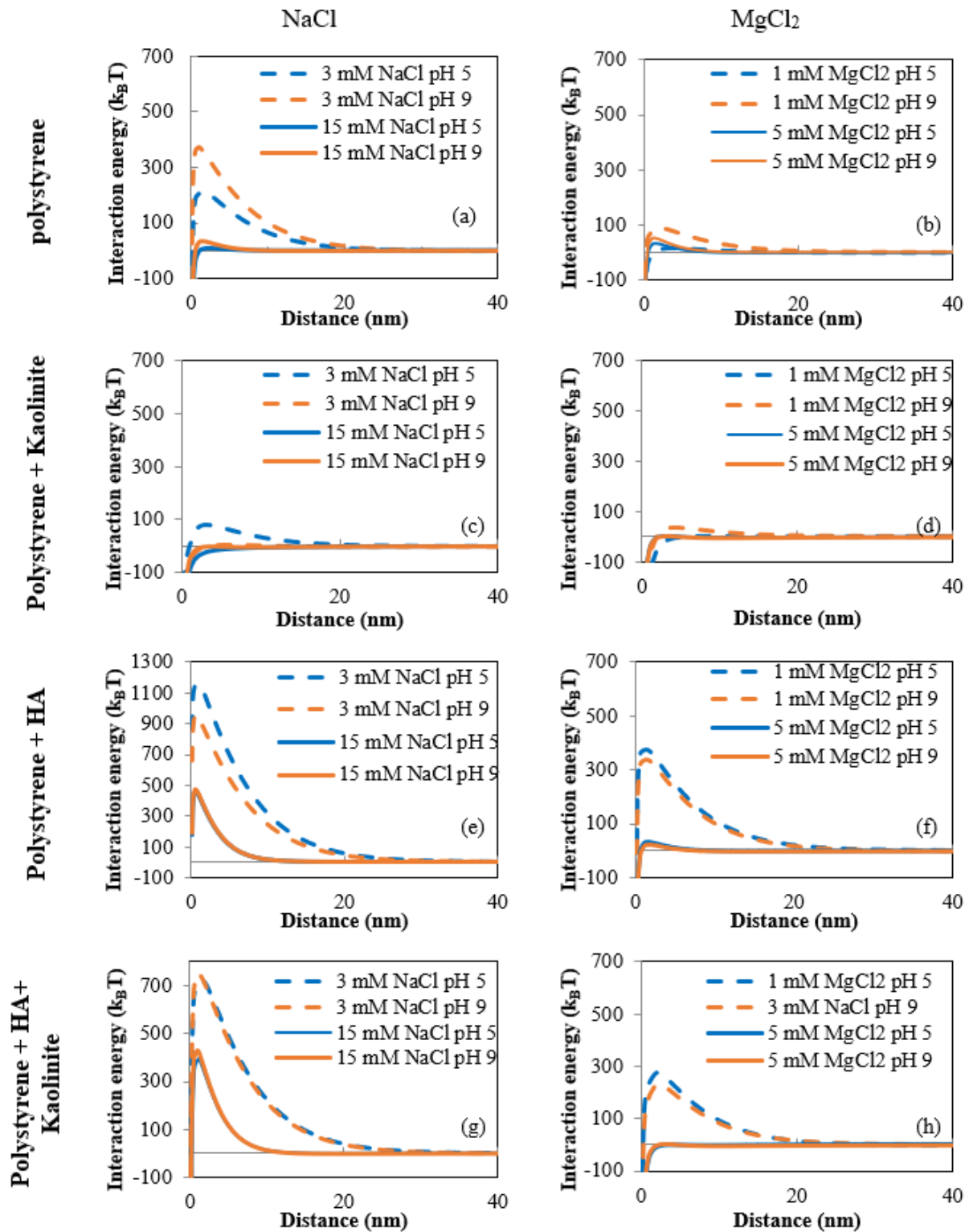


Figure 28. DLVO interaction plots for polystyrene microplastics according to DLVO theory, van der Waals and EDL forces. Different colors symbolize different pH, and dashed lines lower IS for NaCl and MgCl₂. a) polystyrene b) polystyrene+ kaolinite c) polystyrene+ humic acid (HA) d) polystyrene+ HA+ kaolinite

Table 8. Energy Barrier (ϕ_{\max}), Secondary Minimum ($\phi_{2\min}$) in NaCl solutions calculated for polystyrene microplastics based on DLVO theory.

Suspension	NaCl (mM)	pH	ZP (mV)	HDD (nm)	Energy barrier (k _B T)	Secondary min (k _B T)	A (*10 ⁻²⁰ J)
polystyrene	3	5	-26.45	1002	210.4	-0.1	0.4
		9	-33.95	956	370.89	-0.08	0.4
	15	5	-10.6	1383	7.68	-0.96	0.4
		9	-15	1252	33.74	-0.74	0.4
Polystyrene + kaolinite	3	5	-20.03	1809	79.74	-0.44	1.22
		9	-10.5	903	6.42	-0.73	1.22
	15	5	-6.6	4829	N/A	-4.07	1.22
		9	-13.7	5269	N/A	-3.52	1.22
Polystyrene +HA	3	5	-56.95	937	1148.08	-0.05	0.4
		9	-52.35	1100	957.63	-0.06	0.4
	15	5	-39.3	1059	458.1	-0.44	0.4
		9	-39.75	1029	470.51	-0.43	0.4
Polystyrene + kaolinite +HA	3	5	-48.7	821	725.99	-0.28	1.22
		9	-49.5	856	753.82	-0.27	1.22
	15	5	-41.2	1123	392.82	-1.71	1.22
		9	-42.75	1920	431.7	-1.67	1.22

*N/A means not applicable.

Table 9. Energy Barrier (ϕ_{\max}), Secondary Minimum ($\phi_{2\min}$) in MgCl₂ solutions calculated for polystyrene microplastics based on DLVO theory.

Suspension	MgCl ₂ (mM)	pH	ZP (mV)	HDD (nm)	Energy barrier (k _B T)	Secondary min (k _B T)	A (*10 ⁻²⁰ J)
polystyrene	1	5	-10	2111.83	16.64	-0.16	0.4
		9	-18.29	1851	87.2	-0.11	0.4
	5	5	-15	2284.17	33.74	-0.74	0.4
		9	-17	1647.17	50.02	-0.68	0.4
Polystyrene + kaolinite	1	5	-8.6	1846.17	0.93	-0.91	1.22
		9	-15.27	1482.17	32.88	-0.53	1.22
	5	5	-15	1829.83	3.38	-3.38	1.22
		9	-15.05	2010	3.61	-3.38	1.22
Polystyrene + HA	1	5	-34.02	1136.33	327.57	-0.08	0.4
		9	-32.56	1270.33	339.06	-0.08	0.4
	5	5	-14.78	1434.5	32.22	-0.74	0.4
		9	-13.71	1763.33	24.24	-0.78	0.4
Polystyrene + kaolinite + HA	1	5	-32.51	812.5	277.85	-0.34	1.22
		9	-30.08	883.83	228.41	-0.35	1.22
	5	5	-13.38	1816.96	N/A	-3.56	1.22
		9	-15.01	1747.3	3.47	-3.38	1.22

*N/A means not applicable.

4.5 Amine-modified polystyrene stability

This section explores the evaluation of the stability of suspensions containing PSNH₂ MPs with a characteristic size of 1 micrometer in an aqueous environment. The results are presented in Figures 29 to 32 and Tables 10 and 11, where blue and red symbols represent pH 5 and pH 9, respectively. Generally, amine suspensions exhibit stability and have high energy barriers. However, the effects of kaolinite and high ionic strength did influence the behavior of MPs.

Figure 29 show A/A_0 for the PSNH₂ MPs particle suspension as a function of time for the two salts (NaCl and MgCl₂) at two different IS and for the two values of pH (5 and 9). The A/A_0 ratio remained stable for PSNH₂ in all suspensions, except for the high IS NaCl solution at pH 9. The HDD value of 2647 nm (Figure 31 a) is another indication of the instability of this suspension. Upon examining the ZP (Figure 30), it is evident that the ZP values were all positive. Notably, the ZP values for the 15 mM NaCl suspension was relatively large at 23 mV. Moreover, the energy barrier (Figure 32), for the 15 mM NaCl suspension was substantial (110 k_BT). In the case of MgCl₂, the ZP values were notably high, and the HDD values were low. Large energy barriers indicated the dominance of repulsive forces, preventing aggregation.

Upon the addition of kaolinite to PSNH₂ suspension, the A/A_0 ratio was very similar to the suspension without kaolinite. The ratio remained close to 1 for both NaCl and MgCl₂ suspensions, except for the 15 mM NaCl suspension at pH 9. This result correlated with the largest HDD values (1368 nm), least positive ZP (23 mV), and the lowest energy barrier (64 k_BT), and highest secondary minimum (-2.2 k_BT) compared to other conditions (Table 10 and 11).

When HA was added to the PSNH₂ suspension, the ZP values were negative (Figure 30 c and g). As seen in Figure 29, the A/A_0 ratio remained stable for both NaCl and MgCl₂ suspensions

at low IS, but in this case the 15 mM NaCl suspension remained stable at high IS and instability was instead observed for high IS MgCl₂ at both pH 5 and 9. This stability aligned with the larger HDD values (2340 nm at pH 5 and 2392 nm at pH 9), less negative ZP values (-11.4 mV at pH 5 and -12 mV at pH 9), and lower energy barrier values (10 k_BT at pH 5 and 13 k_BT at pH 9) compared to other conditions. Other suspensions exhibited large negative ZP values and high energy barriers, indicating a prevention of aggregation and low HDD (Table 10 and 11).

In the case of HA + kaolinite + PSNH₂ suspensions, the results resembled those of the HA + PSNH₂ suspensions. All of the suspensions, except the high IS MgCl₂ suspensions, displayed stability, with a stable A/A₀ ratio, moderately negative ZP, and low HDD values. High energy barrier values indicate the dominance of repulsive forces. However, the high IS MgCl₂ suspension at both pH 5 and 9 exhibited instability, corresponding to the absence of energy barrier, higher secondary minimum (-3 k_BT), and leading to aggregation. ZP values were less negative, and HDD values were larger.

The various PS-NH₂ suspensions were stable, except for the suspensions containing PS-NH₂ and PS-NH₂ + kaolinite in 15 mM NaCl and pH 9, and PS-NH₂ + HA and PS-NH₂ + HA + kaolinite in 5 mM MgCl₂. This stability is attributed to the positive surface charges of PS-NH₂ compared to the other MPs. These results are consistent with a previous study that found PS-NH₂ stable in media such as (i) ultrapure water, (ii) artificial seawater, and (iii) seawater. There was a decrease in ZP when particles were suspended in seawater, but it remained sufficiently high to ensure repulsive mechanisms ([Tallec et al., 2019](#)). Also, in accordance with a similar study, it was observed that an increase in salinity led to decreased ZP values of both negatively charged PS and positively charged PS-NH₂, resulting in particle aggregation ([Wu et al., 2019](#)).

The addition of HA to plain PS suspensions was found to have an impact on the ZP values, causing them to become more negative (Figure 26). This effect was also observed for amine-modified particles, which initially had a positive charge. Upon the addition of HA, the ZP values shifted from positive to negative (Figure 30). It is inferred that when positively charged particles interacted with negatively charged HA, the HA molecules adsorbed onto the particle surface, leading to the neutralization of the surface charge or its conversion to a negative value. In a study where a low concentration of HA was added to PS-NH₂, it resulted in particle aggregation, as the surface charge was neutralized ([Wu et al., 2019](#)). However, with a further increase in HA concentration, the HDD decreased, indicating enhanced stability of the nanoparticles. This enhanced stability was attributed to the increased adsorption of HA, which induced electrostatic repulsion and steric stabilization ([Wu et al., 2019](#)).

When comparing PS-NH₂ + HA suspensions, especially in MgCl₂ solutions, it is evident that HA had a more pronounced destabilizing impact on PS-NH₂ with positive charges in comparison to plain PS. These findings are consistent with a different study that also observed greater destabilization effects of HA on PSNPs-NH₂ with positive charges compared to negatively surface charged PSNPs-COOH and PSNPs ([Wu et al., 2019](#)). This can be attributed to the absorption of negatively charged HA onto the positively charged particle surface of PS-NH₂, resulting in greater neutralization effects for positively charged PSNPs-NH₂ ([Qu et al., 2010](#)).

These findings align with previous research on the aggregation of polyethylenimine (BPEI)-coated silver nanoparticles influenced by pony lake fulvic acid (PLFA). In their study, the adsorption of PLFA onto the surface of positively charged nanoparticles initially promoted aggregation. However, with more adsorption, the colloidal stability and dispersion of the nanoparticles were improved due to the combined effects of electrostatic hindrance and steric

repulsion ([Jung et al., 2018](#)). Similar effect on micro-scale titanium dioxide particles was found for humic acid. While humic acid enhanced particle aggregation at lower concentration, they hindered aggregation at higher concentration ([Wu et al., 2016](#)). Moreover, adding minor amounts of humic acid into suspensions containing kaolinite leads to an enhancement in colloidal stability. This enhancement can be attributed to alterations in the charge distribution along the particle edges, transitioning from a positive to a negative charge at lower pH. This shift in charge distribution hinders the tendency of particles to aggregate in a face-to-edge arrangement, thereby contributing to enhanced stability in the suspension ([Kretzschmar et al., 1997](#)).

Therefore, the adsorption of HA onto the particle surface affects the surface charge, leading to changes in ZP values and influencing the aggregation behavior. The findings also demonstrate the complex interplay between HA concentration, electrostatic forces, and steric effects in determining the overall stability of the nanoparticles.

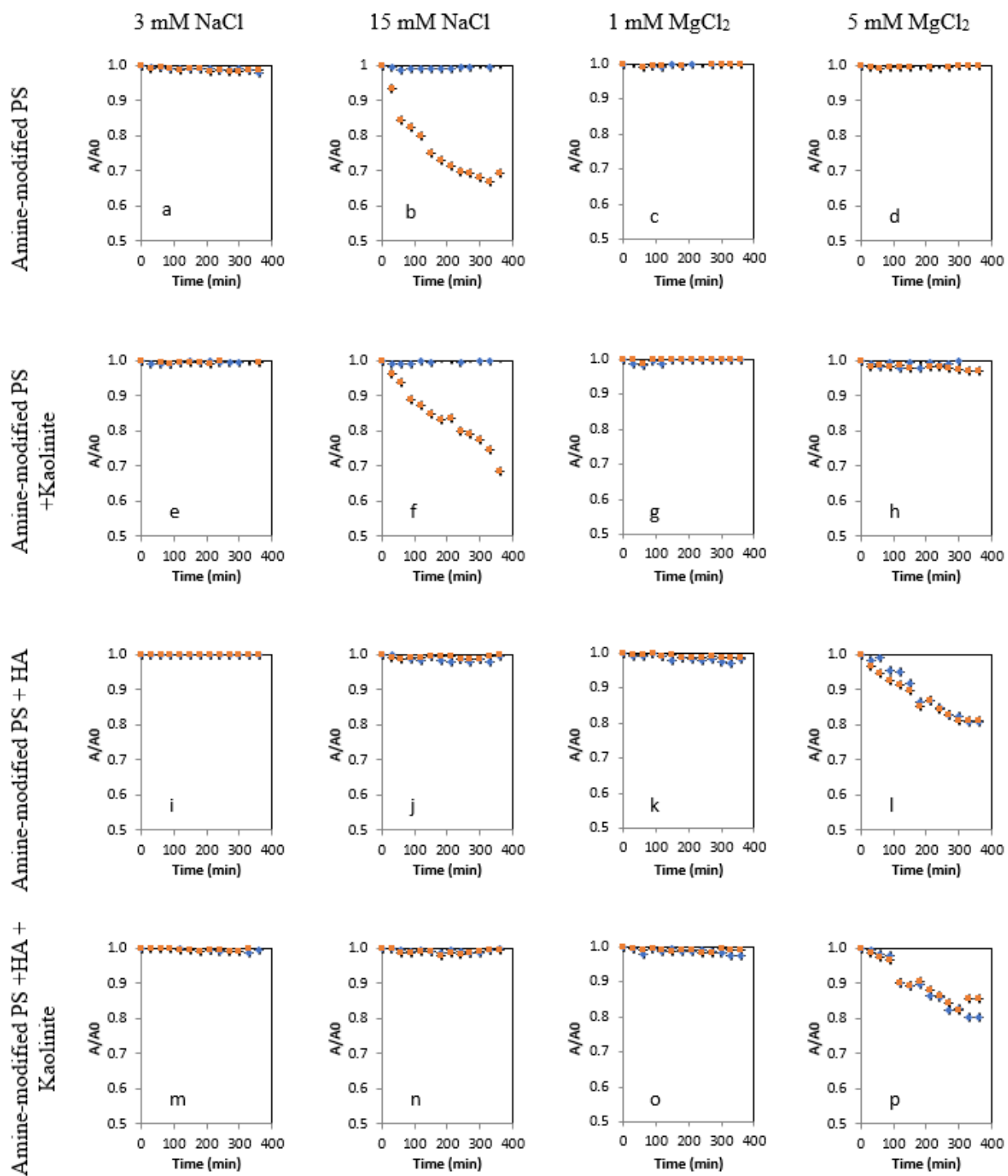


Figure 29. Stability of the amine-modified polystyrene suspensions at pH 5 (blue) and 9 (red) in 3 mM NaCl, 15 mM NaCl, 1 mM MgCl₂, and 5 mM MgCl₂ solutions. Data are expressed as mean \pm standard deviation of duplicate experiments.

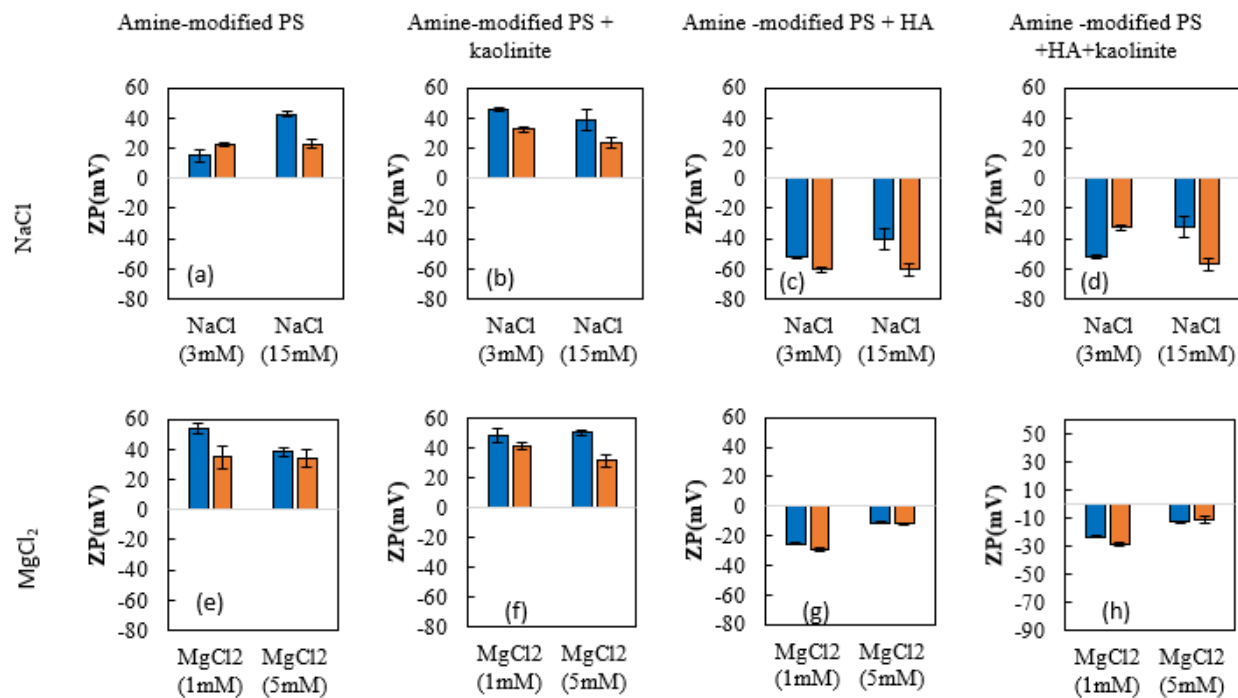


Figure 30. Zeta potential (ZP) of the amine-modified polystyrene suspensions at pH 5 (blue) and 9 (red) in 3 mM NaCl, 15 mM NaCl, 1 mM MgCl₂, and 5 mM MgCl₂ solutions. Data are expressed as mean \pm standard deviation of triplicate measurements.

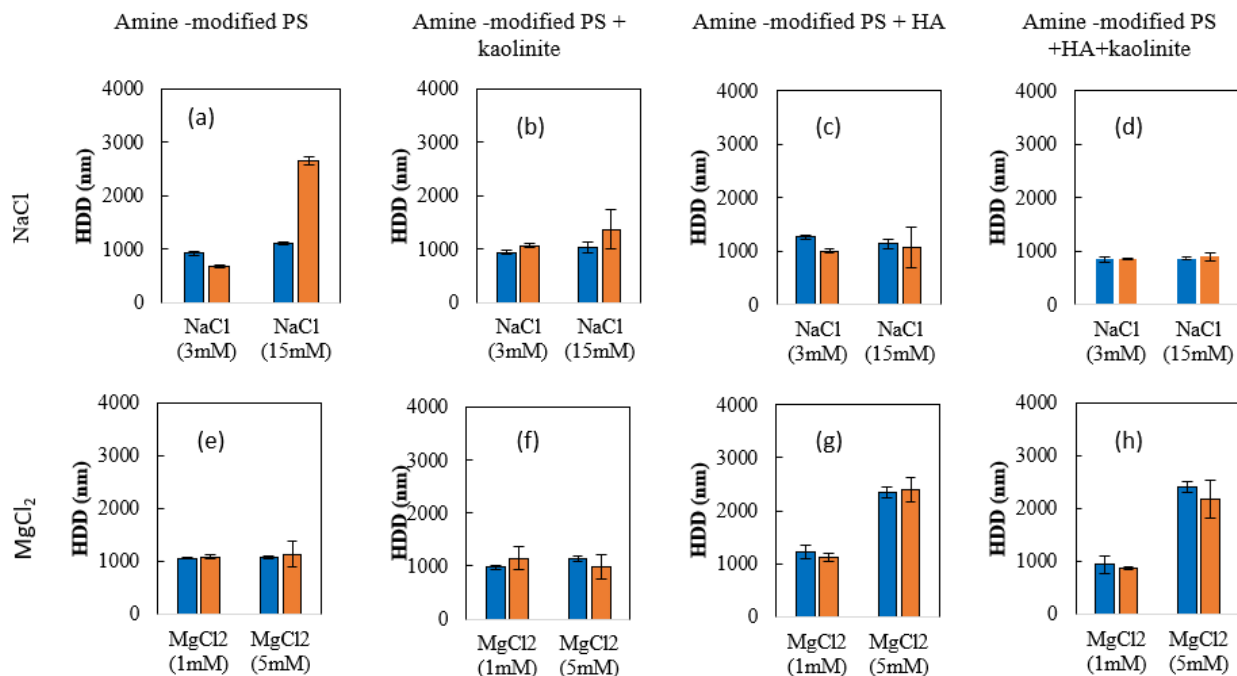


Figure 31. The hydrodynamic diameter (HDD) of the amine-modified polystyrene suspensions at pH 5 (blue) and 9 (red) in 3 mM NaCl, 15 mM NaCl, 1 mM MgCl₂, and 5 mM MgCl₂ solutions. Data are expressed as mean \pm standard deviation of triplicate measurements.

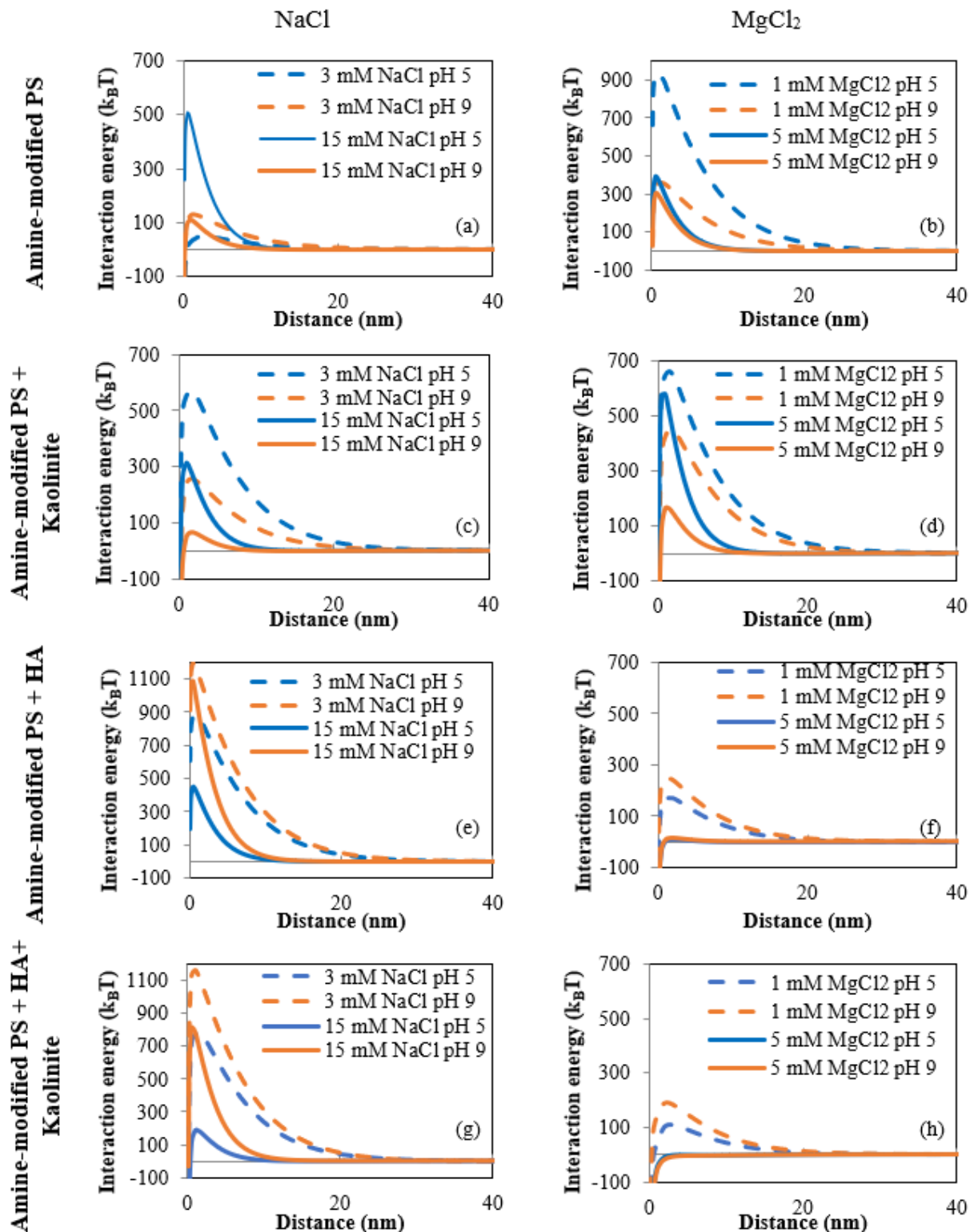


Figure 32. DLVO interaction plots for amine-modified polystyrene (PS-NH₂) according to DLVO theory, van der Waals, and EDL forces. Different colors symbolize different pH, and dashed lines lower IS for NaCl and MgCl₂. a) PS-NH₂ b) PS-NH₂ + kaolinite c) PS-NH₂ + HA d) PS-NH₂ + HA + kaolinite

Table 10. Energy Barrier (ϕ_{\max}), Secondary Minimum ($\phi_{2\min}$) in NaCl solutions calculated for amine-modified polystyrene based on DLVO theory.

Suspension	NaCl (mM)	pH	ZP (mV)	HDD (nm)	Energy barrier (k _B T)	Secondary min (k _B T)	A (*10 ⁻²⁰ J)
Amine-modified PS	3	5	15	921.35	47.96	-0.11	0.4
		9	22.37	674.1	129.32	-0.09	0.4
	15	5	42.75	1106	506.19	-0.38	0.4
		9	23	2647	109.61	-0.52	0.4
Amine-modified PS+Kal	3	5	45.7	931.17	568.78	-0.26	1.22
		9	32.63	1063.5	255.13	-0.3	1.22
	15	5	39.08	1028.28	310.89	-1.6	1.22
		9	23.62	1368.73	63.85	-2.19	1.22
Amine-modified PS+HA	3	5	-52.6	1271	879.61	-0.05	0.4
		9	-60.7	1002.8	1195.63	-0.04	0.4
	15	5	-40.7	1141	451.96	-0.39	0.4
		9	-60.45	1071.56	1085.19	-0.33	0.4
Amine-modified PS+Kal+HA	3	5	-52.4	846.25	780.47	-0.24	1.22
		9	-62.65	866.65	1160.28	-0.22	1.22
	15	5	-32.62	869.3	185.1	-1.77	1.22
		9	-57.15	903.38	812.3	-1.31	1.22

*N/A means not applicable.

Table 11. Energy Barrier (ϕ_{\max}), Secondary Minimum ($\phi_{2\min}$) in MgCl₂ solutions calculated for amine-modified polystyrene based on DLVO theory.

Suspension	MgCl ₂ (mM)	pH	ZP (mV)	HDD (nm)	Energy barrier (k _B T)	Secondary min (k _B T)	A (*10 ⁻²⁰ J)
Amine-modified PS	1	5	53.96	1057.17	929.51	-0.05	0.4
		9	34.81	1083	356.64	-0.07	0.4
	5	5	38.17	1070.17	388.71	-0.4	0.4
		9	34.26	1130.93	298.94	-0.42	0.4
Amine-modified PS + Kal	1	5	48.7	973.7	659.99	-0.25	1.22
		9	41.37	1149.35	449.73	-0.27	1.22
	5	5	50.17	1135.33	579.7	-1.4	1.22
		9	31.3	973.73	162.19	-1.82	1.22
Amine-modified PS +HA	1	5	-25.3	1217.83	172.1	-0.09	0.4
		9	-29.5	1114.83	246.23	-0.08	0.4
	5	5	-11.4	2340.17	10.27	-0.82	0.4
		9	-12	2392.83	13.02	-0.79	0.4
Amine-modified PS +Kal +HA	1	5	-23.4	938.77	107.93	-0.36	1.22
		9	-28.9	874.8	188.11	-0.32	1.22
	5	5	-13.17	2402	N/A	-3.25	1.22
		9	-11.5	2169.7	N/A	-3.39	1.22

*N/A means not applicable.

4.6 Carboxylate-modified polystyrene stability

This section examines suspensions of PS-COOH particles, under the range of conditions studied in sections 4.4 and 4.5. Results are presented in Figures 33 to 36 and Tables 12 to 13.

From Figure 33, the suspensions in NaCl solutions are all stable. Looking at Figure 34 and Table 12, it can be seen that in NaCl solutions, the ZP values for PS-COOH are all moderately to strongly negative, exhibiting a range spanning approximately from -82 mV to -32 mV. The addition of HA to NaCl solutions enhances the negative charge. The lowest value recorded was -82 mV upon the introduction of HA to a suspension with 15 mM NaCl and pH 9. The trends manifested in ZP values are mirrored in other parameters, including the ratio of absorbance (A/A_0) (Figure 33), the HDD values (Figure 35), and the energy barrier (Figure 36). Notably, the introduction of HA triggers a reduction in both ZP and HDD values. This agreement between ZP and HDD values matches the energy barrier findings from the DLVO theory. The calculated high energy barrier values prevent particles from clumping together and improve the suspension's stability.

The role of IS with divalent cation Mg^{2+} was evident in the behavior of ZP, HDD, and energy barrier values. In $MgCl_2$ solutions, the ZP values for PS-COOH were observed to range from approximately -38 mV to -18.5 mV (Figure 34 e to h, Table 13). This result demonstrates how background electrolyte (NaCl or $MgCl_2$) impacts the surface charge of the particles. ZP values in NaCl solutions show a wider range and more negative values compared to $MgCl_2$ solutions. In most cases, this change in ZP values is usually accompanied by a modest increase in the HDD of the particles (Figure 35). This relationship is supported by the energy barrier calculated using the DLVO theory. These observations emphasize the interplay between IS, surface charge, and particle interactions.

The addition of kaolinite only slightly affects the stability and aggregation tendencies of PS-COOH MPs. In general, when kaolinite was added to high IS MgCl_2 solutions, the A/A_0 ratio decreased slightly with time (Figure 33 h), the ZP values of the MPs were less negative (Figure 34 f) and the HDD values increased (Figure 35 f). The calculated energy barrier values were correspondingly eliminated (Figure 36 d). All these factors indicate aggregation. On the other hand, in the case of other suspensions, the ZP range covers a wide span, the HDD values are relatively small, and the energy barrier values are significant. This combination of factors indicates stable suspensions.

In contrast to suspensions of PS-NH₂, suspensions of PS-COOH were found to be stable in 15 mM NaCl, suggesting that the carboxylic acid groups of the PSNPs contributed to their stability. Our results were similar to recent studies that showed increasing IS resulted in PSNPs stability due to the high negative charge on the PSNPs ([Cai et al., 2018](#)). Based on several studies, it has been found that at higher IS, aggregation occurs for plain PS and PS-COOH (sized 25 and 50 nm) ([Della Torre et al., 2014](#); [Tallec et al., 2018](#); [Wegner et al., 2012](#)). However, other studies have shown that for plain PS and PS-COOH sized 100 nm, aggregation did not occur with increasing IS ([Cai et al., 2018](#); [González-Fernández et al., 2018](#)). This indicates that there might be additional variables (e.g., size, surface chemistry and heterogeneity) that affect the stability of MPs, apart from IS, which requires additional investigation ([Alimi et al., 2018](#)).

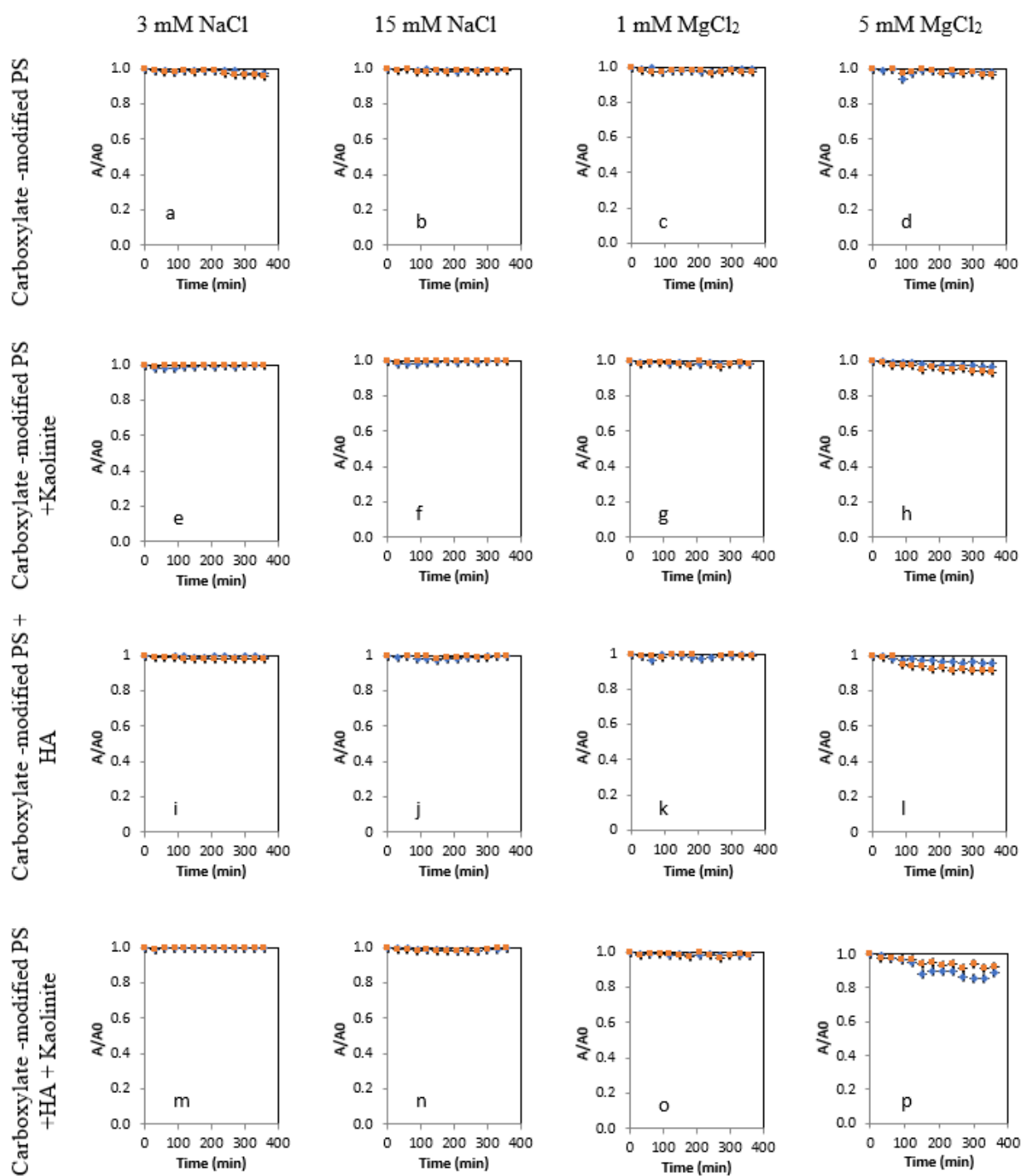


Figure 33. Stability of the carboxylate-modified polystyrene suspensions at pH 5 (blue) and 9 (red) in 3 mM NaCl, 15 mM NaCl, 1 mM MgCl₂, and 5 mM MgCl₂ solutions. Data are expressed as mean \pm standard deviation of duplicate experiments.

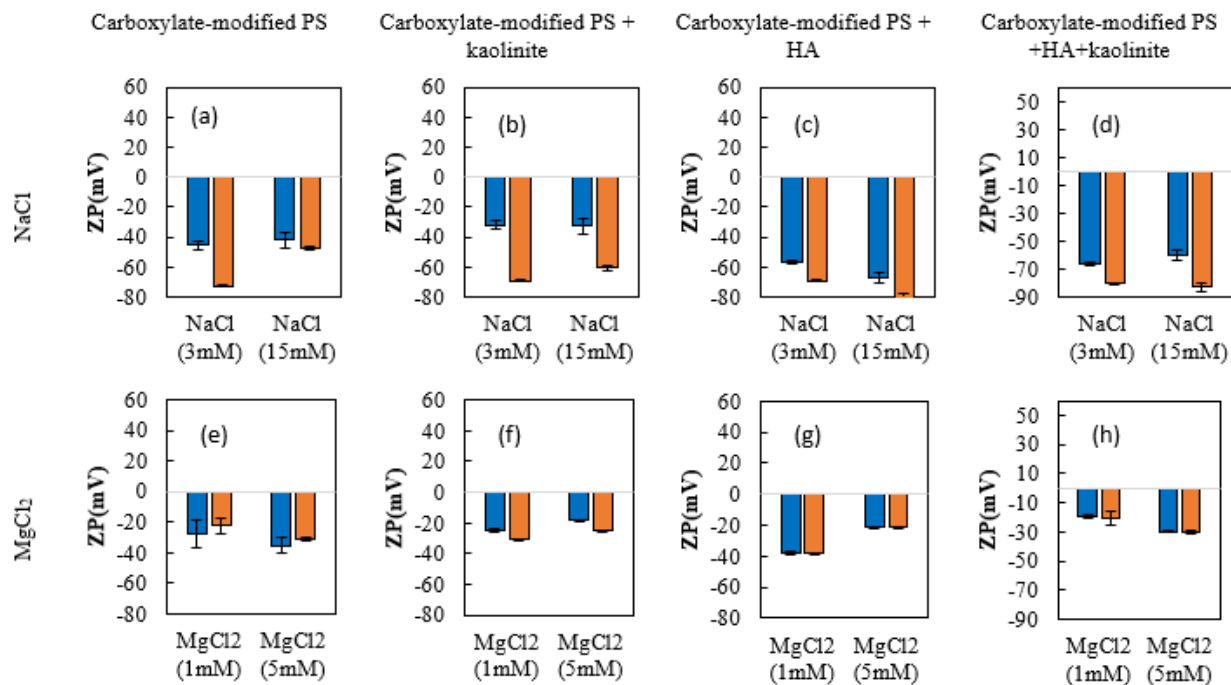


Figure 34. Zeta potential (ZP) of the carboxylate-modified polystyrene suspensions at pH 5 (blue) and 9 (red) in 3 mM NaCl, 15 mM NaCl, 1 mM MgCl₂, and 5 mM MgCl₂ solutions. Data are expressed as mean \pm standard deviation of triplicate measurements.

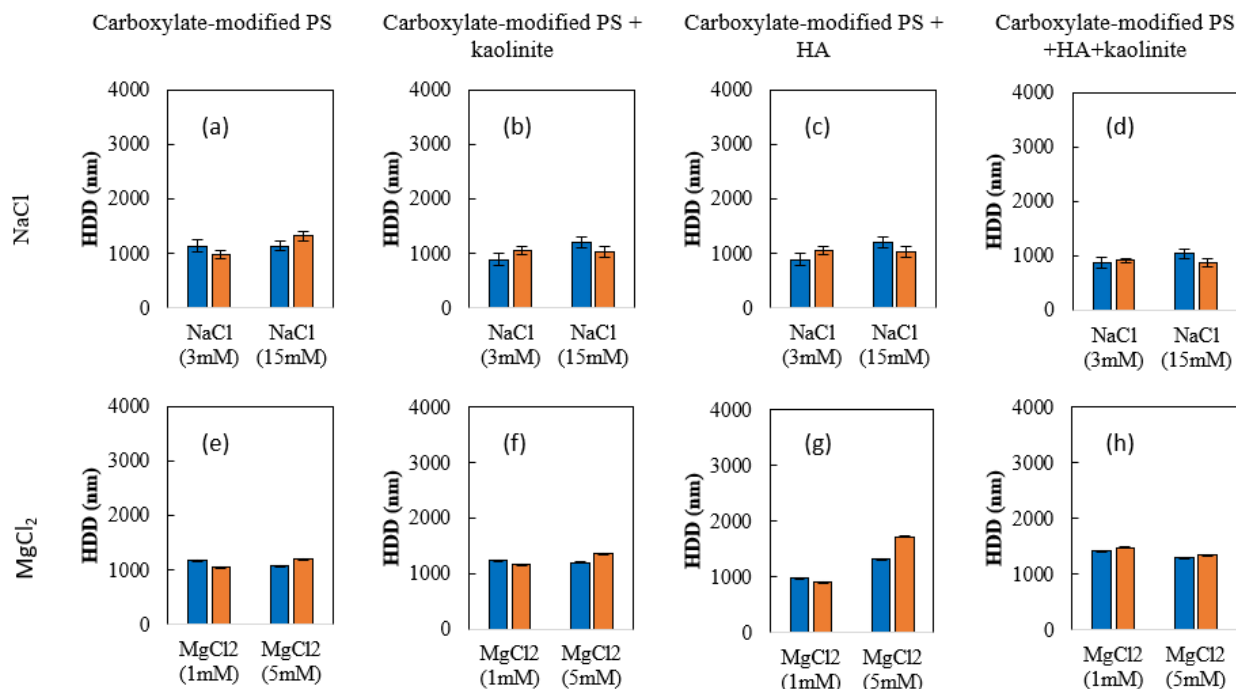


Figure 35. Hydrodynamic diameter (HDD) of the carboxylate-modified polystyrene suspensions at pH 5 (blue) and 9 (red) in 3 mM NaCl, 15 mM NaCl, 1 mM MgCl₂, and 5 mM MgCl₂ solutions. Data are expressed as mean \pm standard deviation of triplicate measurements.

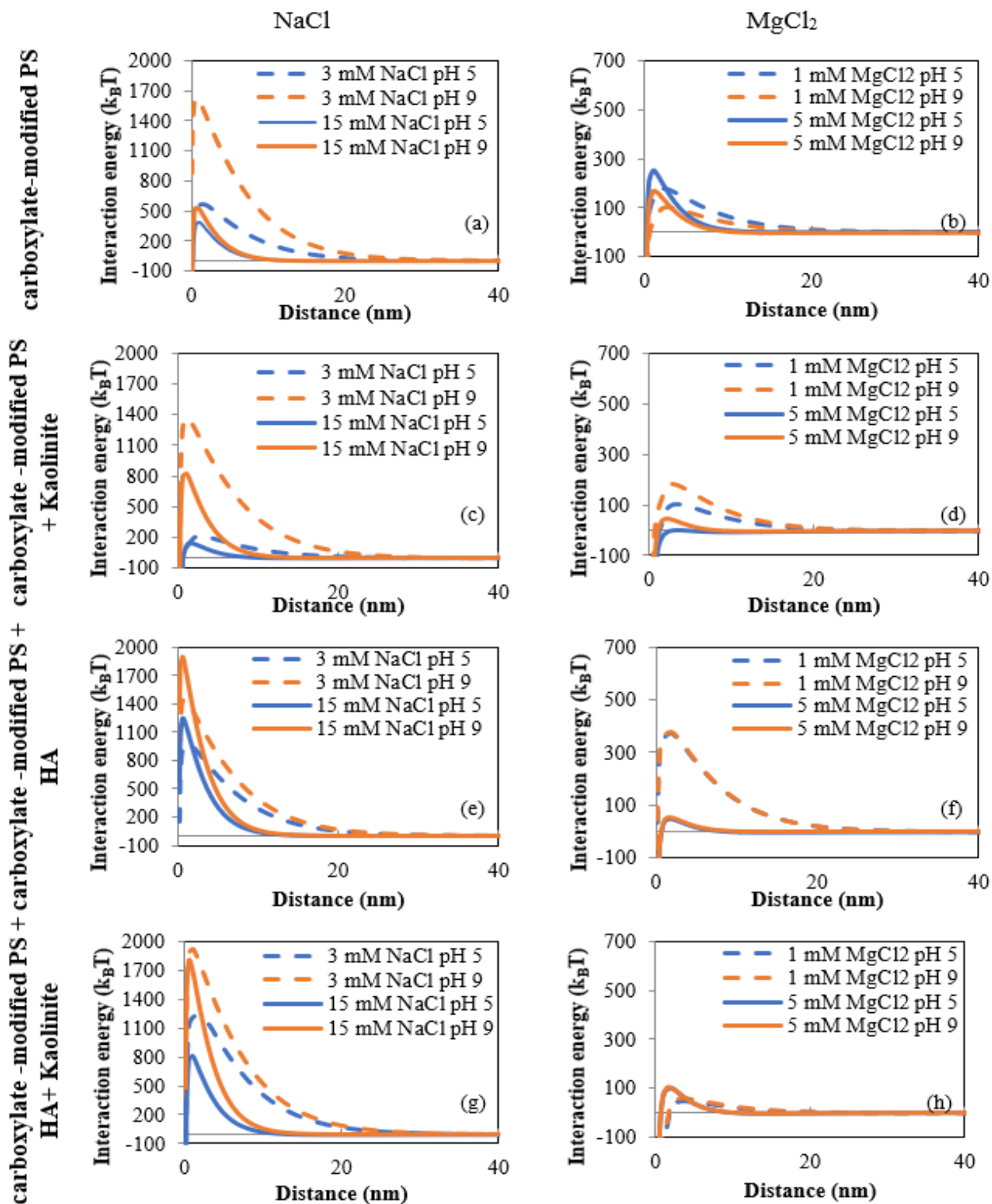


Figure 36. DLVO interaction plots for carboxylate-modified polystyrene suspensions (PS-COOH) according to DLVO theory, van der Waals, and EDL forces. Different colors symbolize different pH, and dashed lines lower IS for NaCl and MgCl₂. a) PS-COOH b) PS-COOH + kaolinite c) PS-COOH + HA d) PS-COOH + kaolinite+ HA

Table 12. Energy Barrier (ϕ_{\max}), Secondary Minimum ($\phi_{2\min}$) in NaCl solutions calculated for carboxylate-modified polystyrene suspensions based on DLVO theory.

Suspension	NaCl (mM)	pH	ZP (mV)	HDD (nm)	Energy barrier (k _B T)	Secondary Minimum (k _B T)	A (*10 ⁻²⁰ J)
Carboxylate-modified PS	3	5	-45.3	1132.5	571.53	-0.22	1.05
		9	-72.55	982.28	1620.55	-0.16	1.05
	15	5	-42.1	1139.5	391.95	-1.27	1.05
		9	-47.45	1321.5	522.06	-1.19	1.05
Carboxylate-modified PS + Kal	3	5	-32.1	886.97	213.26	-0.57	2
		9	-69.1	1050.35	136.57	-0.39	2
	15	5	-32.7	1194.83	140.46	-3.4	2
		9	-60.57	1029.25	826.06	-2.3	2
Carboxylate-modified PS +HA	3	5	-57.15	903.75	964.6	-0.2	1.05
		9	-69	903.75	1447.52	-0.17	1.05
	15	5	-67.25	832.8	1241.64	-1.02	1.05
		9	-81.15	868.15	1895.48	-0.94	1.05
Carboxylate-modified PS +Kal +HA	3	5	-65.93	882.98	1229.71	-0.4	2
		9	-80.67	911.02	1925.68	-0.37	2
	15	5	-60.2	1037.8	813.92	-2.19	2
		9	-82.83	874.17	1809.17	-1.97	2

*N/A means not applicable.

Table 13. Energy Barrier (ϕ_{\max}), Secondary Minimum ($\phi_{2\min}$) in MgCl₂ solutions calculated for carboxylate-modified polystyrene suspensions based on DLVO theory.

Suspension	MgCl ₂ (mM)	pH	ZP (mV)	HDD (nm)	Energy barrier (k _B T)	Secondary Minimum (k _B T)	A (*10 ⁻²⁰ J)
Carboxylate-modified PS	1	5	-27.8	1173.67	177.06	-0.27	1.05
		9	-22.5	1041.38	102.22	-0.31	1.05
	5	5	-35.4	820.07	250.93	-1.3	1.05
		9	-30.8	1208.2	168.23	-1.5	1.05
Carboxylate-modified PS + Kal	1	5	-24.8	1245.64	103.66	-0.67	2
		9	-30.4	1175.83	183.88	-0.59	2
	5	5	-18.55	1204.65	2.01	-5.12	2
		9	-24.87	1353.87	45.23	-4.19	2
Carboxylate-modified PS +HA	1	5	-37.77	985.18	373.09	-0.23	1.05
		9	-38.1	909.1	380.63	-0.23	1.05
	5	5	-21.33	1323.33	49.27	-1.93	1.05
		9	-21.58	1725.17	51.61	-1.91	1.05
Carboxylate-modified PS +Kal +HA	1	5	-19.33	1424	46.73	-0.8	2
		9	-20.58	1482.17	57.22	-0.76	2
	5	5	-30	1300	100.4	-2.18	2
		9	-30.05	1347	101.99	-3.61	2

*N/A means not applicable.

4.7 Comparative analysis of microplastic behavior: insights from three types of MPs

The analysis of stability measures (A/A_0 , HDD, ZP, DLVO) reveals that their agreement is not always consistent, particularly for plain PS samples. Among the examined plain PS samples, plain PS+ kaolinite exhibited the greatest instability, followed by plain PS. In contrast, PS-COOH suspensions demonstrated the highest stability, while PS-NH₂ suspensions generally exhibited stability except for suspensions of IS=15 mM and pH=9 for NaCl solutions in the absence of HA and IS=15mM for MgCl₂ solutions with HA, where suspensions became unstable (Figure 29). For PSMPs, the introduction of kaolinite led to reduced stability, whereas HA enhanced stability. In general, the addition of HA enhanced stability, while the introduction of kaolinite to HA generally decreased stability at higher IS, albeit to a limited extent.

For PS-NH₂ solutions, the addition of HA changed the ZP from positive to negative. For the NaCl solutions, the magnitude of the ZP increased (Figure 37) and correspondingly stability increased. For the MgCl₂ solutions, however, the magnitude of the ZP was reduced (Figures 30e and 30g) and the suspensions were less stable.

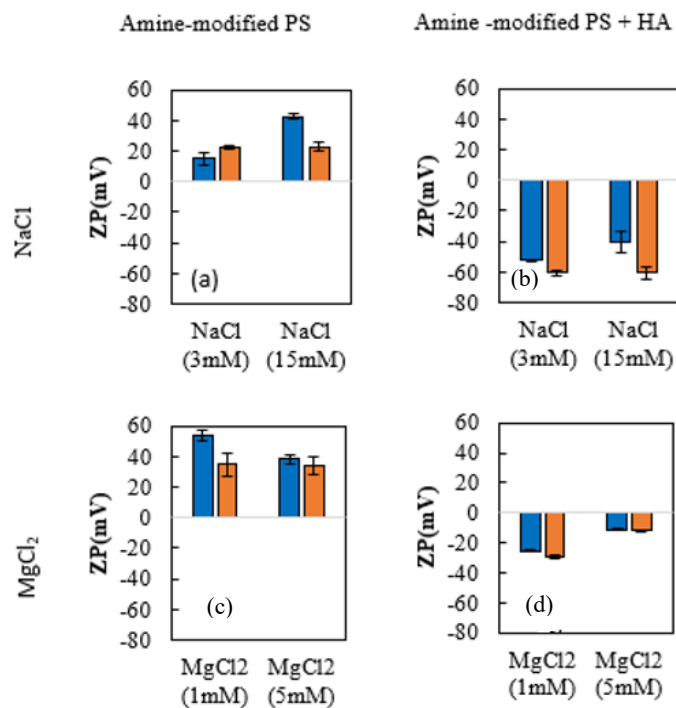


Figure 37. Zeta potential (ZP) of the amine-modified polystyrene suspensions at pH 5 (blue) and 9 (red) in 3 mM NaCl, 15 mM NaCl, 1 mM MgCl₂, and 5 mM MgCl₂ solutions. Data are expressed as mean \pm standard deviation of triplicate measurements.

In contrast, the incorporation of kaolinite had a less consistent effect on ZP values. For plain PS in NaCl solutions, ZP was reduced and at its lowest values, at IS=15mM, the suspensions were less stable (Figure 38). For plain PS in MgCl₂ solutions, and in PS-NH₂ and PS-COOH experiments, the addition of kaolinite generally had little effect on ZP or the stability of the suspensions. Notably, the addition of kaolinite resulted in elevated HDD (Figure 27b). These increased HDD pointed to a higher inclination for MPs aggregation when kaolinite was present, leading to the formation of larger particle clusters. In other experiments, the presence of kaolinite did not have a large effect.

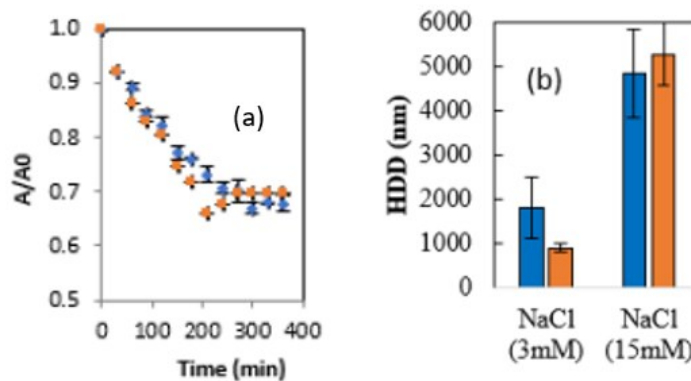


Figure 38. (a). Stability of the polystyrene+ kaolinite suspensions at pH 5 (blue) and 9 (red) in 15 mM NaCl, (b). Hydrodynamic diameter (HDD) of the polystyrene suspensions at pH 5 (blue) and 9 (red) in 3 mM NaCl and 15 mM NaCl solutions

High IS conditions, particularly in $MgCl_2$ solutions, tended to induce greater instability. This reduction in stability was evident in decreased A/A_0 ratios and increased HDD values. This effect was more pronounced for $MgCl_2$ compared to NaCl solutions. Specifically, for NaCl, PS-COOH suspensions remained stable across all scenarios; the ZP and energy barrier decreased when kaolinite was introduced, yet the suspensions remained stable.

As the IS of the solution increased, ZP become less negative for PS and PS-COOH and less positive for PS-NH₂. This decrease in ZP indicated a weakening of repulsive forces and, therefore, a lower energy barrier between microplastic particles, leading to aggregation. Reduced energy barrier indicated weakened repulsion and heightened aggregation potential.

Findings from other research ([Romero-Cano et al., 2001](#)) indicated that the stability of PS and PS-COOH suspensions in NaCl solutions increases as pH increases. This was attributed to the greater adsorption of hydroxyl groups onto the MPs' surface. Consequently, the ZP became more negative, leading to an increase in electrostatic repulsion. In the present work, aligned with this, more negative ZP (Figures 23a and 34a) and higher calculated energy barriers (Figures 28a and

34a) occurred with increasing pH, although corresponding changes in A/A_0 and HDD (Figures 25a&b, 33a&b, 27a and 35a) were not observed.

When considering $MgCl_2$ solutions, most suspensions tended to be less stable compared to their corresponding NaCl solutions with the same IS. The stronger charge screening effect and bridging effect of divalent cations made them more effective in destabilizing the suspensions compared to monovalent cations.

5 Conclusions and Recommendations

5.1 Conclusions

Results from this study help us understand the different factors that affect the stability of polystyrene microplastics (PSMPs). These findings add to the larger discussion about plastic pollution and offer valuable insights for addressing the challenges posed by these persistent pollutants in aquatic environments.

Functional group and zeta potential (ZP). The stability of MPs in aquatic environments is strongly influenced by their surface charge, a key finding supported by numerous studies. MPs with a strong negative surface charge, including plain PS and carboxylate-modified polystyrene (PS-COOH), demonstrated increased stability due to the presence of strong repulsive forces among particles. This outcome was confirmed through ZP measurements, which revealed that more negative ZP values correlated with enhanced stability. Similarly, the stability of amine-modified polystyrene (PS-NH₂), which has a positive surface coating, is correlated with high positive ZP values. These electrostatic repulsive forces played a crucial role in preventing microplastic aggregation by maintaining a distance between particles.

The addition of humic acid (HA) had an interesting effect on the ZP values. HA usually induced a negative shift in ZP values. This amplified the repulsion between particles with negative surface charge and thereby strengthened their stability.

The correlation between ZP values and stability observed across various experimental setups, highlights the significance of surface charge in governing microplastic interactions.

Ionic strength (IS) and salt effects. The stability of MPs in aquatic environments is linked to both the IS of the solution and the specific salt type present. The magnitude of the IS in the solution emerged as a critical determinant affecting the stability of MPs. Notably, with an increase in IS, a general trend of reduced stability became apparent within MPs suspensions. This tendency was particularly prominent in the case of the divalent cation Mg^{2+} . The divalent cations Mg^{2+} played a pivotal role in this process by serving as bridges connecting individual microplastic particles. By performing this bridging function, these cations nullified the repulsive forces that would otherwise maintain particle separation, thereby promoting aggregation.

Notably, microplastic suspensions of plain PS and PS-COOH in NaCl solutions demonstrated broader ZP ranges and more negative ZP values when compared to suspensions in $MgCl_2$ solutions. This contrasting behavior underscores the interplay between the ionic strength of the solution, the surface charge exhibited by MPs, and the interactions among particles.

Kaolinite and Humic Acid. The presence of kaolinite displayed a role in encouraging the aggregation of plain PSMPs in NaCl solutions. Conversely, the introduction of HA had a distinct influence on the HDD of MPs. The presence of HA often contributed to a reduction in HDD values, suggesting a stabilizing effect exerted by HA on microplastic suspensions. These findings aligned with the trends observed in ZP. Greater negativity in ZP values correlated with heightened stability.

The lower HDD in the presence of HA showed the concept of enhanced stability arising from the interaction between HA and MPs, which discouraged particle aggregation. The energy barrier trends mirrored ZP and HDD observations, underscoring their interrelation. This alignment between DLVO theory predictions and experimental results emphasized repulsive forces' central importance in sustaining microplastic suspension stability.

5.2 Recommendations for the future studies

Future investigations should further explore the unique behaviors displayed by PS, PS-NH₂, and PS-COOH nanoparticles across diverse environmental contexts. The following areas offer promising directions for further investigation.

Surface Modification Effects. The differences observed in aggregation tendency and stability among PS, PS-NH₂, and PS-COOH nanoparticles emphasize the significance of surface functionalization. Future studies might broaden the scope to encompass a wider array of functional groups. An exploration of the complex interactions between these functional groups and environmental conditions could provide crucial knowledge for customizing to specific application requirements.

Environmental Complexity. Expanding the research scope to encompass complex aquatic environments, such as natural water bodies, presents the potential for leading outcomes that closely replicate real-world scenarios. Within these more complex environments, the presence of factors such as NOM, diverse pollutants, and an array of ions introduces a layer of complexity that has the potential to change the aggregation behavior and stability of nanoparticles. Therefore, exploring the dynamic interaction between MPs and these complex aquatic environments is not only relevant but also essential to ensure a thorough and accurate assessment of potential hazards of MPs.

Exploring the Effects of pH and Temperature. Another important factor for further investigation are the impact of varying pH and temperature conditions on the behavior of MPs. It is crucial to investigate the effects of these factors on the aggregation, stability, and interfacial interactions of MPs.

Long-Term Stability. While the current study predominantly focused on the short-term stability and aggregation of MPs for 360 min, an essential path for future exploration involves conducting long-term investigations. By monitoring the conduct of these MPs over extended timeframes within aquatic environments, researchers can obtain valuable insights into the behavior of MPs. This extended perspective provides the chance to observe how the stability or aggregation of these MPs might change over time.

6 References:

- Adyel, T. M. (2020). Accumulation of plastic waste during COVID-19. *Science*, 369(6509), 1314-1315.
- Ahmed, R., Hamid, A. K., Krebsbach, S. A., He, J., & Wang, D. (2022). Critical review of microplastics removal from the environment. *Chemosphere*, 133557.
- Akaighe, N., Depner, S. W., Banerjee, S., Sharma, V. K., & Sohn, M. (2012). The effects of monovalent and divalent cations on the stability of silver nanoparticles formed from direct reduction of silver ions by Suwannee River humic acid/natural organic matter. *Science of the total environment*, 441, 277-289.
- Al Harraq, A., & Bharti, B. (2021). Microplastics through the Lens of Colloid Science. *ACS Environmental Au*, 2(1), 3-10.
- Ali, I., Tan, X., Li, J., Peng, C., Naz, I., Duan, Z., & Ruan, Y. (2022). Interaction of microplastics and nanoplastics with natural organic matter (NOM) and the impact of NOM on the sorption behavior of anthropogenic contaminants—A critical review. *Journal of cleaner production*, 134314.
- Alimi, O. S., Farner Budarz, J., Hernandez, L. M., & Tufenkji, N. (2018). Microplastics and nanoplastics in aquatic environments: aggregation, deposition, and enhanced contaminant transport. *Environmental science & technology*, 52(4), 1704-1724.
- Andrady, A. L. (2011). Microplastics in the marine environment. *Marine pollution bulletin*, 62(8), 1596-1605.
- Andrady, A. L. (2017). The plastic in microplastics: A review. *Marine pollution bulletin*, 119(1), 12-22.

- Andrady, A. L., & Neal, M. A. (2009). Applications and societal benefits of plastics. *Philosophical Transactions of the Royal Society B: Biological Sciences*, 364(1526), 1977-1984.
- Anguissola, S., Garry, D., Salvati, A., O'Brien, P. J., & Dawson, K. A. (2014). High content analysis provides mechanistic insights on the pathways of toxicity induced by amine-modified polystyrene nanoparticles. *PloS one*, 9(9), e108025.
- Auta, H. S., Emenike, C. U., & Fauziah, S. H. (2017). Distribution and importance of microplastics in the marine environment: a review of the sources, fate, effects, and potential solutions. *Environment international*, 102, 165-176.
- Badawy, A. M. E., Luxton, T. P., Silva, R. G., Scheckel, K. G., Suidan, M. T., & Tolaymat, T. M. (2010). Impact of environmental conditions (pH, ionic strength, and electrolyte type) on the surface charge and aggregation of silver nanoparticles suspensions. *Environmental science & technology*, 44(4), 1260-1266.
- Bader, R. F. W., Popelier, P. L. A., & Keith, T. A. (1994). Theoretical definition of a functional group and the molecular orbital paradigm. *Angewandte Chemie International Edition in English*, 33(6), 620-631.
- Besseling, E., Quik, J. T., Sun, M., & Koelmans, A. A. (2017). Fate of nano-and microplastic in freshwater systems: A modeling study. *Environmental Pollution*, 220, 540-548.
- Bhargava, S., Chen Lee, S. S., Min Ying, L. S., Neo, M. L., Lay-Ming Teo, S., & Valiyaveetil, S. (2018). Fate of nanoplastics in marine larvae: a case study using barnacles, *Amphibalanus amphitrite*. *ACS Sustainable chemistry & engineering*, 6(5), 6932-6940.
- Bhattacharjee, S. (2016). DLS and zeta potential—what they are and what they are not? *Journal of controlled release*, 235, 337-351.
- Birdi, K. (2016). *Surface chemistry and geochemistry of hydraulic fracturing*: CRC Press.

- Bizmark, N., Schneider, J., Priestley, R. D., & Datta, S. S. (2020). Multiscale dynamics of colloidal deposition and erosion in porous media. *Science Advances*, 6(46), eabc2530.
- Brandon, J. A. (2017). *The distribution of suspended microplastics and nanoplastics in the Northeast Pacific and their effects on zooplankton consumers*: University of California, San Diego.
- Cai, L., Hu, L., Shi, H., Ye, J., Zhang, Y., & Kim, H. (2018). Effects of inorganic ions and natural organic matter on the aggregation of nanoplastics. *Chemosphere*, 197, 142-151.
- Carr, S. A., Liu, J., & Tesoro, A. G. (2016). Transport and fate of microplastic particles in wastewater treatment plants. *Water Research*, 91, 174-182.
- Chekli, L., Zhao, Y., Tijing, L., Phuntsho, S., Donner, E., Lombi, E., . . . Shon, H. (2015). Aggregation behaviour of engineered nanoparticles in natural waters: characterising aggregate structure using on-line laser light scattering. *Journal of Hazardous Materials*, 284, 190-200.
- Chen, Z., Wei, Z., Chen, Y., & Dames, C. (2013). Anisotropic Debye model for the thermal boundary conductance. *Physical Review B*, 87(12), 125426.
- Chorover, J. (2023). Surface charge and zero-charge points.
- Chowdhury, I., Duch, M. C., Mansukhani, N. D., Hersam, M. C., & Bouchard, D. (2014). Deposition and release of graphene oxide nanomaterials using a quartz crystal microbalance. *Environmental science & technology*, 48(2), 961-969.
- Chowdhury, I., Mansukhani, N. D., Guiney, L. M., Hersam, M. C., & Bouchard, D. (2015). Aggregation and stability of reduced graphene oxide: complex roles of divalent cations, pH, and natural organic matter. *Environmental science & technology*, 49(18), 10886-10893.
- Cole, M., Lindeque, P., Halsband, C., & Galloway, T. S. (2011). Microplastics as contaminants in the marine environment: a review. *Marine pollution bulletin*, 62(12), 2588-2597.

- Cross, W., Ma, S., Winter, R., & Kellar, J. (1999). FT-IR/ATR and SEM study of colloidal particle deposition. *Colloids and Surfaces A: Physicochemical and Engineering Aspects*, 154(1-2), 115-125.
- Danso, D., Chow, J., & Streit, W. R. (2019). Plastics: microbial degradation, environmental and biotechnological perspectives. *Applied and environmental microbiology*, AEM. 01095-01019.
- Darabi, M., Majeed, H., Diehl, A., Norton, J., & Zhang, Y. (2021). A review of microplastics in aquatic sediments: Occurrence, fate, transport, and ecological impact. *Current Pollution Reports*, 7, 40-53.
- Debroy, A., George, N., & Mukherjee, G. (2022). Role of biofilms in the degradation of microplastics in aquatic environments. *Journal of Chemical Technology & Biotechnology*, 97(12), 3271-3282.
- Della Torre, C., Bergami, E., Salvati, A., Faleri, C., Cirino, P., Dawson, K., & Corsi, I. (2014). Accumulation and embryotoxicity of polystyrene nanoparticles at early stage of development of sea urchin embryos *Paracentrotus lividus*. *Environmental science & technology*, 48(20), 12302-12311.
- Dong, S., Yu, Z., Huang, J., & Gao, B. (2022). Fate and transport of microplastics in soils and groundwater *Emerging contaminants in soil and groundwater systems* (pp. 301-329): Elsevier.
- Dong, Z., Qiu, Y., Zhang, W., Yang, Z., & Wei, L. (2018). Size-dependent transport and retention of micron-sized plastic spheres in natural sand saturated with seawater. *Water Res.*, 143, 518-526. doi:<https://doi.org/10.1016/j.watres.2018.07.007>

- Dong, Z., Zhu, L., Zhang, W., Huang, R., Lv, X., Jing, X., . . . Qiu, Y. (2019). Role of surface functionalities of nanoplastics on their transport in seawater-saturated sea sand. *Environmental Pollution*, 255, 113177.
- Eerkes-Medrano, D., Thompson, R. C., & Aldridge, D. C. (2015). Microplastics in freshwater systems: a review of the emerging threats, identification of knowledge gaps and prioritisation of research needs. *Water Research*, 75, 63-82.
- Filby, A. (2010). *Interaction of colloids with mineral surfaces: a microscopical and nanoscopical approach*. Karlsruhe, Univ., Diss., 2009.
- Garvey, C. J., Imp  rator-Clerc, M., Rouzi  re, S., Gouadec, G., Boyron, O., Roweczyk, L., . . . Ter Halle, A. (2020). Molecular-scale understanding of the embrittlement in polyethylene ocean debris. *Environmental science & technology*, 54(18), 11173-11181.
- Gonz  lez-Fern  ndez, C., Tallec, K., Le Go  c, N., Lambert, C., Soudant, P., Huvet, A., . . . Paul-Pont, I. (2018). Cellular responses of Pacific oyster (*Crassostrea gigas*) gametes exposed in vitro to polystyrene nanoparticles. *Chemosphere*, 208, 764-772.
- Hahladakis, J. N., Velis, C. A., Weber, R., Iacovidou, E., & Purnell, P. (2018). An overview of chemical additives present in plastics: Migration, release, fate and environmental impact during their use, disposal and recycling. *Journal of Hazardous Materials*, 344, 179-199.
- Harrison, J. P., Hoellein, T. J., Sapp, M., Tagg, A. S., Ju-Nam, Y., & Ojeda, J. J. (2018). Microplastic-associated biofilms: a comparison of freshwater and marine environments. *Freshwater microplastics: emerging environmental contaminants?*, 181-201.
- He, L., Wu, D., Rong, H., Li, M., Tong, M., & Kim, H. (2018). Influence of nano-and microplastic particles on the transport and deposition behaviors of bacteria in quartz sand. *Environmental science & technology*, 52(20), 11555-11563.

https://www.clays.org/sourceclays_source_and_special/.

- Ibrahim, A., Hiripitiyage, Y., Peltier, E. F., & Sturm, B. S. (2018). *Investigation of the response mechanisms of halophilic and mixed culture aerobic granular sludge under hypersaline conditions*. Paper presented at the WEFTEC 2018.
- Israelachvili, J. N. (2011a). *Intermolecular and surface forces*: Academic press.
- Israelachvili, J. N. (2011b). Van der Waals forces. *Intermolecular and surface forces*, 107-132.
- Jans, H., Liu, X., Austin, L., Maes, G., & Huo, Q. (2009). Dynamic light scattering as a powerful tool for gold nanoparticle bioconjugation and biomolecular binding studies. *Analytical chemistry*, 81(22), 9425-9432.
- Jung, Y., Metreveli, G., Park, C.-B., Baik, S., & Schaumann, G. E. (2018). Implications of pony lake fulvic acid for the aggregation and dissolution of oppositely charged surface-coated silver nanoparticles and their ecotoxicological effects on *Daphnia magna*. *Environmental science & technology*, 52(2), 436-445.
- Kalliola, S., Repo, E., Sillanpää, M., Arora, J. S., He, J., & John, V. T. (2016). The stability of green nanoparticles in increased pH and salinity for applications in oil spill-treatment. *Colloids and Surfaces A: Physicochemical and Engineering Aspects*, 493, 99-107.
- Kontogeorgis, G. M., & Kiil, S. (2016). *Introduction to applied colloid and surface chemistry*: John Wiley & Sons.
- Kretzschmar, R., Sticher, H., & Hesterberg, D. (1997). Effects of adsorbed humic acid on surface charge and flocculation of kaolinite. *Soil Science Society of America Journal*, 61(1), 101-108.
- Kvale, K., & Oschlies, A. (2023). Recovery from microplastic-induced marine deoxygenation may take centuries. *Nature Geoscience*, 16(1), 10-12.

- Lafi, Z. M. S. (2020). *FORMULATION AND FUNCTIONALIZATION OF APTAMER-GUIDED pH-SENSITIVE LIPOSOMES FOR TARGETED DRUG DELIVERY OF ECHINOMYCIN-CYCLODEXTRIN COMPLEX INTO CANCER CELLS*. University of Jordan.
- Lei, L., Liu, M., Song, Y., Lu, S., Hu, J., Cao, C., . . . He, D. (2018). Polystyrene (nano) microplastics cause size-dependent neurotoxicity, oxidative damage and other adverse effects in *Caenorhabditis elegans*. *Environmental Science: Nano*, 5(8), 2009-2020.
- Li, L., Sillanpää, M., & Risto, M. (2016). Influences of water properties on the aggregation and deposition of engineered titanium dioxide nanoparticles in natural waters. *Environmental Pollution*, 219, 132-138.
- Li, M., He, L., Zhang, X., Rong, H., & Tong, M. (2020). Different surface charged plastic particles have different cotransport behaviors with kaolinite☆ particles in porous media. *Environmental Pollution*, 267, 115534.
- Li, M., Zhang, X., Yi, K., He, L., Han, P., & Tong, M. (2021). Transport and deposition of microplastic particles in saturated porous media: Co-effects of clay particles and natural organic matter. *Environmental Pollution*, 287, 117585.
- Li, S., Liu, H., Gao, R., Abdurahman, A., Dai, J., & Zeng, F. (2018). Aggregation kinetics of microplastics in aquatic environment: Complex roles of electrolytes, pH, and natural organic matter. *Environmental Pollution*, 237, 126-132.
- Li, X., Mei, Q., Chen, L., Zhang, H., Dong, B., Dai, X., . . . Zhou, J. (2019). Enhancement in adsorption potential of microplastics in sewage sludge for metal pollutants after the wastewater treatment process. *Water Research*, 157, 228-237.

- Lin, D., Story, S. D., Walker, S. L., Huang, Q., Liang, W., & Cai, P. (2017). Role of pH and ionic strength in the aggregation of TiO₂ nanoparticles in the presence of extracellular polymeric substances from *Bacillus subtilis*. *Environmental Pollution*, 228, 35-42.
- Lin, D., Tian, X., Wu, F., & Xing, B. (2010). Fate and transport of engineered nanomaterials in the environment. *Journal of environmental quality*, 39(6), 1896-1908.
- Ling, X., Yan, Z., & Lu, G. (2022). Vertical transport and retention behavior of polystyrene nanoplastics in simulated hyporheic zone. *Water Research*, 219, 118609.
- Liu, J., Ma, Y., Zhu, D., Xia, T., Qi, Y., Yao, Y., . . . Chen, W. (2018). Polystyrene nanoplastics-enhanced contaminant transport: role of irreversible adsorption in glassy polymeric domain. *Environmental science & technology*, 52(5), 2677-2685.
- Long, M., Paul-Pont, I., Hegaret, H., Moriceau, B., Lambert, C., Huvet, A., & Soudant, P. (2017). Interactions between polystyrene microplastics and marine phytoplankton lead to species-specific hetero-aggregation. *Environmental Pollution*, 228, 454-463.
- Luan, L., Wang, X., Zheng, H., Liu, L., Luo, X., & Li, F. (2019). Differential toxicity of functionalized polystyrene microplastics to clams (*Meretrix meretrix*) at three key development stages of life history. *Marine pollution bulletin*, 139, 346-354.
- Lunov, O., Syrovets, T., Loos, C., Nienhaus, G. U., Mailänder, V., Landfester, K., . . . Simmet, T. (2011). Amino-functionalized polystyrene nanoparticles activate the NLRP3 inflammasome in human macrophages. *ACS nano*, 5(12), 9648-9657.
- Lv, X., Dong, Q., Zuo, Z., Liu, Y., Huang, X., & Wu, W.-M. (2019). Microplastics in a municipal wastewater treatment plant: Fate, dynamic distribution, removal efficiencies, and control strategies. *Journal of cleaner production*, 225, 579-586.
- Matter, F., Luna, A. L., & Niederberger, M. (2020). From colloidal dispersions to aerogels: How to master nanoparticle gelation. *Nano Today*, 30, 100827.

- Mattsson, K., Jovic, S., Doverbratt, I., & Hansson, L. (2018). An emerging matter of environmental urgency. *Microplastic contamination in aquatic environments*, 379-399.
- McNutt, M. (2017). Production, use, and fate of all plastics ever made. *Science Advances*, 19.
- Novich, B. E., & Ring, T. A. (1984). Colloid stability of clays using photon correlation spectroscopy. *Clays and Clay minerals*, 32, 400-406.
- Oriekhova, O., & Stoll, S. (2018). Heteroaggregation of nanoplastic particles in the presence of inorganic colloids and natural organic matter. *Environmental Science: Nano*, 5(3), 792-799.
- Park, S.-J., & Seo, M.-K. (2011). *Interface science and composites* (Vol. 18): Academic Press.
- Pradel, A., Ferreres, S., Veclin, C., El Hadri, H., Gautier, M., Grassl, B., & Gigault, J. (2021). Stabilization of fragmental polystyrene nanoplastic by natural organic matter: insight into mechanisms. *ACS ES&T Water*, 1(5), 1198-1208.
- Qu, X., Hwang, Y. S., Alvarez, P. J., Bouchard, D., & Li, Q. (2010). UV irradiation and humic acid mediate aggregation of aqueous fullerene (nC60) nanoparticles. *Environmental science & technology*, 44(20), 7821-7826.
- Ramirez, L., Ramseier Gentile, S., Zimmermann, S., & Stoll, S. (2019). Behavior of TiO₂ and CeO₂ nanoparticles and polystyrene nanoplastics in bottled mineral, drinking and Lake Geneva waters. Impact of water hardness and natural organic matter on nanoparticle surface properties and aggregation. *Water*, 11(4), 721.
- Raval, N., Maheshwari, R., Kalyane, D., Youngren-Ortiz, S. R., Chougule, M. B., & Tekade, R. K. (2019). Importance of physicochemical characterization of nanoparticles in pharmaceutical product development *Basic fundamentals of drug delivery* (pp. 369-400): Elsevier.
- Rezaei, M., Riksen, M. J., Sirjani, E., Sameni, A., & Geissen, V. (2019). Wind erosion as a driver for transport of light density microplastics. *Science of the total environment*, 669, 273-281.

- Rochman, C. M., & Hoellein, T. (2020). The global odyssey of plastic pollution. *Science*, 368(6496), 1184-1185.
- Romero-Cano, M., Martin-Rodriguez, A., & De las Nieves, F. (2001). Electrosteric stabilization of polymer colloids with different functionality. *Langmuir*, 17(11), 3505-3511.
- Rosenboom, J.-G., Langer, R., & Traverso, G. (2022). Bioplastics for a circular economy. *Nature Reviews Materials*, 7(2), 117-137.
- Selvamani, V. (2019). Stability studies on nanomaterials used in drugs *Characterization and biology of nanomaterials for drug delivery* (pp. 425-444): Elsevier.
- Shams, M., Alam, I., & Chowdhury, I. (2020). Aggregation and stability of nanoscale plastics in aquatic environment. *Water Research*, 171, 115401.
- Shams, M., Alam, I., & Chowdhury, I. (2021). Interactions of nanoscale plastics with natural organic matter and silica surfaces using a quartz crystal microbalance. *Water Research*, 197, 117066.
- Sharma, V. K., Ma, X., Guo, B., & Zhang, K. (2021). Environmental factors-mediated behavior of microplastics and nanoplastics in water: A review. *Chemosphere*, 271, 129597.
- Shen, M.-H., Yin, Y.-G., Booth, A., & Liu, J.-F. (2015). Effects of molecular weight-dependent physicochemical heterogeneity of natural organic matter on the aggregation of fullerene nanoparticles in mono-and di-valent electrolyte solutions. *Water Research*, 71, 11-20.
- Singh, N., Tiwari, E., Khandelwal, N., & Darbha, G. K. (2019). Understanding the stability of nanoplastics in aqueous environments: effect of ionic strength, temperature, dissolved organic matter, clay, and heavy metals. *Environmental Science: Nano*, 6(10), 2968-2976.
- Smith, P. H. (1935). Plastics Come of Age. *Scientific American*, 152(1), 5-7.
- Sobeck, D. C., & Higgins, M. J. (2002). Examination of three theories for mechanisms of cation-induced biofloculation. *Water Research*, 36(3), 527-538.

- Sun, J., Dai, X., Wang, Q., Van Loosdrecht, M. C., & Ni, B.-J. (2019). Microplastics in wastewater treatment plants: Detection, occurrence and removal. *Water Research*, *152*, 21-37.
- Talleg, K., Blard, O., González-Fernández, C., Brotons, G., Berchel, M., Soudant, P., . . . Paul-Pont, I. (2019). Surface functionalization determines behavior of nanoplastic solutions in model aquatic environments. *Chemosphere*, *225*, 639-646.
- Talleg, K., Huvet, A., Di Poi, C., González-Fernández, C., Lambert, C., Petton, B., . . . Paul-Pont, I. (2018). Nanoplastics impaired oyster free living stages, gametes and embryos. *Environmental Pollution*, *242*, 1226-1235.
- Tan, M., Liu, L., Zhang, M., Liu, Y., & Li, C. (2021). Effects of solution chemistry and humic acid on the transport of polystyrene microplastics in manganese oxides coated sand. *Journal of Hazardous Materials*, *413*, 125410.
- Wang, C., Wang, R., Huo, Z., Xie, E., & Dahlke, H. E. (2020). Colloid transport through soil and other porous media under transient flow conditions—A review. *Wiley Interdisciplinary Reviews: Water*, *7*(4), e1439.
- Wang, H., Dong, Y.-n., Zhu, M., Li, X., Keller, A. A., Wang, T., & Li, F. (2015). Heteroaggregation of engineered nanoparticles and kaolin clays in aqueous environments. *Water Research*, *80*, 130-138.
- Wang, J., Zhao, X., Wu, A., Tang, Z., Niu, L., Wu, F., . . . Fu, Z. (2021). Aggregation and stability of sulfate-modified polystyrene nanoplastics in synthetic and natural waters. *Environmental Pollution*, *268*, 114240.
- Wang, P., Qi, N., Ao, Y., Hou, J., Wang, C., & Qian, J. (2016). Effect of UV irradiation on the aggregation of TiO₂ in an aquatic environment: Influence of humic acid and pH. *Environmental Pollution*, *212*, 178-187.

- Wang, T., Wang, L., Li, X., Hu, X., Han, Y., Luo, Y., . . . Wang, L. (2017). Size-dependent regulation of intracellular trafficking of polystyrene nanoparticle-based drug-delivery systems. *ACS Applied Materials & Interfaces*, *9*(22), 18619-18625.
- Wang, X., Li, Y., Zhao, J., Xia, X., Shi, X., Duan, J., & Zhang, W. (2020). UV-induced aggregation of polystyrene nanoplastics: effects of radicals, surface functional groups and electrolyte. *Environmental Science: Nano*, *7*(12), 3914-3926.
- Wang, X., Liu, L., Zheng, H., Wang, M., Fu, Y., Luo, X., . . . Wang, Z. (2020). Polystyrene microplastics impaired the feeding and swimming behavior of mysid shrimp *Neomysis japonica*. *Marine pollution bulletin*, *150*, 110660.
- Wegner, A., Besseling, E., Foekema, E. M., Kamermans, P., & Koelmans, A. A. (2012). Effects of nanopolystyrene on the feeding behavior of the blue mussel (*Mytilus edulis* L.). *Environmental Toxicology and Chemistry*, *31*(11), 2490-2497.
- Wessel, C. C., Lockridge, G. R., Battiste, D., & Cebrian, J. (2016). Abundance and characteristics of microplastics in beach sediments: insights into microplastic accumulation in northern Gulf of Mexico estuaries. *Marine pollution bulletin*, *109*(1), 178-183.
- Wright, S. L., & Kelly, F. J. (2017). Plastic and human health: a micro issue? *Environmental science & technology*, *51*(12), 6634-6647.
- Wu, J., Jiang, R., Lin, W., & Ouyang, G. (2019). Effect of salinity and humic acid on the aggregation and toxicity of polystyrene nanoplastics with different functional groups and charges. *Environmental Pollution*, *245*, 836-843.
- Wu, W.-M., Yang, J., & Criddle, C. S. (2017). Microplastics pollution and reduction strategies. *Frontiers of Environmental Science & Engineering*, *11*, 1-4.

- Wu, X., Lyu, X., Li, Z., Gao, B., Zeng, X., Wu, J., & Sun, Y. (2020). Transport of polystyrene nanoplastics in natural soils: Effect of soil properties, ionic strength and cation type. *Science of the total environment*, 707, 136065.
- Wu, Y., & Cheng, T. (2016). Stability of nTiO₂ particles and their attachment to sand: Effects of humic acid at different pH. *Science of the total environment*, 541, 579-589.
- Xiao, Y., Tan, Z., Yin, Y., Guo, X., Xu, J., Wang, B., . . . Liu, J. (2018). Application of hollow fiber flow field-flow fractionation with UV–Vis detection in the rapid characterization and preparation of poly (vinyl acetate) nanoemulsions. *Microchemical Journal*, 137, 376-380.
- Xinjie Wang, N. B., Daniel C.W. Tsang, Binoy Sarkar, Lauren Bradney, Yang Li,. (2021). A review of microplastics aggregation in aquatic environment: Influence factors, analytical methods, and environmental implications. *Journal of Hazardous Materials*, 402, 123496.
- Zhang, C., Wang, C., Cao, G., Wang, D., & Ho, S.-H. (2020). A sustainable solution to plastics pollution: An eco-friendly bioplastic film production from high-salt contained *Spirulina* sp. residues. *Journal of Hazardous Materials*, 388, 121773.
- Zhou, D., Abdel-Fattah, A. I., & Keller, A. A. (2012). Clay particles destabilize engineered nanoparticles in aqueous environments. *Environmental science & technology*, 46(14), 7520-7526.
- Zhu, M., Wang, H., Keller, A. A., Wang, T., & Li, F. (2014). The effect of humic acid on the aggregation of titanium dioxide nanoparticles under different pH and ionic strengths. *Science of the total environment*, 487, 375-380.

7 Appendix

7.1 Product specification of polystyrene

SIGMA-ALDRICH

sigma-aldrich.com

Website: www.sigmaaldrich.com
Email USA: techserv@sial.com
Outside USA: eurtechserv@sial.com

Product Specification

Product Name:

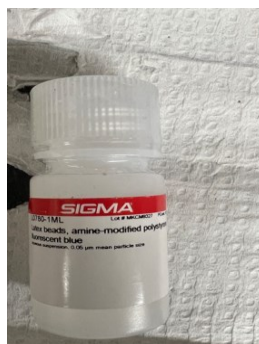
Latex beads, amine-modified polystyrene, fluorescent red - aqueous suspension, 1.0 µm mean particle size

Product Number:

L2778

MDL:

MFCD00131492



TEST

Specification

Appearance (Color)	Faint Pink to Very Dark Red
Appearance (Form)	Suspension
Latex Type	Conforms
Polystyrene	
Surface Functional Group	Conforms
Amine-modified	
Density	1.04 - 1.05 g/ml
Solid Content	
Approximately 2.5%	
Mean Particle Diameter	0.9 - 1.1 micron
Standard Deviations	0.05 - 0.09 micron
Dye Content	0.4 - 0.6 %
Red fluorescent dye with maximum excitation of 505 nm to 585 nm and maximum emission of 550 nm to 645 nm	

Sigma-Aldrich warrants, that at the time of the quality release or subsequent retest date this product conformed to the information contained in this publication. The current Specification sheet may be available at Sigma-Aldrich.com. For further inquiries, please contact Technical Service. Purchaser must determine the suitability of the product for its particular use. See reverse side of invoice or packing slip for additional terms and conditions of sale. 1 of 1

7.2 Product specification of amine-modified polystyrene

SIGMA-ALDRICH®

sigma-aldrich.com

Website: www.sigmaaldrich.com

Email USA: techserv@sial.com

Outside USA: eurtechserv@sial.com

Product Specification

Product Name:

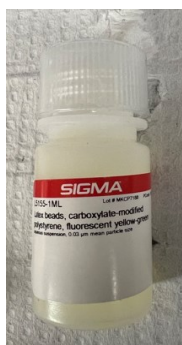
Latex beads, carboxylate-modified polystyrene, fluorescent yellow-green - aqueous suspension, 1.0 µm mean particle size

Product Number:

L4655

MDL:

MFCD00131492



TEST

Specification

Appearance (Color)	Yellow
Appearance (Form)	Suspension
Miscellaneous Supplier Data	Conforms
Latex Type, Polystyrene	
Miscellaneous Supplier Data	Conforms
Surface Functional Groups	
Carboxylate Modified	
Miscellaneous Supplier Data	1.045 - 1.055
Density	
Solid Content	2.4 - 2.6 %
Miscellaneous Supplier Data	0.90 - 1.10 micron
Mean Diameter	
Miscellaneous Supplier	Data > 0.008 meq _
Charge Density	
Miscellaneous Supplier Data	
Preservative, 0.1% Sodium Azide	

Specification: PRD.0.ZQ5.10000017820

Sigma-Aldrich warrants, that at the time of the quality release or subsequent retest date this product conformed to the information contained in this publication. The current Specification sheet may be available at Sigma-Aldrich.com. For further inquiries, please contact Technical Service. Purchaser must determine the suitability of the product for its particular use. See reverse side of invoice or packing slip for additional terms and conditions of sale.

7.3 Product specification of carboxylate-modified polystyrene

SIGMA-ALDRICH®

sigma-aldrich.com

3050 Spruce Street, Saint Louis, MO 63103, USA

Website: www.sigmaaldrich.com

Email USA: techserv@sial.com

Outside USA: eurtechserv@sial.com

Product Specification

Product Name:

Latex beads, polystyrene - 1.1 µm mean particle size

Product Number: **LB11**

MDL: MFCD00131491

TEST	Specification
Appearance (Color)	White
Appearance (Form)	Suspension
Size	1.0 - 1.2 micron
Particle Diameter	

Specification: PRD.0.ZQ5.10000021305



PROPERTIES

form

aqueous suspension.

Composition

Solids, 10%

mean particle size

1.1 µm

7.4 Specification of humic acid

Description

Metal chelator; pigments. Humic acid is used as a soil supplement in agriculture and human nutritional supplement. It is used to improve the growth and cultivation of crops, citrus, turf, flowers. It is also used to improve the strength of organically-deficient soils. It is utilized to stimulate the immune system and treating the influenza, avian flu, swine flu and other viral infections.

This Thermo Scientific Chemicals brand product was originally part of the Alfa Aesar product portfolio. Some documentation and label information may refer to the legacy brand. The original Alfa Aesar product / item code or SKU reference has not changed as a part of the brand transition to Thermo Scientific Chemicals.

Specifications

Chemical Name or Material	Humic acid
MDL Number	MFCD00147177
Quantity	25 g
CAS	1415-93-6
Solubility Information	Slightly soluble in water,with much swellingSoluble in organic solvents like acetone and benzenol. Slightly soluble in water.

Physical Form

Crystalline Powder

Chemical Identifiers

CAS

1415-93-6

MDL Number

MFCD00147177

Safety and Handling

EINECSNumber: 215-809-6

RTECSNumber: MT6544000

TSCA: Yes

Recommended Storage: Ambient temperatures

7.5 Specification of kaolinite

Kaolin KGa-2, (high-defect)

ORIGIN: Probably lower tertiary (stratigraphic sequence uncertain)

County of Warren, State of Georgia, USA

LOCATION: 33°19' N-82°28' W approximately, topographic map Bowdens Pond, Georgia N 3315-W 8222.5/7.5, Collected from face of Purvis pit, October 4, 1972.

CHEMICAL COMPOSITION (%): SiO₂: 43.9, Al₂O₃: 38.5, TiO₂: 2.08, Fe₂O₃: 0.98, FeO: 0.15, MnO: n.d., MgO: 0.03, CaO: n.d., Na₂O: <0.005, K₂O: 0.065, P₂O₅: 0.045, S: 0.02, Loss on heating: -550°C: 12.6; 550-1000°C: 1.17, F:0.02.

CATION EXCHANGE CAPACITY (CEC): 3.3 meq/100g

SURFACE AREA: N₂ area: 23.50 +/- 0.06 m²/g

THERMAL ANALYSIS: DTA: endotherm at 625°C, exotherm at 1005°C, TG: dehydroxylation weight loss 13.14% (theory 14%) indicating less than 7% impurities.

INFRARED SPECTROSCOPY: Typical spectrum for less crystallized kaolinite, however the mineral is not extremely disordered since the band at 3669 cm⁻¹ is still present in the spectrum.

STRUCTURE: Al₂Si₂O₅(OH)₄- (Catr Ktr)[Al_{3.66} Fe(III).07 Mntr Mgtr Ti.16][Si_{4.00}]O₁₀(OH)₈, Octahedral charge:.16, Tetrahedral charge:0.00, Interlayer charge:.16, Unbalanced charge:.15, Extra Si:.04

Density of kaolinite is 2.68 g/cm³